CONCENTRATION AND VELOCITY MEASUREMENTS IN SUSPENSIONS FLOWING THROUGH A RECTANGULAR CHANNEL

Thesis by

Philip Alan Hookham

In Partial Fulfillment of the Requirements

for the Degree of

Doctor of Philosophy

California Institute of Technology

Pasadena, California

1986

(Submitted October 18, 1985)

to Ralph, the dog

If I have not seen as far as other men,

it is because there are too damn many giants in the way.

-Anonymous

ACKNOWLEDGEMENTS

It is very unfortunate that my original advisor, Professor William H. Corcoran , was not able to witness the completion of this work. I wish that I could have thanked him for his help and guidance. His concern for the overall development of his students' professional abilities was very unusual.

I would like to thank Professor L. Gary Leal for "adopting" me and guiding me through the completion of my thesis.

I would also like to thank George Griffith for all of his help in the construction of the experimental apparatus, and John Yehle for his assistance with electronics.

This project was made possible by a grant from the Donald E. Baxter Foundation. I would also like to acknowledge the receipt of a William H. Corcoran Fellowship during my final summer at Caltech (Thanks Rita!).

My tenure as a graduate student was enriched by the presence of many of my fellow students. In particular, Puvin and Brian were (usually) there when a break from the rigors of research was needed.

Most of all, I would like to thank Malina for being such a *sweetie*

ABSTRACT

A method to measure particle concentrations in dilute to moderately concentrated transparent liquid-solid suspensions was developed. The method uses a dual-beam laser-Doppler anemometer system. Particle concentrations were determined by counting the number of signals from fluorescently-dyed tracer particles per unit time. Using this method, both the velocities and concentrations of suspended particles were obtained.

Velocity and concentration measurements were made in suspensions of neutrally-buoyant polystyrene-divinylbenzene spheres 27, 50, and 70 μm in diameter flowing in a rectangular channel with 800 μm spacing between walls. Measurements were made in the central plane of the flow channel, thus approximating two-dimensional flow. Dilute-suspension (particle volume fraction Φ_m=0.001) experiments were performed both at Reynolds numbers that were low enough so that inertial effects were unimportant (particle Reynolds number $Re_p<10^{-3}$), and Reynolds numbers at which inertial effects were significant ($Re_p=10^{-3}-10^{-1}$). Concentrated-suspension (Φ_m=0.02–0.25) experiments were done at low Re_p only.

For the dilute suspensions at low Re, small peaks in the concentration distributions were found near the flow channel walls, which were attributed to an entrance effect. At higher Re, lateral migration of particles due to inertia was observed. The spheres migrated toward a lateral equilibrium position about 0.6 times the distance from the flow channel centerline to the walls, as demonstrated previously by others. The measured concentration profiles were compared to a previously published theory for the lateral migration of a single sphere, and it was found that the peaks near the equilibrium positions in the measured concentration distributions were somewhat broader than those predicted by the theory, presumably due to particle-particle interactions.

Non-uniform concentration profiles were observed for the concentrated suspensions. The concentration profiles became somewhat peaked in the center of the channel as Φ_m and/or sphere diameter increased, particularly for the 50 and 70 μm sphere suspensions, and for these suspensions the velocity profiles were blunted for $\Phi_m \geq 0.10$. A model velocity profile calculation indicated that the shape of the concentration profiles could satisfactorily account for the shape of the velocity profiles, except possibly for the suspensions of 70 μm spheres.

TABLE OF CONTENTS

LIST OF SYMBOLS

a	sphere radius
B	parameter in viscosity equation of Krieger and Dougherty
C	measured number of cycles per burst
d	spacing between flow channel walls
$\bar{f}_v$	average Doppler frequency
$G(s)$	function defined by Ho and Leal (1974)
$I_{S_{max}}$	maximum scattered intensity from a bright fringe
$I_{S_{min}}$	minimum scattered intensity from a dark fringe
K	parameter in viscosity equation of Krieger and Dougherty
L_e	hydrodynamic entrance length
n	number of particles
n_D^{20}	refractive index at 20 degrees Centigrade
$<N>$	average rate of particles passing through the measurement volume
P	pressure
R	tube radius
Re	Reynolds number
Re_p	Reynolds number relevant to flow near a particle
s	dimensionless lateral coordinate ($s=(1+\bar{Y})/2$)
S/N	signal-to-noise ratio
t	time
t_B	time needed for a particle to traverse the measurement volume
U	velocity
$\bar{U}$	normalized velocity

$\langle U(y) \rangle$ measured average velocity at point y

U_B bulk velocity

U_{max} maximum velocity (at channel centerline)

V Doppler signal visibility function

X streamwise coordinate

y lateral coordinate

$\bar{Y}$ dimensionless lateral coordinate ($\bar{Y}=y/(d/2)$)

μ viscosity

μ_0 suspending fluid viscosity

ρ_0 suspending fluid density

σ standard deviation

τ_{yx} shear stress exerted in the x direction on a surface normal to the y direction

Φ volume fraction of particles

Φ_m mean volume fraction of particles

$\langle \Phi \rangle$ measured time-averaged volume fraction of particles

1. INTRODUCTION AND BACKGROUND

The flow of suspensions in channels and tubes is important in a number of practical applications, such as the flow of suspended coal particles in pipes, and blood flow in membrane-type artificial kidneys. Much experimental and theoretical effort has been spent on studying suspension flow, as can be seen from review articles (Jeffrey and Acrivos, 1976; or Jinescu, 1974; for example). There remains much to be investigated regarding the flow of suspensions, however, particularly suspensions that are relatively concentrated. The prediction of the behavior of such suspensions is based mostly on empirical approaches, because the complicated interactions between particles present makes theoretical analysis difficult. Thus there is a need for experimental data in order to better understand the flow of concentrated suspensions.

One phenomenon observed in flowing suspensions which has never been adequately explained is the blunting of the velocity profiles of neutrally buoyant suspensions of rigid particles in Poiseuille flow at very low Reynolds numbers, when when the particle diameter is not small compared to the tube diameter. The classic experimental study of this phenomenon was done by Karnis et al. (1966a). Using microcinematography, Karnis et al. measured velocity profiles in tube flow of suspensions of neutrally buoyant rigid spheres, rods,and discs (for particle Reynolds numbers $Re_p<10^{-5}$). The particle volume fraction Φ_m ranged from 0.085 to 0.41, and the ratio of particle radius to tube radius a/R ranged from 0.024 to 0.112. The velocity profiles of the particle phase were determined by observing the motion of tracer spheres of the same size but different refractive index as the bulk of the particles. Liquid velocity profiles were approximated by observing the motions of a small number of aluminum tracer particles less than 25 μm in size.

For low enough Φ_m and a/R, the particle and fluid velocities were identical and parabolic. As Φ_m and/or a/R were increased, the fluid and particle velocities were still equal but the velocity profiles became blunted in the center of the tube. Blunting occured for a/R=0.02 and Φ_m>0.35, or a/R=0.04 and Φ_m>0.20, for example. There was a region of radius R_c in the center of the channel where there was no measurable velocity gradient. In this region the particles did not rotate, nor did they translate radially. For $R>R_c$ the particles did rotate and exhibited erratic radial displacements. If Φ_m and/or a/R were increased sufficiently, complete plug flow resulted. The observed velocity profiles were independent of flow rate.

The apparent viscosities of the suspensions were measured in a Couette viscometer and were found to be independent of shear rate. Also, the measured pressure drop increased linearly with flow rate. These results indicate that the observed blunting of the velocity profiles was not caused by non-Newtonian bulk properties of the suspensions. The concentration profiles of the suspended particles across the tube diameter were approximated by counting the number of tracer spheres in a given section of the tube. Since relatively few particles were counted, there was a substantial error of at least 10% in the measured concentrations . Within this experimental error, however, the concentration profiles were found to be flat. The authors concluded that the blunting was caused by a "wall effect," i.e., "a region of high viscosity consisting of suspension, bounded by a region of low viscosity at the wall." No mechanism was given to explain how this wall effect would result in the observed velocity profiles, however.

Blunting of velocity profiles for suspensions of neutrally-buoyant rigid spheres in tube flow has also been observed at higher Re_p, where inertial effects can be important (Karnis et al., 1966b, Re_p=0.0025-0.018). These investigators observed increasing blunting of velocity profiles with increasing time (or dis-

tance along the tube), and attributed this phenomenon to inertia-induced inward migration of particles. They based this conclusion in part on the visual observation of a particle-depleted layer near the wall, which increased in thickness over time, corresponding to the increase in blunting of the velocity profiles. McMahon and Parker (1975) used a microwave Doppler flowmeter to measure flow properties of suspensions of neutrally-buoyant rigid spheres. A "plug flow area" was calculated from the experimental data by determining the fraction of the total scattered power which was at the maximum frequency, this corresponding to the maximum velocity (the velocity in the plug flow region). The plug flow region was found to increase in area with increasing flow rate. Also, there appeared to be a particle-depleted region near the wall whose thickness increased with increasing Re. These effects were attributed to increasing particle migration due to inertia with increasing Re. Goto and Kuno (1982) observed optically an increase in the size of a particle-depleted layer with increasing Re for neutrally-buoyant suspensions of rigid spheres. Concentration profiles were not measured in any of these experiments, so it is not known if the particle concentration profiles were non-uniform away from the wall.

From the above it is apparent that a technique which would allow the accurate and rapid measurement of particle concentrations as well as velocities in flowing suspensions would be useful. Techniques which require the insertion of a probe into the flow are inappropriate for two-phase flows, since they disrupt the flow and can become clogged. Such an approach was used by Fenton and Stukel (1976), who made measurements of local particle concentration in fully developed turbulent duct flow by inserting a fiber-optic probe into the flow. Although they were able to overcome clogging problems, the size of the probe limits its use to large flow systems.

An optical technique, such as laser-Doppler anemometry (LDA), which is

non-invasive, needs no calibration, and has a short response time, would thus seem best suited to such measurements. While LDA has traditionally been used as a velocity measurement technique, its use as a concentration-measurement technique has been limited. The use of a dual-beam LDA system to measure particle concentrations was proposed by Farmer (1972). His method determined the number density of particles directly from the Doppler signal visibility. The visibility V is defined as:

$$V = \frac{\left(I_{S_{max}} - I_{S_{min}}\right)}{\left(I_{S_{max}} + I_{S_{min}}\right)} , \qquad (1.1)$$

where $I_{S_{max}}$ is the maximum scattered intensity from a bright fringe and $I_{S_{min}}$ is the corresponding minimum scattered intensity from the next consecutive dark fringe. His technique required that the particles were illuminated uniformly by the fringe pattern, however, which meant that the particle size had to be much smaller than the fringe spacing. Since the fringe spacing is usually only a few microns, his technique would be limited to small particle sizes.

Another method for measuring particle concentration and size using an LDA system was demonstated by Lee and Srinivasan (1978). Concentrations were determined by counting the number of "bursts" per unit time, after using certain discrimination procedures. The technique could only be used in dilute suspensions, however. This limitation arises because, using this technique, it is not possible to tell how many particles are in the measurement volume, if there are more than one in it at a time. Thus the suspension concentration has to be low enough that the probability that there is more than one particle in the measuring volume at a time is small.

More recently, Kowalewski (1984) measured concentration and velocity profiles in concentrated "droplet suspensions" flowing in a tube. The velocity

and concentration profiles were measured in two separate experiments, with identical suspensions for the two experiments, except that a fluorescent dye was added to the droplets for the concentration measurements. The concentrations were found by measuring the degree of absorption of a laser beam by the droplets. The spatial resolution of the concentration measurement technique was about 100 μm, which was determined by the laser beam waist diameter. The velocities were measured using a conventional dual-beam laser-Doppler anemometer. The spatial resolution of the velocity measurement technique, which was limited by the laser beam waist diameter and the beam intersection angle, was about 100 μm. The maximum droplet volume fraction used was 0.40. Aside from the undesirability of having to conduct two separate experiments, the method appeared to work well for emulsions. It is not clear if the method would be usable in a suspension, however.

An optical method for measuring concentrations in suspensions was demonstrated very recently (Gregory, 1985). The method was based on measuring the turbidity fluctuations in a suspension by measuring the fluctuations in light from an LED transmitted through the suspension with a photodetector. The maximum suspension concentration usable with technique was only on the order of 1%, however. This maximum concentration is governed by the sensitivity of the photodetector to fluctuations in the signal transmitted through the suspension.

None of the above methods allows the rapid and accurate measurement of velocities and concentrations in a concentrated suspension of solid particles. A method capable of doing so was therefore developed. The technique uses a modified dual-beam laser-Doppler anemometer to measure both velocities and concentrations. The modification was necessary in order to make measurements in the small flow channel (800 μm spacing between walls) used, and will be

discussed in the experimental methods section. The concentration measurement technique is similar to that used by Lee and Srinivasan, except that the concentration was determined by counting the number of fluorescent tracer particles passing through the a given point in the flow channel per unit time, while optically filtering out the signal from the bulk of the particles, thus allowing its use in concentrated suspensions. The techniques allowed the nearly (see section 2.3.4.) simultaneous measurement of velocity and concentration profiles in a suspension with a volume concentration of particles up to 25%. In addition there is no particular restriction on particle size, since Doppler bursts are produced by a wide range of particle sizes. The suspended particles and suspending fluid have to be reasonably transparent, however.

The following describes the experimental techniques and our results for dilute and concentrated suspensions flowing in a rectangular channel. The width of the flow channel was much larger than the depth, so that two-dimensional flow was approximated. A rectangular channel was used rather than a tube to eliminate problems caused by refraction of the incident or scattered light at curved surfaces. The spheres were neutrally-buoyant, to simplify the analysis of the experiments by eliminating the effects of gravity. Since relatively large particles (27-70 μm diameter) were used, non-hydrodynamic effects such as Brownian motion were not expected to be important.

1.1. REFERENCES

Farmer, W. M. 1972 *Appl. Optics* **11** , 2603.

Fenton, D. L. and J. J. Stukel 1976 *Int. J. Multiphase Flow* **3** , 141.

Goto, H., and H. Kuno 1982 *J. Rheology* **26** , 387.

Gregory, J. 1985 *J. Colloid Interface Sci.* **165** , 357.

Jeffrey, D. J. and A. Acrivos 1976 *A.I.Ch.E. J.* **22** , 417.

Jinescu, V. *Int. Chem. Eng.* **14** , 397.

Karnis, A., H. L. Goldsmith, and S. G. Mason 1966a J. Colloid Interface Sci. **22** , 531.

Karnis, A., H. L. Goldsmith, and S. G. Mason 1966b *Can. J. Chem. Eng.* **44** , 181.

Kowalewski, T. A. *Experiments in Fluids* **2** , 213.

Lee, S. L. and J. Srinivasan 1978 *Int. J. Multiphase Flow* **4** , 141.

McMahon, T. A., and R. R. Parker 1975 *Trans. Soc. Rheology* **19** , 445.

2. DILUTE SUSPENSIONS

2.1. INTRODUCTION

This chapter contains descriptions of the experimental methods used, the experimental apparatus, and experimental results for dilute suspensions. The dilute-suspension experiments were done as a check on the validity of the experimental method, and as a basis for comparison with concentrated suspension measurements. The experimental results are compared to theoretical predictions based upon a previously published theory for inertial migration of a single sphere in two-dimensional flow.

2.2. EXPERIMENTAL METHODS

The fundamentals of the experimental techniques will first be presented, followed by the details of the equipment used.

2.2.1. VELOCITY MEASUREMENT

The basic principles of the velocity measurement technique, laser-Doppler anemometry, will not be discussed here. A number of textbooks exist which describe this method in detail (Durst et al., 1976; Durrani and Greated, 1977; or Drain, 1980). The features of the present experimental system which differ from a conventional laser-Doppler system, will, however, be discussed next.

A very thin flow channel (800 μm spacing between walls) was used for the experiments. This was done mainly to minimize the distance that the laser light had to travel in the suspension, and thus improve the transmission of the incident and scattered light through the suspension. Since the flow channel was so small, a conventional laser-Doppler system could not be used. A modified laser-Doppler system was necessary, because the length of the measurement volume for a conventional LDA system, which is the factor limiting its spatial resolution, is usually on the order of one millimeter (1000 microns). Thus such

a system would not be able to resolve a velocity profile in the present flow channel. A modified LDA system, based on the one developed by Chung (1980), was therefore used. The system is shown schematically in Figure 2-1.

The LDA system shown in Figure 2-1 is a variation of a dual-beam (differential-Doppler) system. In this figure, the flow channel is oriented vertically (the flow direction is up or down), while the magnifying lens and photomultiplier tube are in the same horizontal plane as the region of intersection of the laser beams (they "stick out of the page"). The region of intersection of the laser beams, which is normally called the measurement volume, more than spans the distance between the walls of the channel. (Note that the region of intersection of the laser beams actually has an elliptical cross-section, rather than the diamond-shape shown.) The scattered light produced by particles passing through the beam intersection is collected by a magnifying lens, which magnifies it about ten times. The image of the beam intersection (shown here as an arrow) is then projected onto a plate with a narrow slit cut into it. The light which passes through this slit is collected by the photomultiplier tube. Thus the photomultiplier tube effectively collects light from only a small portion (about 6%) of the beam intersection at a time. This portion is the effective measurement volume, and will henceforth be referred to as the measurement volume. The photomultiplier tube is oriented at an angle of about 20 degrees with respect to the normal to the plane of the incident laser beams (the z direction). Chung showed that if the parameters of the optical system (the magnification and the angle of the photodetector with respect to the z axis) are chosen properly, then a distance along the axis of the measurement volume y is linearly related to a horizontal distance in the projected image. Therefore, a velocity profile may be resolved by translating the slit across the image of the measurement volume.

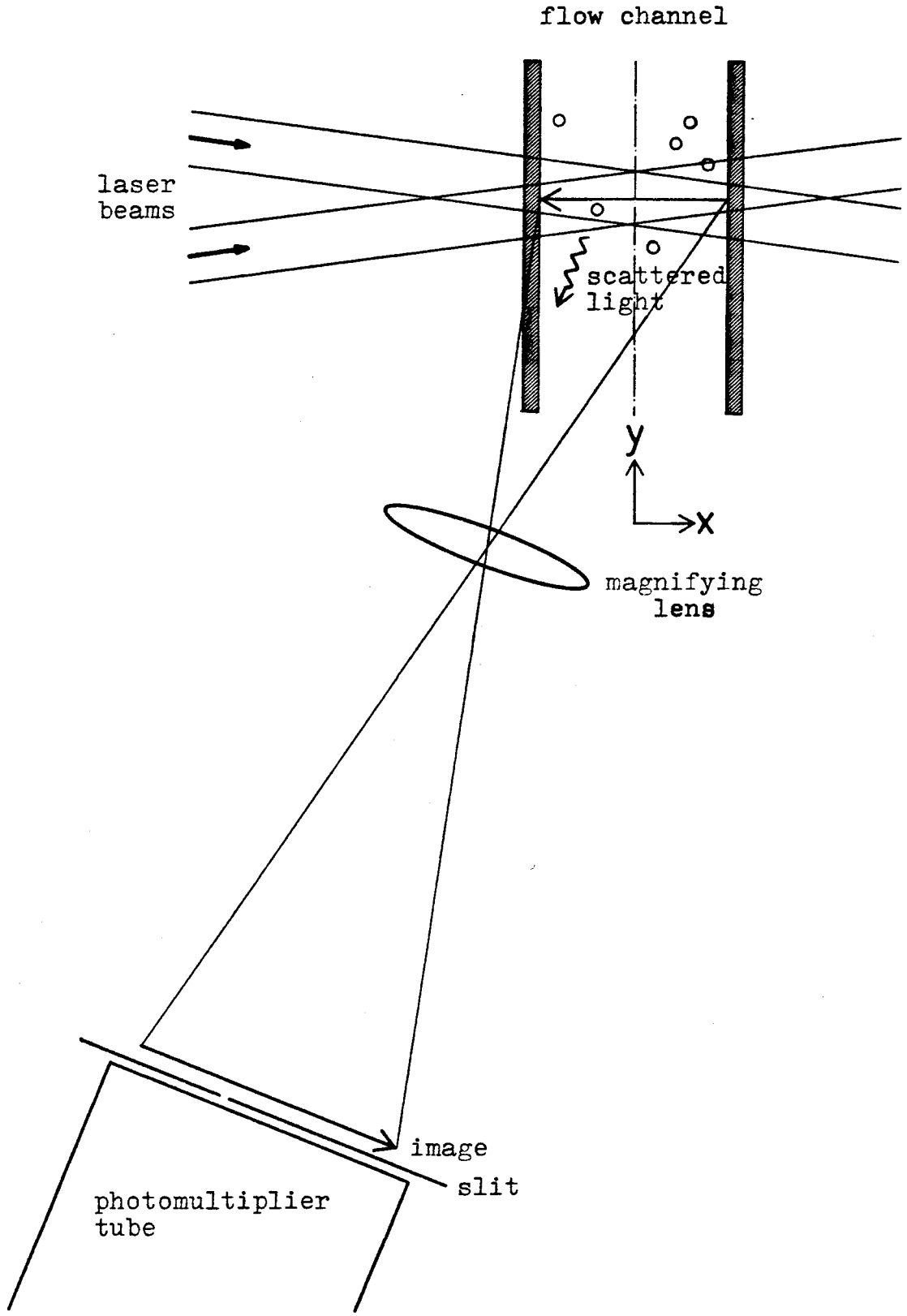

Figure 2-1. Modified LDA system.

The spatial resolution of the LDA system depends upon the magnification and the slit width. The resolution of the present system was about 50 microns, but in principle it could have been less with a smaller slit or higher magnification. It was not logical to use a smaller measurement volume in the present experiments, since the size of the measurement volume was already on the order of the particle size. For other applications, a smaller measurement volume might be desirable, however. Some difficulties might be encountered with a smaller measurement volume. First, as the slit width is decreased and/or the magnification is increased, the signal amplitude decreases. Second, as the measurement volume size decreases, changes in alignment of the optics become magnified. Changes in alignment of the optics and/or position of the flow channel with temperature were sometimes found to be a problem, even with the present system, and would become more severe for smaller measurement volumes. This difficulty would probably be the limiting factor for the spatial resolution of this type of LDA system.

2.2.2. CONCENTRATION MEASUREMENT

The concentration measurement technique is based on counting the number of spheres passing through the measurement volume per unit time. The basic approach is similar to that of Lee and Srinivasan (1978), but modified for use in concentrated suspensions by the use of fluorescent tracer particles, as indicated earlier. When a particle passes through the measurement volume, the photodetector produces a characteristic signal known as a burst, as shown in Figure 2-2. The bursts are shown as they appear after filtration to remove the dc pedestal and high frequency ac noise. By simply counting the number of bursts occuring in a given period of time, the concentration at a given point may be determined.

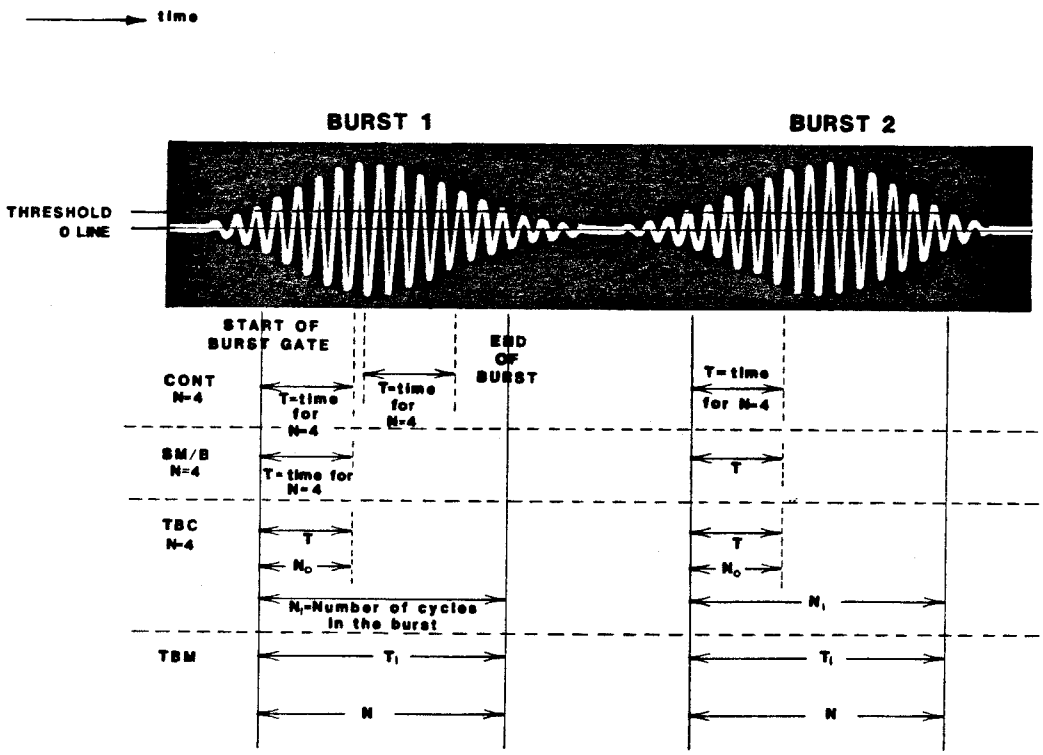

Figure 2-2. Laser-Doppler bursts.

When making velocity measurements with this technique, it is desirable to count only bursts from particles whose centers have passed through the measurement volume. If this condition is met, then an absolute, rather than a relative, concentration measurement can be made. The measurement will also be more accurate, since then each particle will be counted only once. It was therefore necessary to develop a method for determining if the particle centers had passed through the measurement volume. Since the amplitude of the scattered signal from a particle will be less if the particle does not pass entirely through the measurement volume (and hence all of the scattered light does not reach the photodetector) as shown in Figure 2-3, then amplitude discrimination may be used to determine if a particle center has passed through the measurement volume. The amplitude of the signal also depends on the particle size, but for relatively uniform-sized particles as were used, this is not very important. Thus by requiring the amplitude of each burst to exceed a certain threshold value (see Figure 2-2), only signals from particles whose centers have passed through the measurement volume will be counted. The actual setting of the threshold must be determined empirically. This determination was made by adjusting the threshold until the measured particle concentration was approximately equal to the actual concentration of the suspension.

We have so far been assuming that the amplitude of the scattered signal from a given particle is independent of the lateral (y) position of the particle in the flow channel. This would not be true if the laser beam intersection diameter varied across the channel width. To demonstrate that this assumption is reasonable; the dimensions of the beam intersection region have been calculated (see Adrian, 1980, for example) and plotted relative to the flow channel walls in Figure 2-4. Here the envelope of the beam intersection is defined as the points where the beam intensity falls to e^{-2} of its maximum value. By making the beam intersection length much larger than the spacing between flow channel

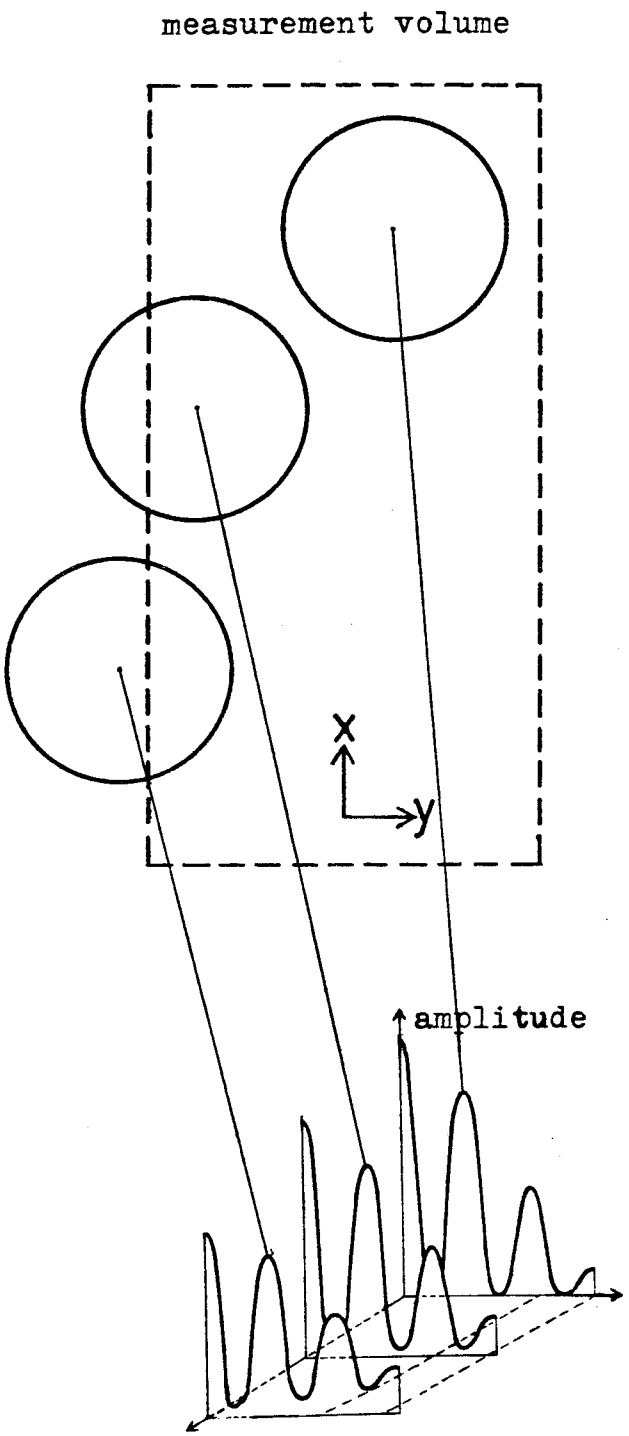

Figure 2-3. Dependence of amplitude of scattered signal upon particle position within measurement volume. Cross-section of measurement volume in x-y plane is shown.

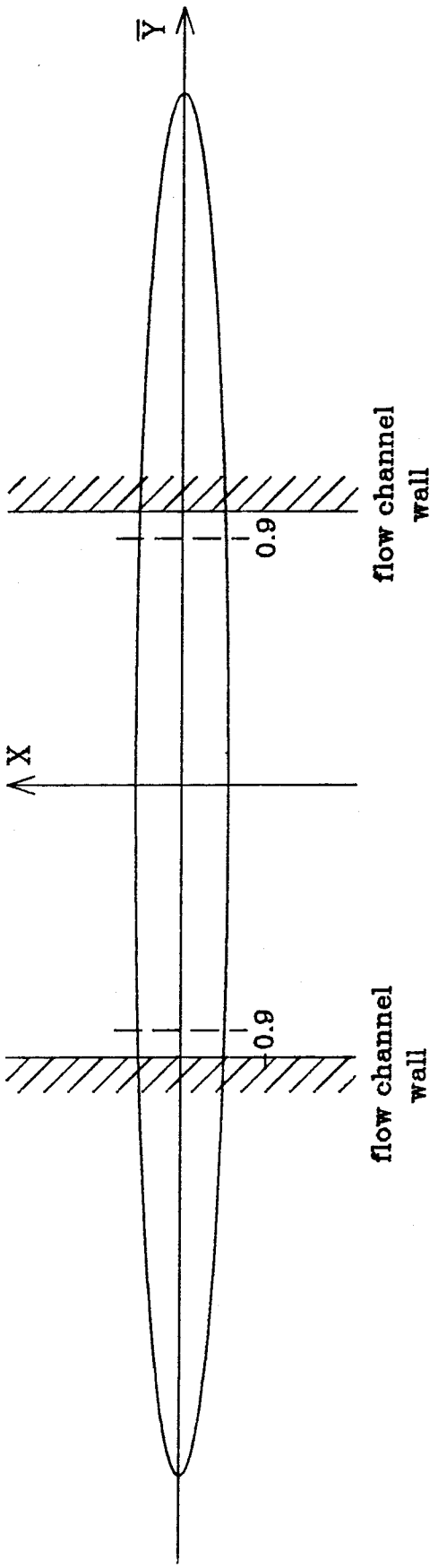

Figure 2-4. Beam intersection shape.

walls, measurements are made only in the central core of the beam intersection region, and thus the above assumption is valid.

Since they used a larger flow system, Lee and Srinivasan electronically discriminated against signals produced by particles outside the core of the measurement volume. The design of the present experimental system made such discrimination unnecessary, since the flow was physically restricted to the core of the measurement volume.

The concentration measurement method is as follows. If n bursts are counted over a period of time Δt , then the average number of particles $\langle N \rangle$ passing through the measurement volume per unit time is simply:

$$\langle N \rangle = \frac{n}{\Delta t} \quad . \tag{2.1}$$

Since the number of particles passing through a given point y will be proportional to the local velocity U(y) at that point, the local time-averaged concentration $\langle \Phi(y) \rangle$ is given by:

$$\langle \Phi(y) \rangle = \frac{\langle N(y) \rangle}{U(y)} \quad . \tag{2.2}$$

As indicated in Chapter 1, the above method has a serious limitation when used in a suspension. Its use is limited to suspension concentrations that are sufficiently low that the probability of having more than one particle in the measurement volume at a given time is small. This condition is necessary because, using this method, it is difficult to determine the number of particles in the measurement volume, if there is more than one. This condition would seem to limit the method to relatively dilute suspensions. For example, for 27 micron diameter spheres in the present experimental system, the maximum concentration would be around 1%. However, in the present experiment this limitation was circumvented in the following way. A small concentration of tracer particles, which were identical to the bulk particles except that they had a

fluorescent dye attached to their surfaces, was introduced into the suspension. When these particles are in the measurement volume, they fluoresce at a wavelength which is different than the wavelength of the incident laser light. By placing an optical filter in front of the photodetector, the scattered light from the majority of the particles is thus blocked and only the fluorescent light from the tracer particles passes through. In effect, we make the concentrated suspension optically dilute. Since the concentration of the tracer particles can be set arbitrarily, the above condition, which now applies only to the tracer particles, can be satisfied for any bulk concentration. Thus, assuming that the tracer particles are representative of the rest of the suspension, concentration profiles can be measured in a concentrated suspension.

The maximum allowable concentration of tracer spheres was determined as follows: Assuming that the number of particles in the measurement volume at a given time is governed by a Poisson distribution, the probability that more than one particle was in the measurement volume was calculated for a given bulk concentration. For a bulk concentration $\Phi_m = 0.001$, this probability was calculated to be 0.5%. Thus the case of more than one particle in the measurement volume could be ignored, provided the tracer particle concentration was less than about 0.1% by volume.

2.2.3. ERRORS IN VELOCITY MEASUREMENT

Certain conditions can affect the accuracy of the velocity measurements, and these are discussed here. Namely, we consider the effect of concentration or velocity gradients within the measurement volume on the accuracy of the velocity measurements.

When calculating the average velocity $\langle U(y) \rangle$ it may be necessary to account for the effect of gradients in velocity or concentration in the measurement volume. If there is a velocity gradient in the measurement volume, then

the measured velocity will be biased upward, since more faster-moving particles will be counted than slower-moving particles. To correct for this bias when calculating <U> at low data rates, the individual velocity points were weighted by t_{Bi}, the time for each particle to traverse the measurement volume (TSI 1982):

$$<U> = \frac{\sum_{i=1}^{n} U_i t_{Bi}}{\sum_{i=1}^{n} t_{Bi}} \quad . \tag{2.3}$$

Since

$$U_i \approx f_{Vi} = \frac{C_i}{t_{Bi}} \quad , \tag{2.4}$$

where f_{Vi} is the measured Doppler frequency and C_i is the measured number of cycles for particle i, then substituting (2.4) into (2.3)

$$<U> \approx \bar{f}_v = \frac{\sum_{i=1}^{n} C_i}{\sum_{i=1}^{n} t_{Bi}} = \frac{\text{sum of cycles for n particles}}{\text{sum of transit times for n particles}} \quad . \tag{2.5}$$

The quantities C_i and t_{Bi} were directly measured by the signal processor.

For the present experiment, the effect of this correction was small, due to the small width of the measurement volume, and the absence of large velocity gradients.

Gradients in concentration within the measurement volume could also potentially affect <U>. To determine if the velocity profiles were affected, the velocity profiles were compared to the parabolic velocity profiles expected for a dilute suspension of particles. Concentration gradients usually did not affect

<U>, except in one instance. If there was a high concentration gradient near the wall, which was usually the case, the velocity measurements were affected. The resulting measured velocities were then too high, apparently as a result of the higher concentration of faster-moving particles in that region, relative to the slower-moving particles. There were more faster-moving particles in this region because both the concentration and velocity increased as the distance from the wall increased. This limited the minimum distance from the wall at which accurate velocity measurements could be made, since it was apparently not possible to correct for this bias. In order to correct for this bias it would be necessary to know the concentration gradient within the measurement volume, which was not measured. In such cases, the local concentration $<\Phi(y_i)>$ was calculated using a velocity value obtained by extrapolation from the remaining velocity points.

2.3. EXPERIMENTAL APPARATUS

2.3.1. LASER-DOPPLER SYSTEM

The experimental setup is illustrated schematically in Figure 2-5. The individual components are as follows: the laser was a Spectra Physics model 165-00 argon-ion laser, operated at the 488 nanometer wavelength with a power setting of 0.4 watts; the basic LDA system was made by DISA (now Dantec) and consisted of a model 55L88 LDA transducer and photomultiplier (pm) tube, and a model 55L70 LDA control unit. The LDA transducer split the laser beam into two beams spaced 4 cm. apart. These beams were then passed through a focusing lens with a 30 cm. focal length, producing a beam intersection half-angle of 3.81 degrees. This produced a measurement volume 2000 microns long and 133 microns wide at the e^{-2} points. The frequency counter was a TSI model 1980B, which included a model 1998 data interface module. The velocity and concentration data were transmitted digitally through this interface to a Digital Equipment Corporation

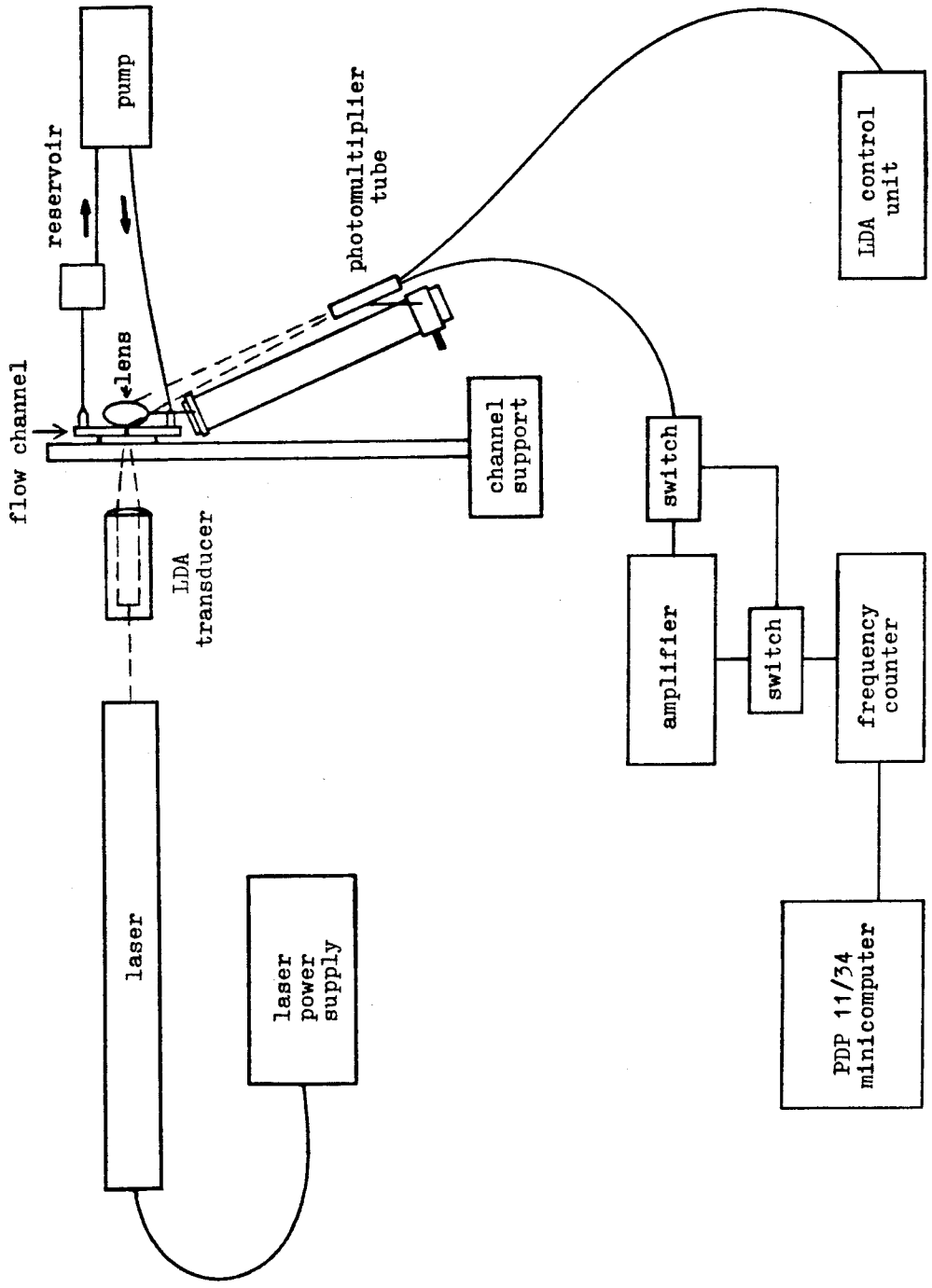

Figure 2-5. Experimental system.

(DEC) PDP 11/34 minicomputer, using a DEC DR11-W direct-memory access board. A Hewlett-Packard HP 461A ac amplifier was used to amplify the signal from the fluorescent particles before processing. The magnifying lens was a Nikon 50 mm. f/2.8 photographic enlarger lens. The f/8 aperture of the lens was used. The slit mounted on the front of the pm tube was 0.28 mm. wide by 8.6 mm. high. The slit/pm tube combination was mounted on a precision positioning device, which allowed placement of the slit/pm tube combination along the image of the measurement volume with an accuracy of at least 0.025 mm. The magnifying lens and pm tube were mounted on an optical rail made by the Los Angeles Scientific Instrument Company.

2.3.2. FLOW SYSTEM

The flow channel is drawn to scale in Figure 2-6. The channel itself consisted of two 0.64 cm.×2.51 cm.×30.3 cm. pieces of optically ground and polished plate glass with a magnesium fluoride anti-reflection coating, which were made by Oriel corporation. The anti-reflection coating reduced the reflectivity to about 1.5% per surface. The refractive index of the glass was 1.52. The glass plates were glued together at the edges with epoxy. The spacing between the glass plates was 0.0789 cm. The identical entry and exit sections were machined from Lucite blocks. The flow channel was mounted on a metal bracket, which was attached to a device that could position the flow channel accurately in the x, y, or z directions. Measurements at different downstream positions were therefore made by moving the flow channel, rather than the optics. Moving the optics would have been impractical due to the time-consuming realignment required. The pump used was a Harvard Apparatus model 951 infusion-withdrawal pump, which maintained a (nearly) continuous flow of suspension through the closed-loop flow system. Fifty $cm.^3$ capacity syringes were used in the pump. The four fastest flow rates produced by the pump were used:

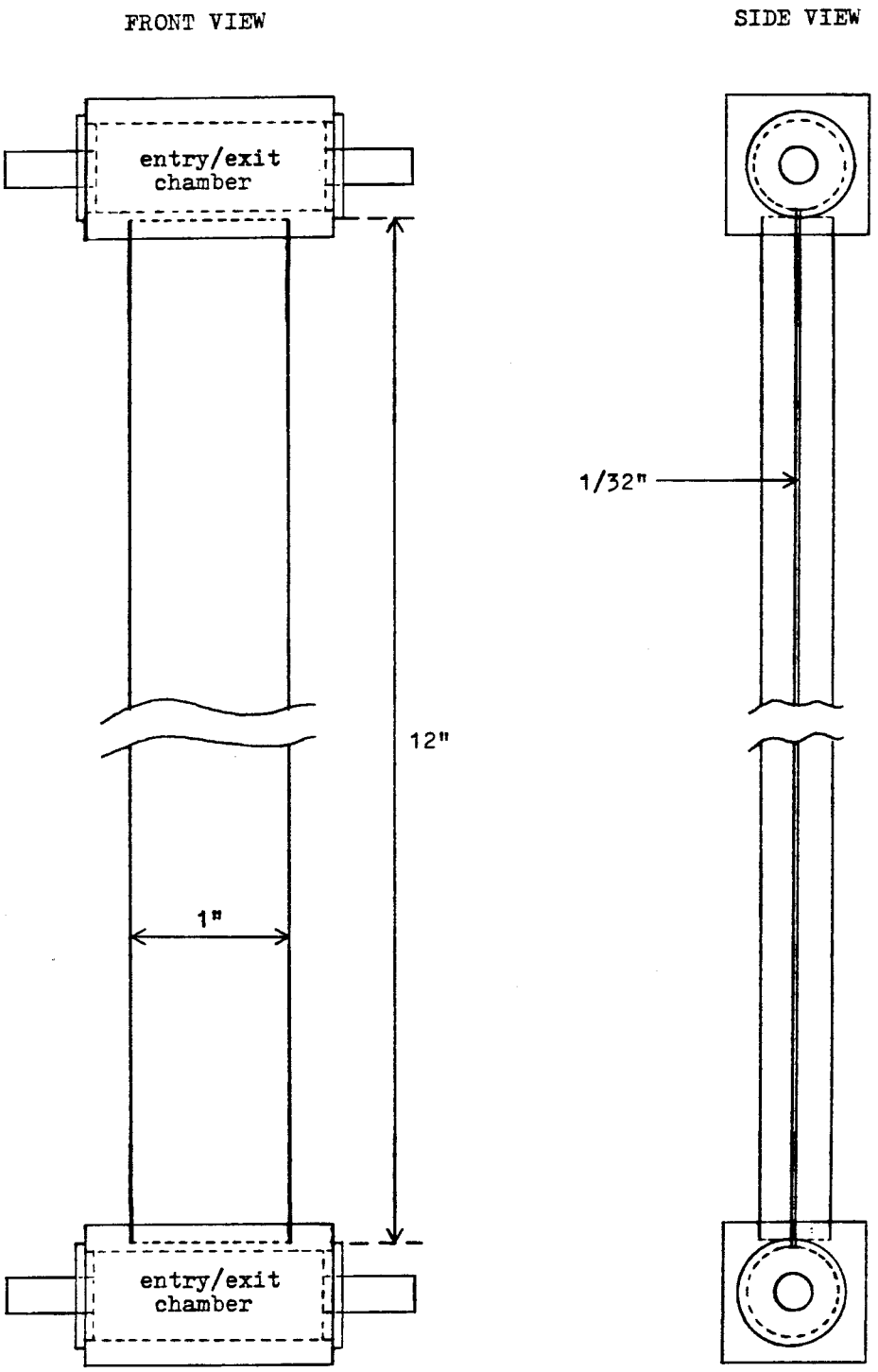

Figure 2-6. Flow channel.

0.192 $cm.^3$ $sec.^{-1}$, 0.382 $cm.^3$ $sec.^{-1}$, 0.765 $cm.^3$ $sec.^{-1}$, and 1.90 $cm.^3$ $sec.^{-1}$. The flow system was filled through the reservoir, which was constantly stirred during the experiments with an electric stirrer.

The hydrodynamic entrance length of the flow channel L_e, defined as the distance downstream of the channel entry where the centerline velocity reaches 99% of its fully developed value, was calculated using the result of Schlichting (1955) for parallel plates. L_e/d was always less than 0.4 for the fluids used.

2.3.3. SUSPENSIONS

The particles used in the suspensions were polystyrene-divinylbenzene copolymer spheres with mean diameters and standard deviations of 26.7±4.4 μm, 50.1±8.7 μm, and 70±7 μm. Polystryene spheres were used because of their availability, their ability to be dyed wth a fluorescent dye, and because their density was close to that of water and other fluids. The mean sizes and standard deviations of the 27 and 50 μm particles were measured with a Coulter Counter. For the 70 μm particles, the supplier's (Particle Information Services) data is shown. Figures 2-7 to 2-9 contain photographs of the spheres taken with a phase contrast microscope. The density of the particles was about 1.052 $g./cm.^{-3}$ (The density varied very slightly with particle size). Three liquid mixtures were used: a glycerine-water mixture with a viscosity μ_0=2.0 centipoise, and a refractive index n_D^{20}=1.3613, a triethylene glycol-1,2-propanediol-water mixture with μ_0=19.4 and n_D^{20}=1.4222, and a triethylene glycol-1,2-propanediol mixture with μ_0=48.6 and n_D^{20}=1.4355. The densities of these liquids were matched to the average particle densities by adjusting the composition of the liquid mixtures. The initial composition of the liquid mixtures was calculated using the densities of the pure liquids, then the density of the mixture was adjusted by trial and error until the spheres were neutrally buoyant (i.e., until the particles neither settled out nor rose to the top over a

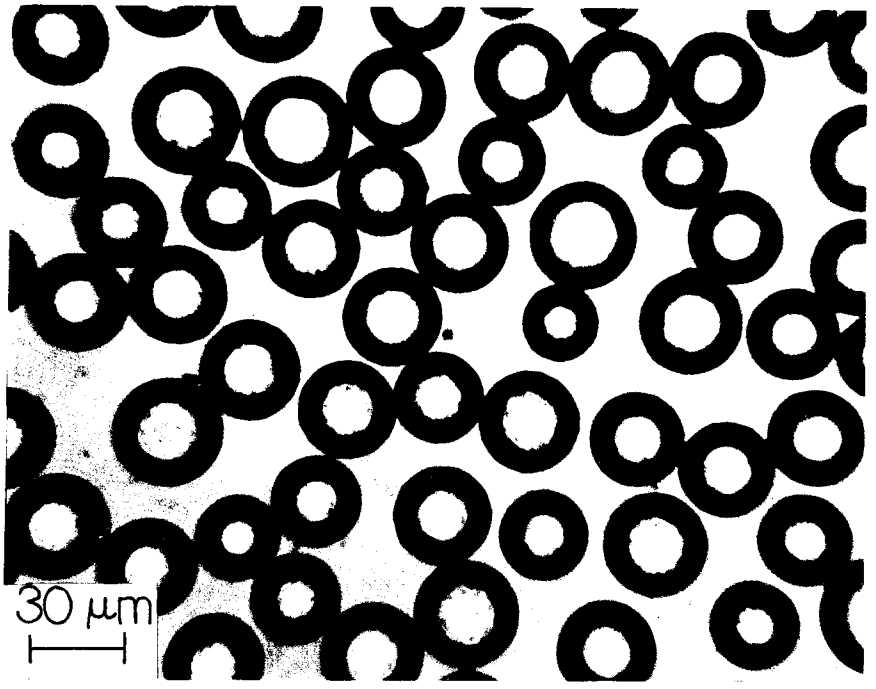

Figure 2-7. Photomicrograph of 27 micron diameter spheres.

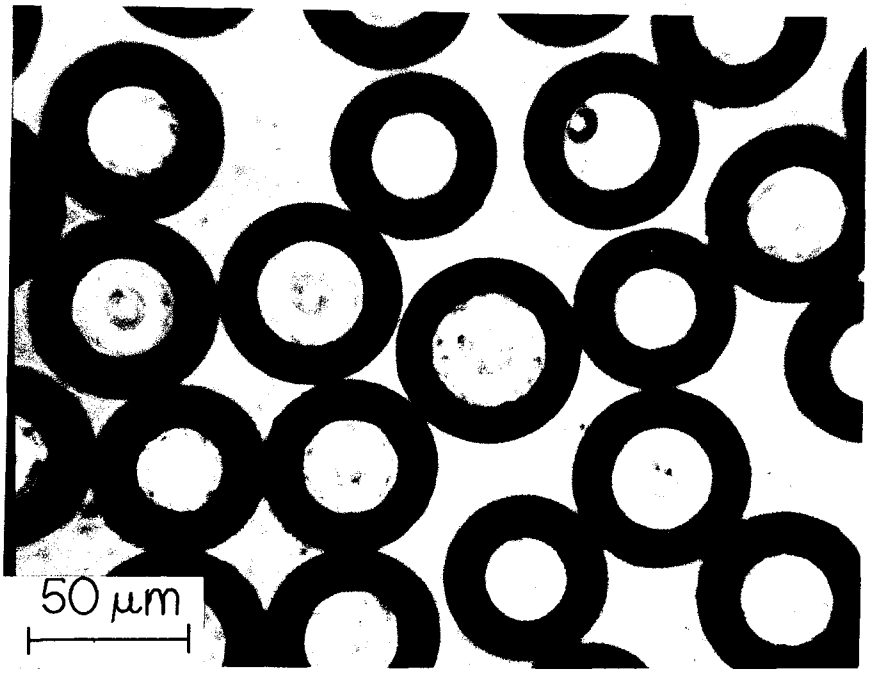

Figure 2-8. Photomicrograph of 50 micron diameter spheres.

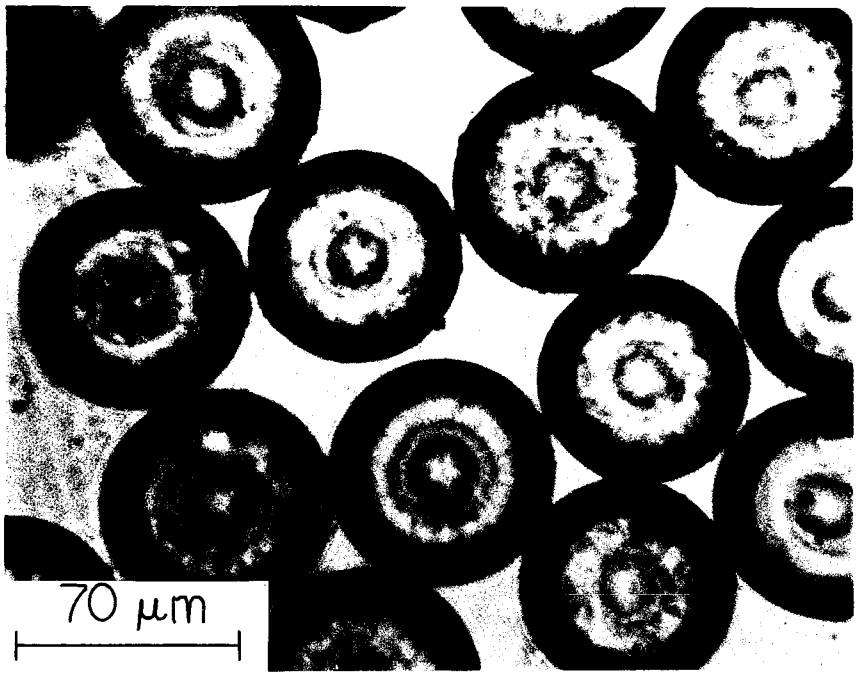

Figure 2-9. Photomicrograph of 70 micron diameter spheres.

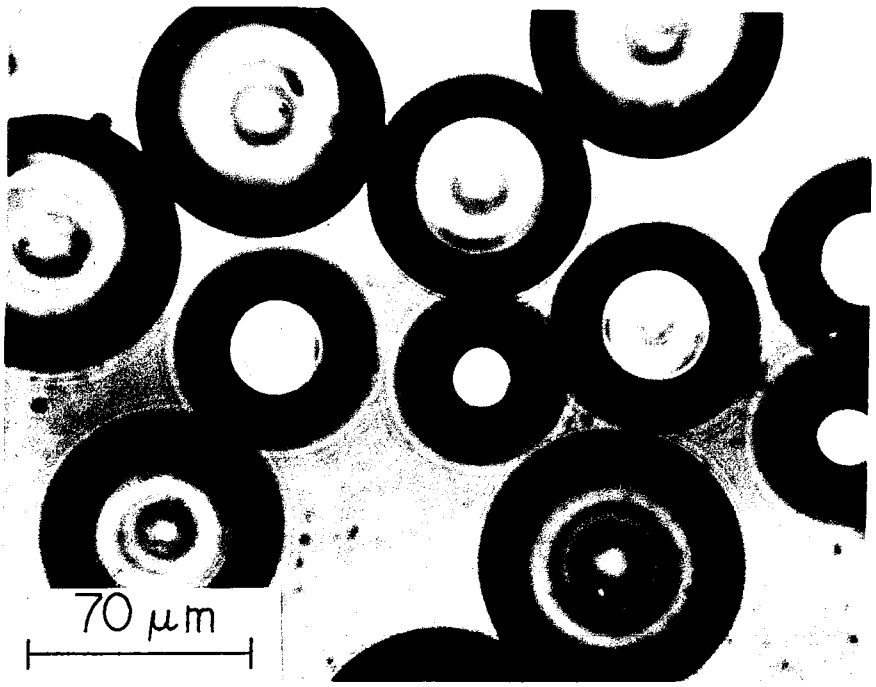

Figure 3-4. Photomicrograph of 70 micron diameter spheres used in concentrated-suspension experiments.

period of days). All of the fluids used were transparent.

The fluorescent dye was Rhodamine-6G. A number of other fluorescent dyes were tried, including Fluorescein and Rhodamine B. Rhodamine-6G was found to give the strongest signal. The procedure used to dye the particles, which was based on a procedure obtained from Dow Diagnostics, was as follows:

1. Dissolve about 1 gram of Rhodamine-6G in 50 ml. of pyridine with a few ml. of methanol added. Do this in a fume hood.
2. Add about 4 grams of dry copolymer spheres to the dye solution.
3. Stir gently at room temperature overnight.
4. Remove the solvent and excess dye by filtration on a fritted-glass funnel. Do not wash the particles with more solvent.
5. Place the dyed copolymer spheres in a vacuum dessicator and apply a vacuum for 4 hours (dry-ice trap) in order to remove residual solvent.
6. Suspend the particles in a Triton X-100/water mixture (.05 g./200 g.) and stir for 3 hours.
7. Filter off the Triton X-100 mixture on a fritted-glass funnel.
8. Repeat steps 6 and 7 until the dye in the aqueous phase is reduced to an acceptable level. The particles are now ready to use.

The fluorescent dye did not dissolve appreciably in the fluids used when attached to the spheres using the above procedure.

Figure 2-10 shows size distributions measured for the undyed and dyed 27 μm spheres as measured by the Coulter Counter. The size distributions of the dyed and undyed spheres are very similar, within the accuracy of the measurement technique.

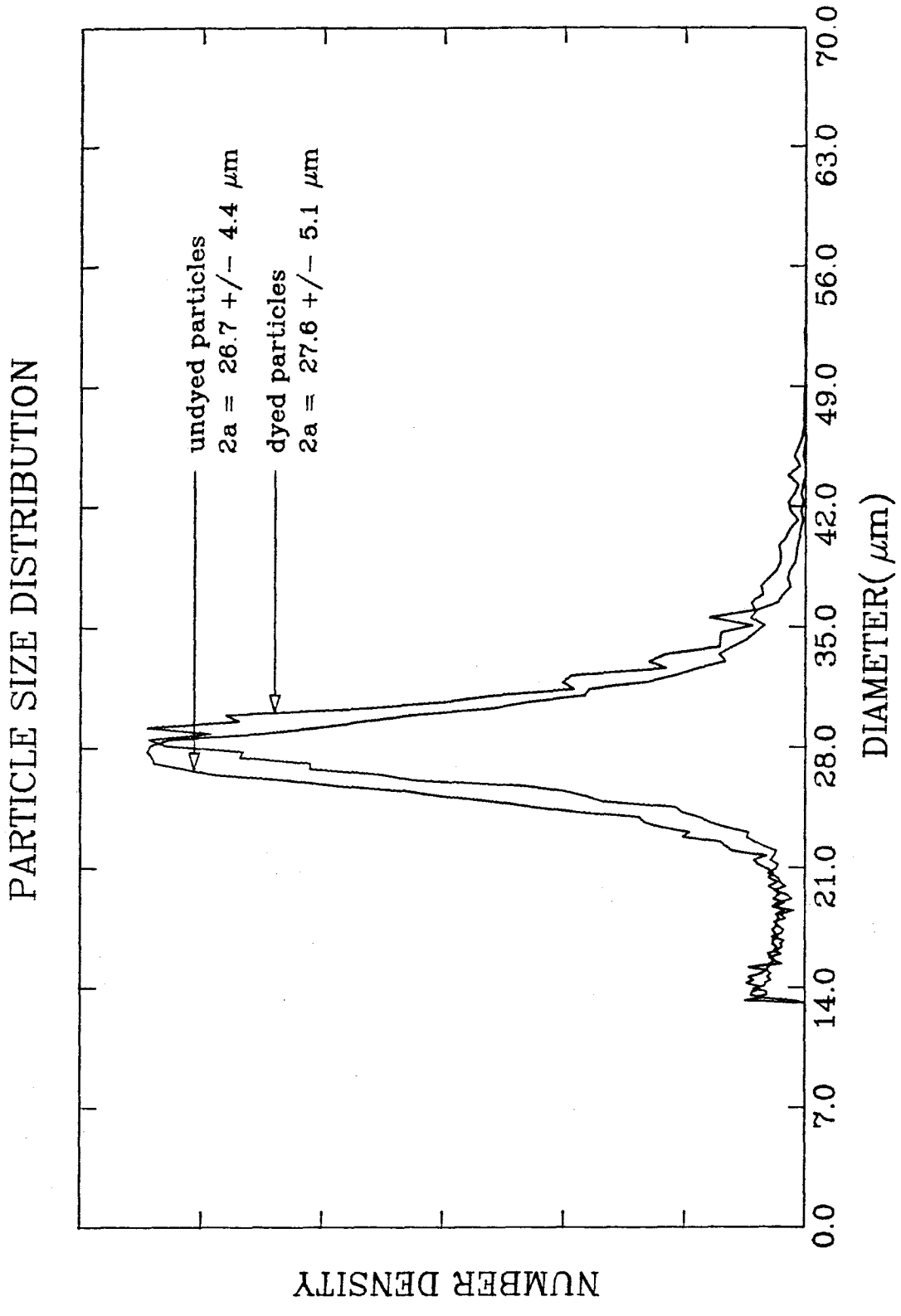
PARTICLE SIZE DISTRIBUTION
undyed particles
2a = 26.7 +/- 4.4 μm
dyed particles
2a = 27.6 +/- 5.1 μm
NUMBER DENSITY
DIAMETER(μm)
0.0
7.0
14.0
21.0
28.0
35.0
42.0
49.0
56.0
63.0
70.0

Figure 2-10.

2.3.4. DATA COLLECTION PROCEDURE

The data collection procedure was as follows: The flow system was filled with 160-165 ml. of the fluid, and 0.15-0.2 g. of dyed spheres were added, giving a mean volume fraction of dyed spheres $\Phi_m \approx 0.001$. The suspension was circulated continuously through the flow system. The slit/pm tube combination was placed at one end of the measurement volume image, i.e., near one wall. At each position the velocity was first measured using the "regular" scattered signal (488 nanometer wavelength) from the spheres. (Initially, it was intended to use the fluorescent signal for velocity measurements. It was not possible to obtain a sufficiently good signal to noise ratio with this signal to make velocity measurements, however.) The signals were required to have at least 8 cycles above the threshold value in order to be measured. Since the frequency counter was used in the "total burst mode" (TBM in Figure 2-2), the number of cycles measured per particle varied somewhat. In the total burst mode, the number of cycles C_i above the threshold and the time period per burst t_{Bi} were measured. The number of individual data points desired (n), usually 100 to 250, was input to a computer program. The computer then obtained the required number of data points from the frequency counter and calculated an average velocity and the standard deviation of the individual velocity data points for each position y_i.

The concentration was then measured by placing the optical filter, a Wratten number 12 photographic gelatin filter, in front of the pm tube and amplifying the signal 20 dB before it was input to the frequency counter. These signals were also required to have at least 8 cycles above the threshold value in order to be measured. The time for a given number of particles, usually 1000 to 2000, to pass through the measurement volume was measured using the computer program. The concentration at that point was then calculated using $\langle N(y_i) \rangle$ and $\langle U(y_i) \rangle$. Afterward, the slit was moved and the process was

repeated for each data point, until the opposite side of the image was reached. Two to three hours were typically needed to measure both the velocity and concentration profiles.

After the last point was measured, the slit was moved back to the opposite side of the image and the first velocity point was re-measured. This was necessary to check for drifting of the measurement volume image due to any slight changes in the positions of the optics or the flow channel. If the image had drifted substantially, the data was rejected and the experiment was re-done. It was found that small temperature fluctuations in the laboratory, even a few tenths of a degree, could cause significant changes in optical alignment. When the laboratory temperature control system was functioning properly, however, acceptable results were usually obtained. The experiments were done at 21.0 degrees centigrade.

2.4. EXPERIMENTAL RESULTS AND DISCUSSION

Table 2-1 is a list of all experiments that were done in the dilute concentration regime (Φ_m=0.001), along with the conditions for each experiment. Here μ_0 is the suspending fluid viscosity in centipoise, a is the mean sphere radius, U_B is the measured bulk velocity of the suspension, X is the distance downstream of the inlet where each measurement was made, ρ_0 is the fluid (and sphere) density, and d is the spacing between channel walls. Re_p is defined as follows:

$$Re_p = \frac{U_{max}\, a\, \rho_0\, a}{\mu_0 \quad d} \quad , \tag{2.6}$$

where U_{max} is the maximum (centerline) velocity of the susension. Data sets 1-6 are for high viscosity fluids, corresponding to low particle Reynolds numbers (Re_p). The remaining data sets are for low viscosity liquids, corresponding to higher Re_p, and hence significant inertial forces.

Table 2-1

Number	μ_0 (cp.)	2a (cm.×10^4)	U_B (cm./sec.)	X (cm.)	Flow Direction	Re_p
1	19.4	27	1.93	1.0	down	0.00036
2	19.4	27	1.93	15.2	down	0.00036
3	19.4	27	1.93	15.2	up	0.00036
4	19.4	27	3.85	15.2	up	0.00072
5	48.6	50.	1.93	1.0	down	0.00050
6	48.6	70.	1.93	29.5	up	0.00097
7	2.0	27	0.95	15.2	down	0.0017
8	2.0	27	0.95	15.2	up	0.0017
9	2.0	27	1.93	1.0	down	0.0035
10	2.0	27	1.93	15.2	down	0.0035
11	2.0	27	1.93	15.2	up	0.0035
12	2.0	27	1.93	29.5	up	0.0035
13	2.0	27	3.85	15.2	down	0.0069
14	2.0	27	3.85	15.2	up	0.0069
15	2.0	27	9.68	1.0	down	0.018
16	2.0	27	9.68	15.2	down	0.018
17	2.0	27	9.68	15.2	up	0.018
18	2.0	27	9.68	29.5	up	0.018
19	2.0	50	0.95	15.2	down	0.0059
20	2.0	50	0.95	15.2	up	0.0059
21	2.0	50	1.93	1.0	down	0.012
22	2.0	50	1.93	15.2	down	0.012
23	2.0	50	1.93	15.2	up	0.012
24	2.0	50	1.93	29.5	up	0.012
25	2.0	50	3.85	15.2	down	0.024
26	2.0	50	3.85	15.2	up	0.024
27	2.0	50	9.68	1.0	down	0.060
28	2.0	50	9.68	15.2	down	0.060
29	2.0	50	9.68	15.2	up	0.060
30	2.0	50	9.68	29.5	up	0.060
31	2.0	70	1.93	1.0	down	0.024
32	2.0	70	1.93	29.5	up	0.024
33	2.0	70	3.85	1.0	down	0.047
34	2.0	70	3.85	17.5	up	0.047
35	2.0	70	3.85	29.5	up	0.047
36	2.0	70	9.68	1.0	down	0.12
37	2.0	70	9.68	10.0	down	0.12
38	2.0	70	9.68	13.0	down	0.12
39	2.0	70	9.68	20.5	up	0.12
40	2.0	70	9.68	29.5	up	0.12

Figure 2-11 is a plot of velocity ($\overline{U}$) and concentration ($\overline{\Phi}$) profiles for data set 4. The velocity points (crosses) are plotted along with a polynomial curve-fit (solid line). A parabolic velocity profile (dashed line) is presented for

VELOCITY AND CONCENTRATION PROFILES

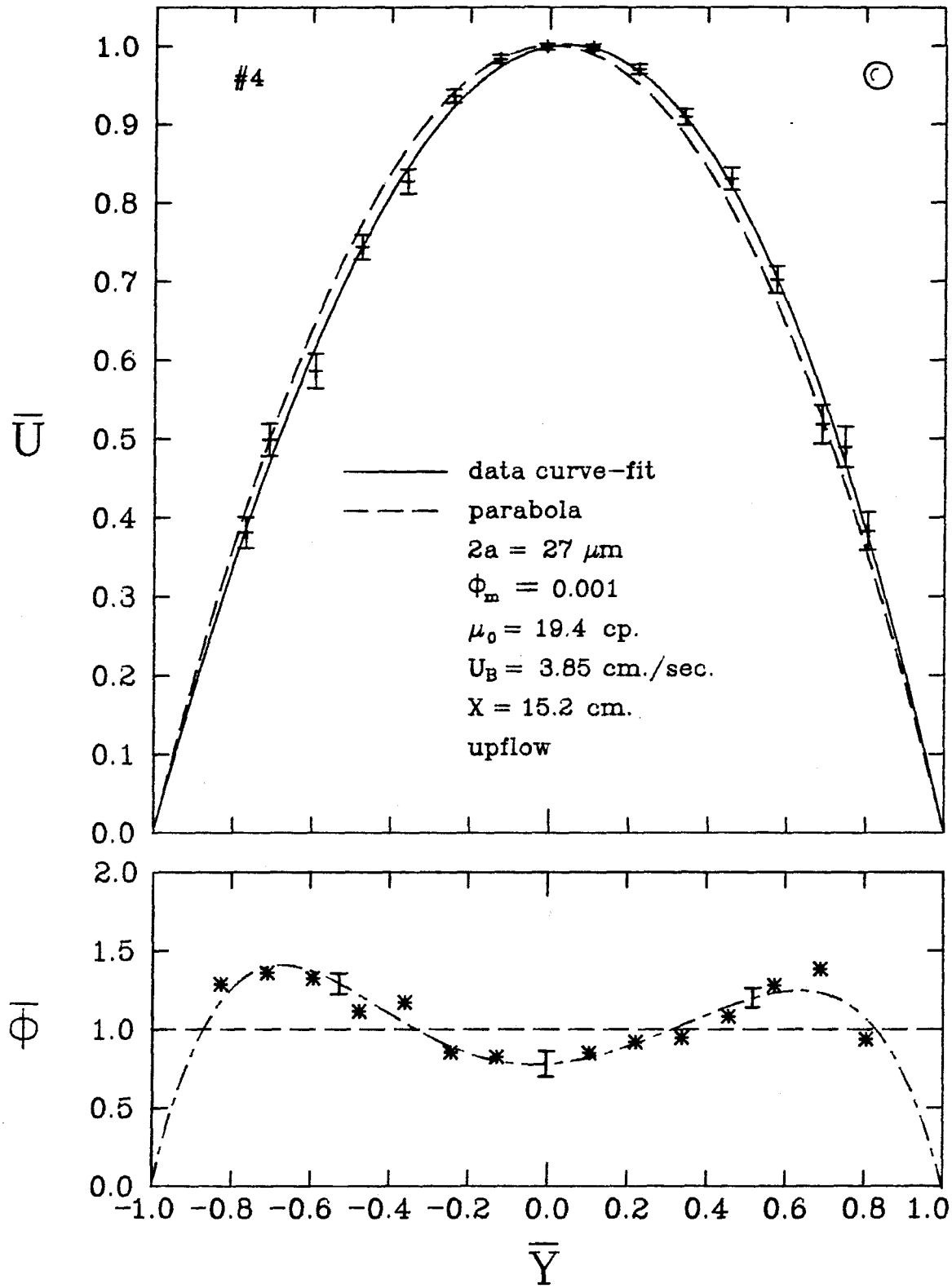

Figure 2-11.

comparison. The parabolic velocity profile was determined from U_B. The measured velocity profile was normalized by making the area under it equal to the area under the parabolic profile. The normalized concentration $\bar{\Phi}$ is defined as follows:

$$\bar{\Phi} = \frac{<\Phi(y_i)>}{\Phi_m} \quad . \tag{2.7}$$

The concentration data points, along with a polynomial curve-fit, are also shown. The normalized position coordinate $\bar{Y}$ is defined as:

$$\bar{Y} = \frac{y}{(d/2)} \quad . \tag{2.8}$$

The error bars on the velocity data points represent 95% confidence limits (assuming the data are normally distributed) calculated as follows (Perry, 1973):

$$\text{error bar length} = \frac{1.96\sigma}{\sqrt{n}} \quad , \tag{2.9}$$

where

$$\sigma = \left[\frac{\sum_{i=1}^{n} (U_i - \bar{U})^2}{(n-1)} \right]^{1/2} \quad . \tag{2.10}$$

Error bars were also calculated for the concentration data of data set 4 for three positions in the channel. Since it is not possible to make a concentration measurement from a single particle, the error bars for the concentration data were calculated in a slightly different manner than for the velocity data. In a separate experiment, the concentrations at $\bar{Y} \approx -0.55$, $\bar{Y} \approx 0.0$, and $\bar{Y} \approx 0.55$ were measured five times at each position (5 measurements of 1000 points each). The error bars at each position were then calculated as for the velocity data, using these five points. Due to the excessive time required for these measure-

ments, they were only carried out for one data set for the dilute suspensions. The error bars provide some guidance as to the extent of the concentration error in other experiments, however.

The circle in the upper right-hand corner of the figure indicates the size of the sphere relative to the channel spacing.

From the figure it is evident that the measured velocity profile is very close to the parabolic velocity profile that would be expected for a dilute suspension. The slight skewness is probably due to experimental scatter of the velocity points, particularly at low velocities. All of the dilute suspension velocity profiles were parabolic within experimental error, and hence will not be discussed further.

In order to make measurements as a function of downstream position, it was usually convenient to simply change the flow direction from upward to downward to effectively change the downstream position, rather than moving the flow channel. For example, if the channel was positioned relative to the laser so that a measurement was made near the inlet of the channel and the flow was downward, a measurement far downstream could be obtained by simply reversing the flow direction without moving the flow channel. This procedure should produce the same result as making a measurement at the other end of the channel, since the particles were neutrally buoyant and the channel was symmetric relative to its midpoint. Nevertheless, a check was performed on this assumption, by measuring concentration profiles as a function of U_B at the midpoint of the channel (15.2 cm. downstream) for upward and downward flows and comparing the results (Figures 2-12 to 2-14). The concentration profiles for upward and downward flows are very similar, within experimental error, thus confirming our assumption. The result may also be viewed as an indication that the spheres are in fact neutrally buoyant.

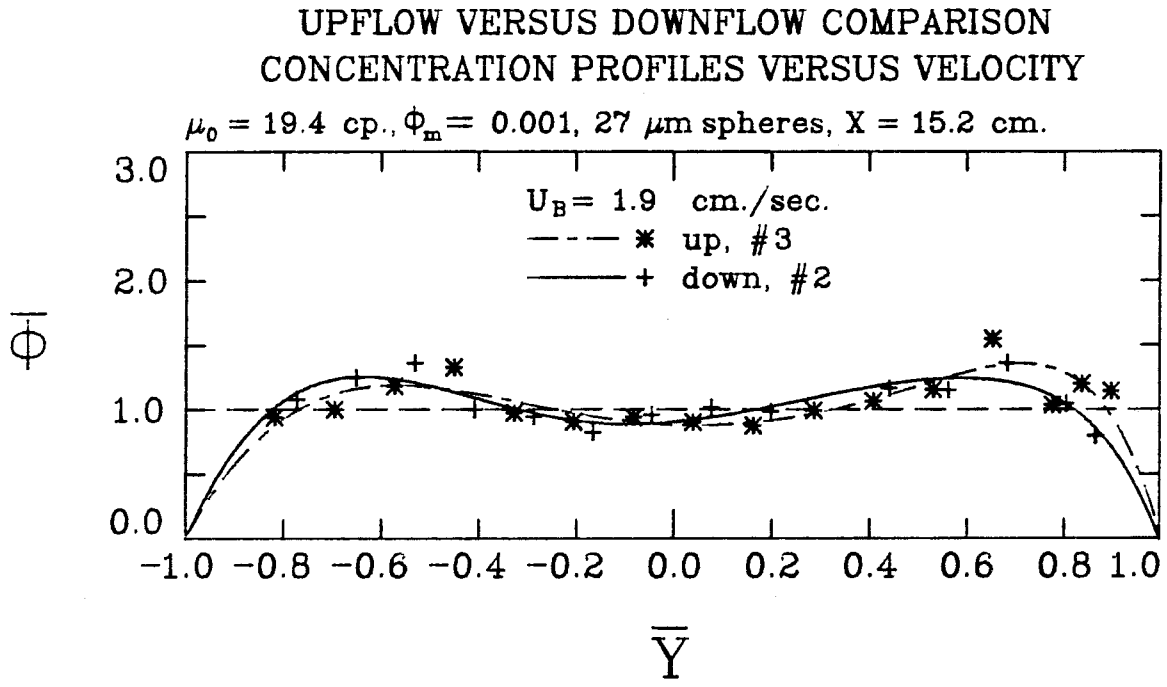
UPFLOW VERSUS DOWNFLOW COMPARISON
CONCENTRATION PROFILES VERSUS VELOCITY
μ_0 = 19.4 cp., Φ_m = 0.001, 27 μm spheres, X = 15.2 cm.
U_B = 1.9 cm./sec.
up, #3
down, #2
3.0
2.0
1.0
0.0
$\overline{\Phi}$
-1.0 -0.8 -0.6 -0.4 -0.2 0.0 0.2 0.4 0.6 0.8 1.0
$\overline{Y}$

Figure 2-12.

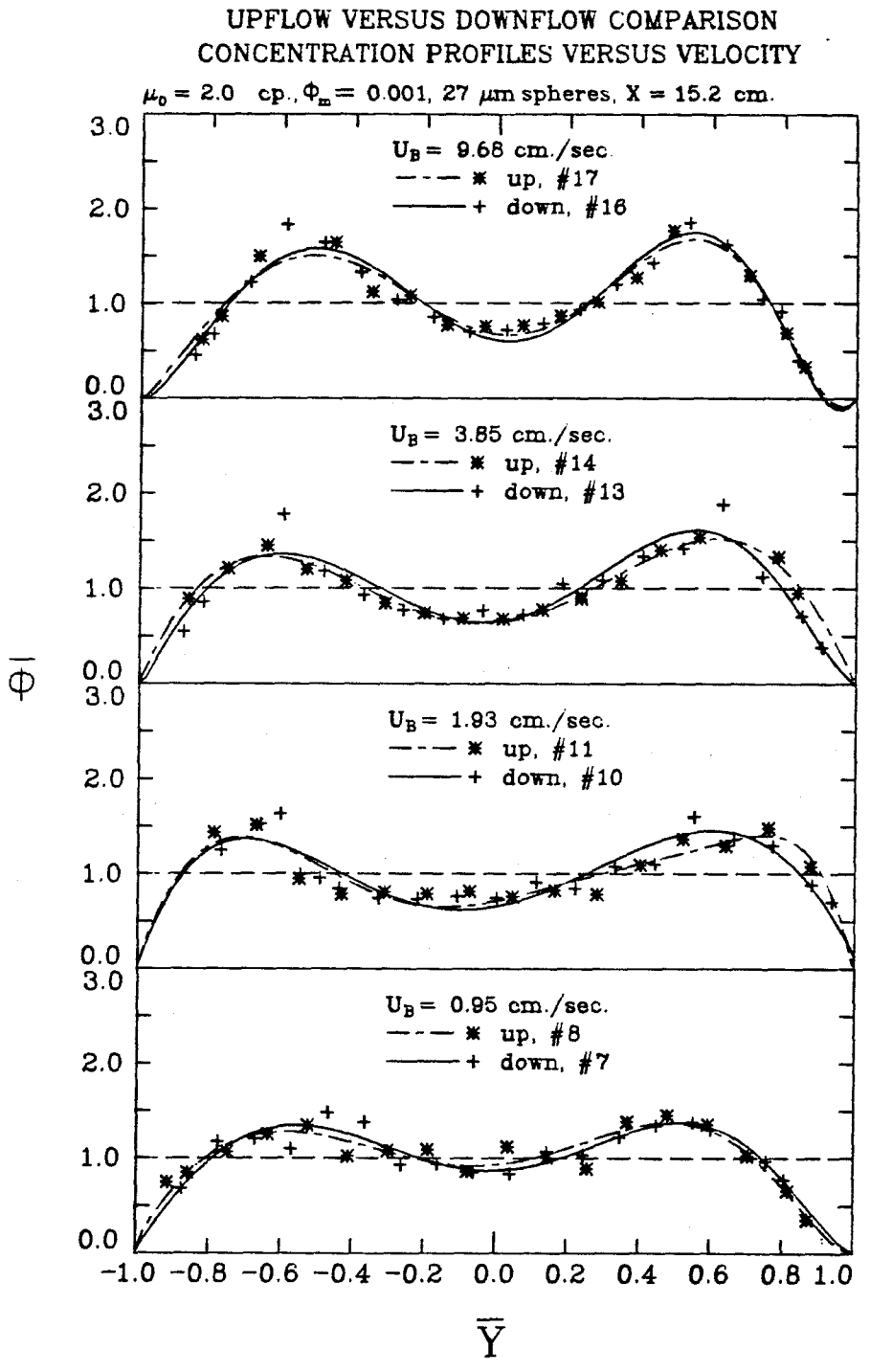
UPFLOW VERSUS DOWNFLOW COMPARISON
CONCENTRATION PROFILES VERSUS VELOCITY
μ_0 = 2.0 cp., Φ_m = 0.001, 27 μm spheres, X = 15.2 cm.
U_B = 9.68 cm./sec.
* up, #17
+ down, #16
U_B = 3.85 cm./sec.
* up, #14
+ down, #13
U_B = 1.93 cm./sec.
* up, #11
+ down, #10
U_B = 0.95 cm./sec.
* up, #8
+ down, #7
$\bar{\Phi}$
$\bar{Y}$
3.0
2.0
1.0
0.0
-1.0 -0.8 -0.6 -0.4 -0.2 0.0 0.2 0.4 0.6 0.8 1.0

Figure 2-13.

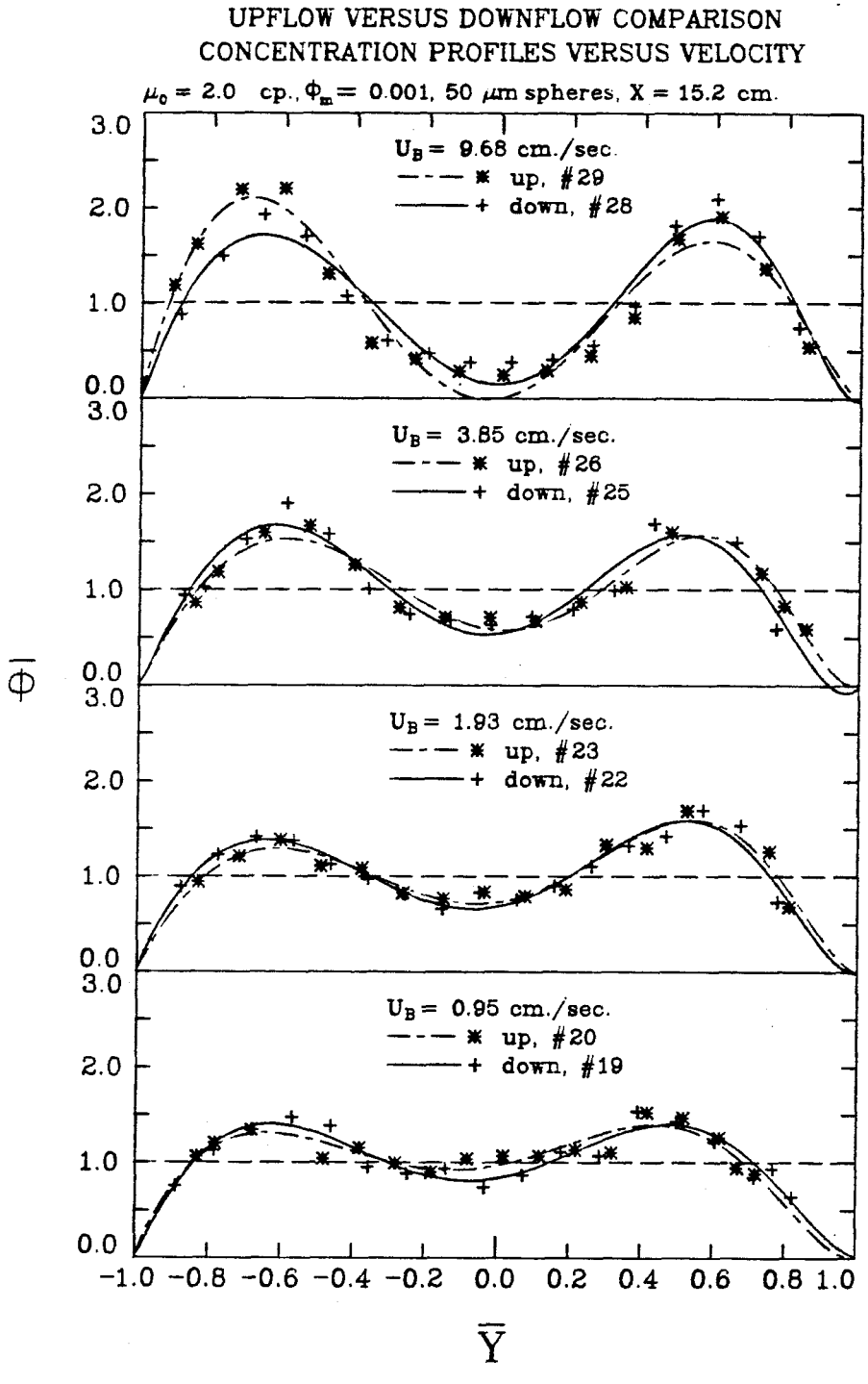
UPFLOW VERSUS DOWNFLOW COMPARISON
CONCENTRATION PROFILES VERSUS VELOCITY
μ_0 = 2.0 cp., Φ_m = 0.001, 50 μm spheres, X = 15.2 cm.
U_B = 9.68 cm./sec.
* up, #29
+ down, #28
U_B = 3.85 cm./sec.
* up, #26
+ down, #25
U_B = 1.93 cm./sec.
* up, #23
+ down, #22
U_B = 0.95 cm./sec.
* up, #20
+ down, #19
$\bar{\Phi}$
$\bar{Y}$
3.0
2.0
1.0
0.0
-1.0 -0.8 -0.6 -0.4 -0.2 0.0 0.2 0.4 0.6 0.8 1.0

Figure 2-14.

Let us now systematically discuss all of our results for dilute suspensions, beginning with the low Reynolds number data sets (1-6). For this regime, where inertial forces are unimportant (and hence no lateral migration is expected, see Bretherton, 1962), the concentration profiles should not vary with downstream position. This is shown to be true in Figure 2-15, which shows concentration profiles for 27 μm diameter spheres near the channel inlet (1.0 cm. downstream), and at the channel midpoint (15.2 cm. downstream).

Figure 2-16 shows concentration profiles as a function of sphere size for 27, 50, and 70 μm diameter particles. There is a small peak near the wall for the 27 μm particles, which becomes somewhat larger for the 50 and 70 μm diameter particles. Since inertial forces are negligible for these cases, these peaks cannot be caused by inward migration of particles. The only apparently reasonable explanation for such peaks would be an entrance effect. Maude and Yearn (1967) observed similar peaks for dilute suspensions of neutrally-buoyant spheres in tube flow. They attributed the formation of the peaks, at least in part, to the inward displacement of spheres on streamlines near the flow tube entry. That the entry geometry of a tube could cause such peaks in concentration near the wall was demonstrated theoretically by Bitbol and Quemada (1981). This seems to be a reasonable explanation for the present observations, except that given this explanation the "wall peak" should be farther from the wall for larger particles, which doesn't seem to be true. The spatial resolution of the concentration measurement technique may not be adequate to show this effect of particle size, however. The observed increase in peak height with increasing particle diameter would follow from this explanation, however.

The higher Re_p results will be discussed next. Figures 2-17 to 2-24 contain concentration profiles plotted versus downstream position for the three sphere sizes used, at three different bulk velocities. A few observations can be made

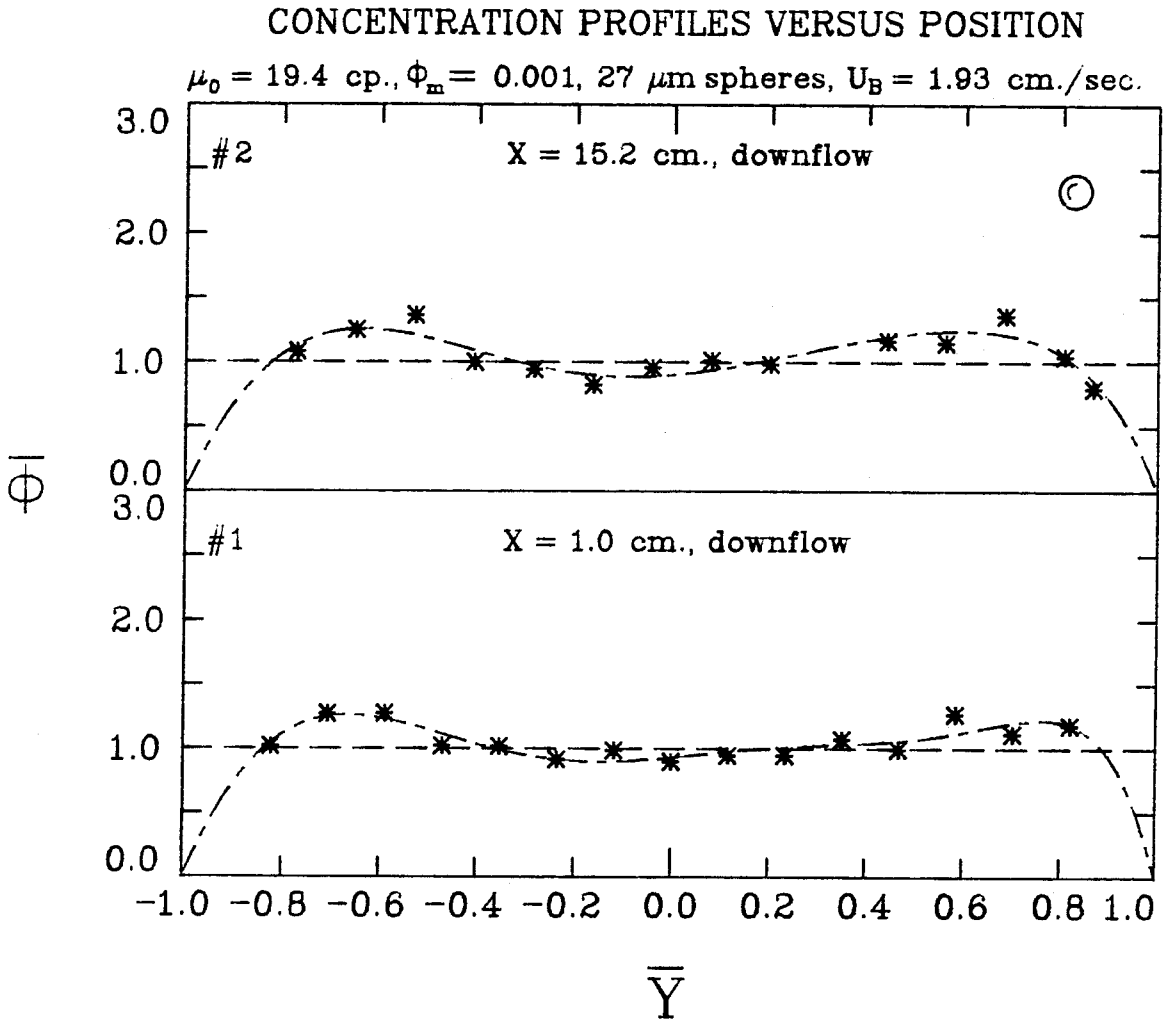
CONCENTRATION PROFILES VERSUS POSITION
μ_0 = 19.4 cp., Φ_m = 0.001, 27 μm spheres, U_B = 1.93 cm./sec.
#2
X = 15.2 cm., downflow
#1
X = 1.0 cm., downflow
3.0
2.0
1.0
0.0
$\overline{\Phi}$
-1.0 -0.8 -0.6 -0.4 -0.2 0.0 0.2 0.4 0.6 0.8 1.0
$\overline{Y}$

Figure 2-15.

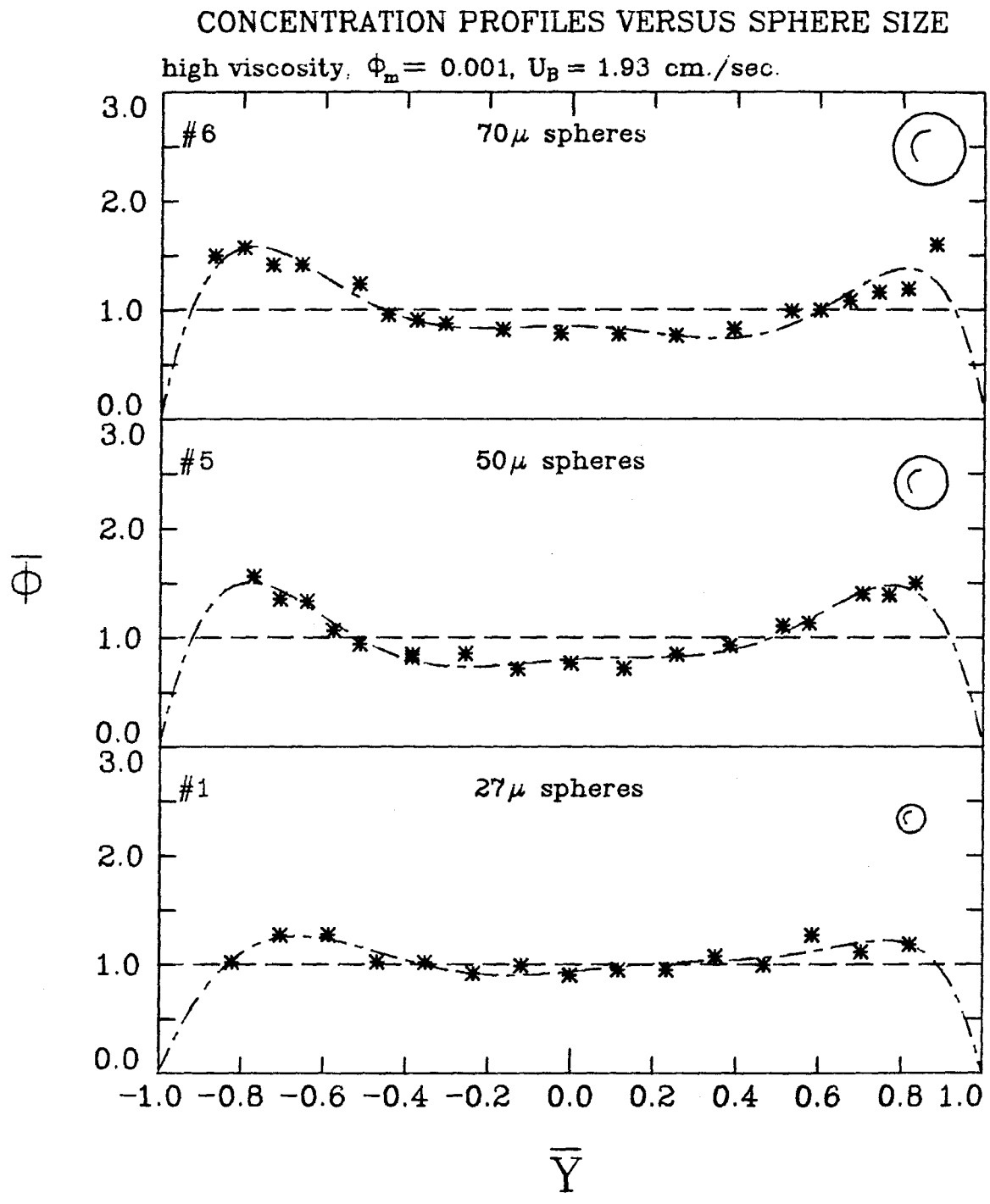
CONCENTRATION PROFILES VERSUS SPHERE SIZE
high viscosity, Φ_m = 0.001, U_B = 1.93 cm./sec.
#6
70μ spheres
#5
50μ spheres
#1
27μ spheres
3.0
2.0
1.0
0.0
$\overline{\Phi}$
−1.0 −0.8 −0.6 −0.4 −0.2 0.0 0.2 0.4 0.6 0.8 1.0
$\overline{Y}$

Figure 2-16.

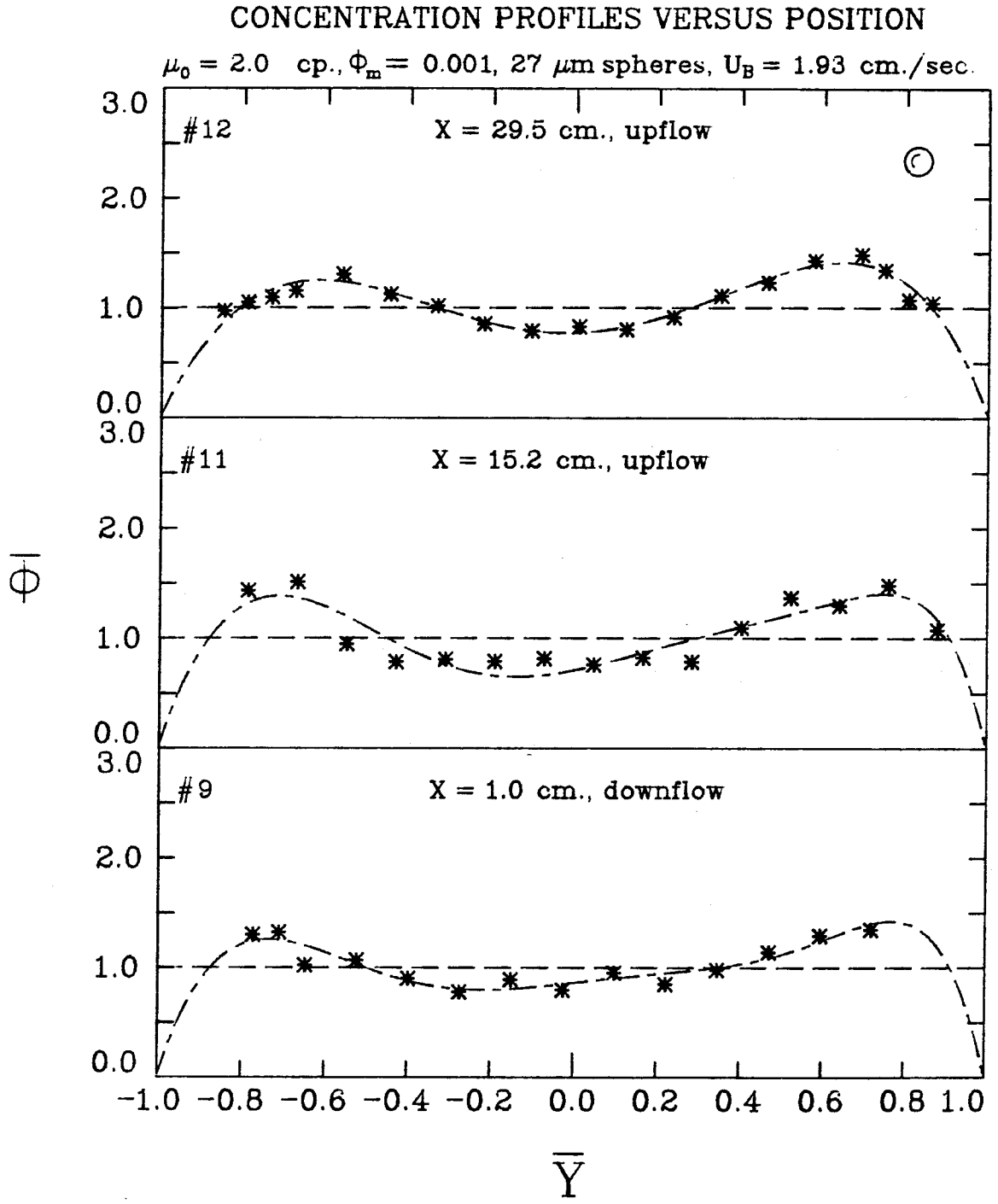
CONCENTRATION PROFILES VERSUS POSITION
μ_0 = 2.0 cp., Φ_m = 0.001, 27 μm spheres, U_B = 1.93 cm./sec.
#12
X = 29.5 cm., upflow
#11
X = 15.2 cm., upflow
#9
X = 1.0 cm., downflow
3.0
2.0
1.0
0.0
$\overline{\Phi}$
-1.0 -0.8 -0.6 -0.4 -0.2 0.0 0.2 0.4 0.6 0.8 1.0
$\overline{Y}$

Figure 2-17.

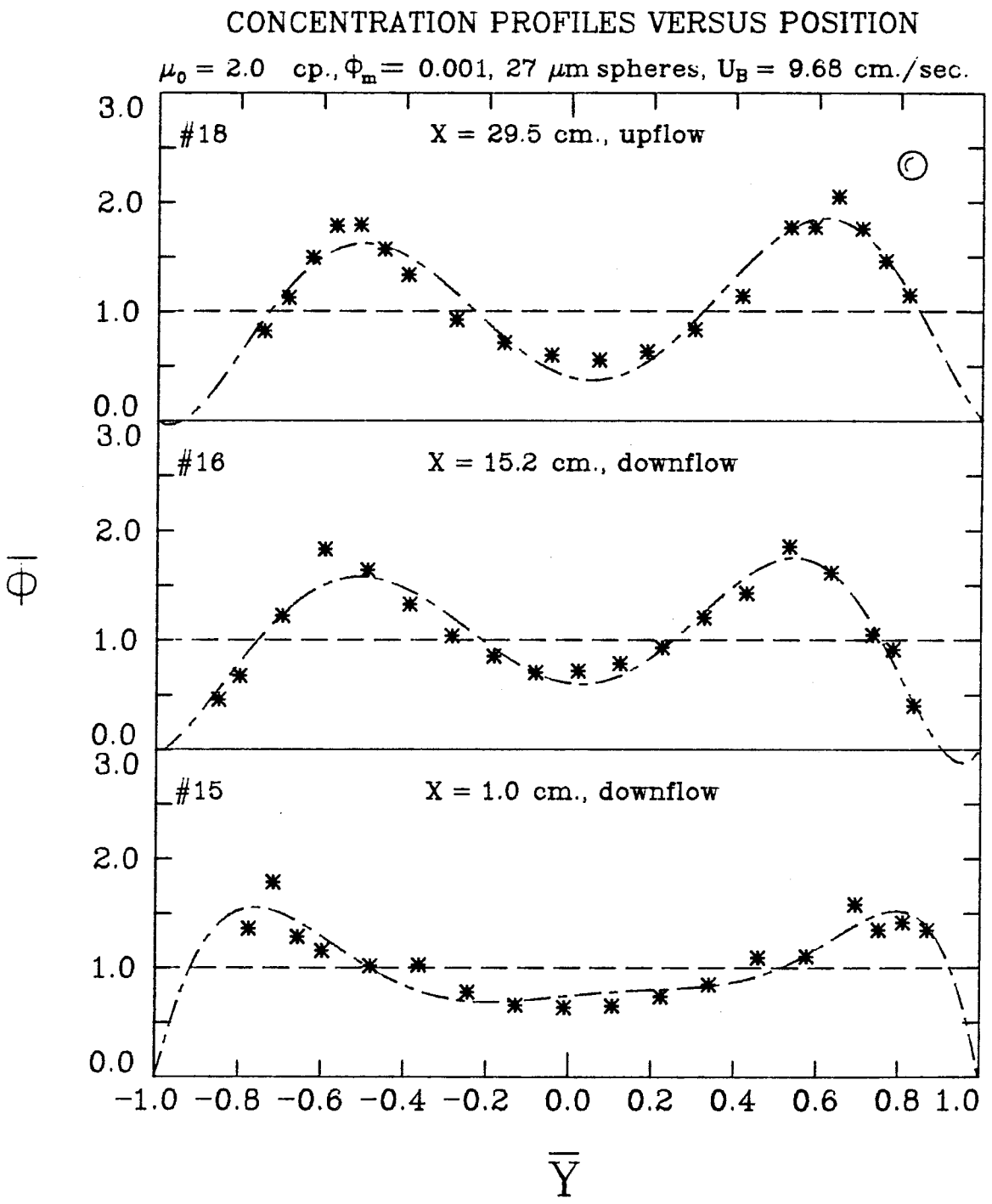
CONCENTRATION PROFILES VERSUS POSITION
μ_0 = 2.0 cp., Φ_m = 0.001, 27 μm spheres, U_B = 9.68 cm./sec.
#18
X = 29.5 cm., upflow
#16
X = 15.2 cm., downflow
#15
X = 1.0 cm., downflow
3.0
2.0
1.0
0.0
$\overline{\Phi}$
-1.0 -0.8 -0.6 -0.4 -0.2 0.0 0.2 0.4 0.6 0.8 1.0
$\overline{Y}$

Figure 2-18.

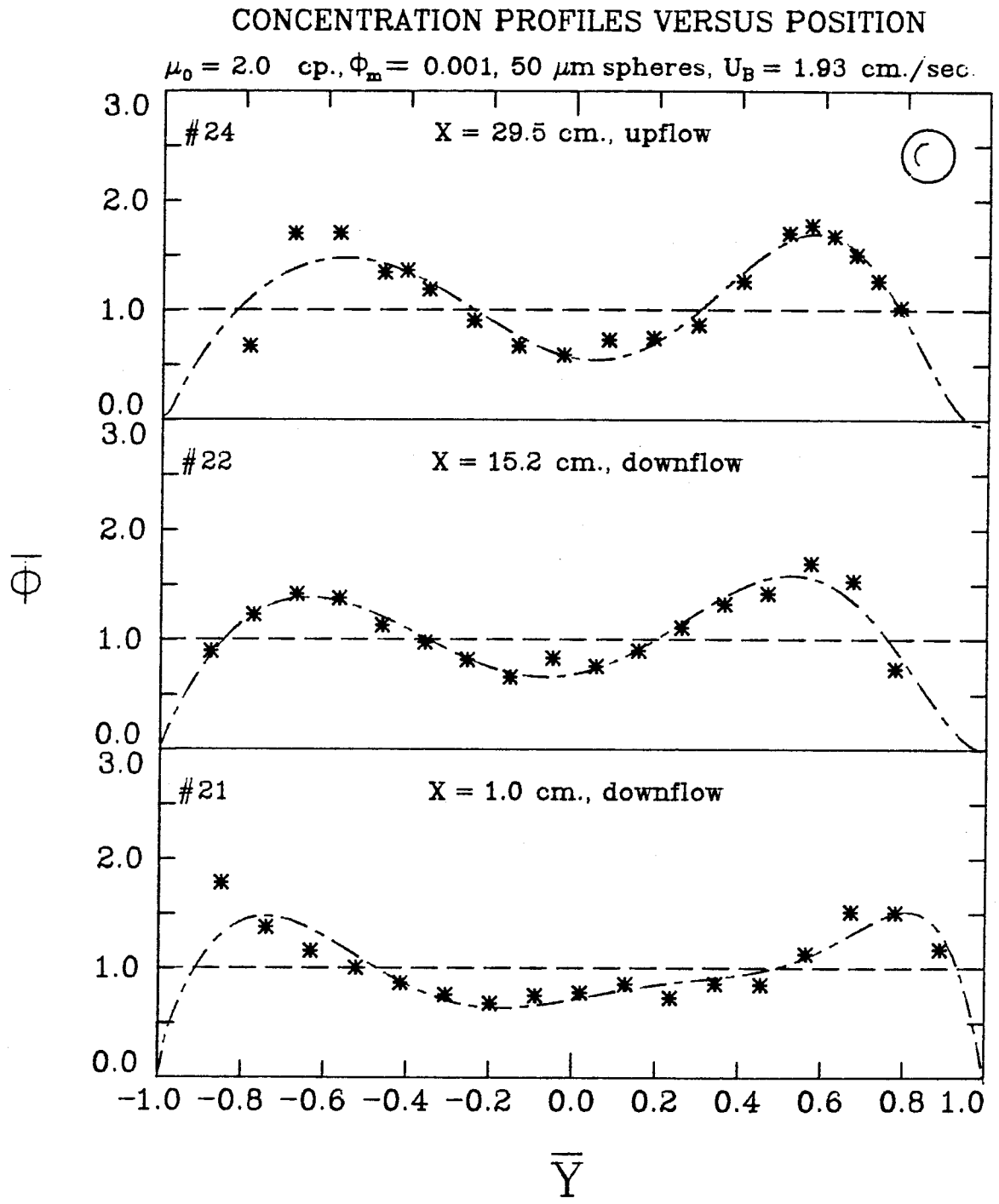
CONCENTRATION PROFILES VERSUS POSITION
μ_0 = 2.0 cp., Φ_m = 0.001, 50 μm spheres, U_B = 1.93 cm./sec.
#24
X = 29.5 cm., upflow
#22
X = 15.2 cm., downflow
#21
X = 1.0 cm., downflow
3.0
2.0
1.0
0.0
$\overline{\Phi}$
-1.0 -0.8 -0.6 -0.4 -0.2 0.0 0.2 0.4 0.6 0.8 1.0
$\overline{Y}$

Figure 2-19.

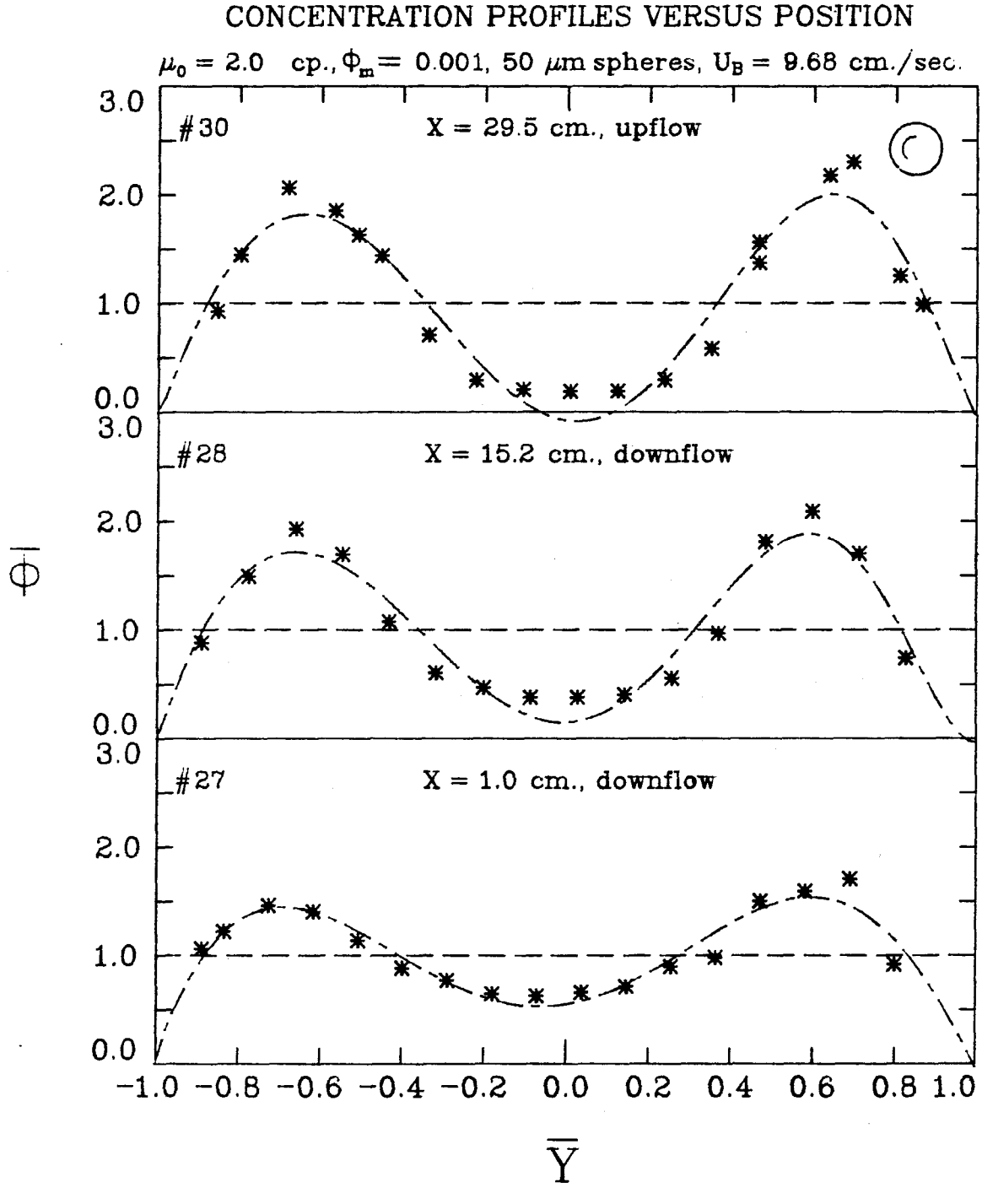
CONCENTRATION PROFILES VERSUS POSITION
μ_0 = 2.0 cp., Φ_m = 0.001, 50 μm spheres, U_B = 9.68 cm./sec.
#30
X = 29.5 cm., upflow
#28
X = 15.2 cm., downflow
#27
X = 1.0 cm., downflow
3.0
2.0
1.0
0.0
$\overline{\Phi}$
-1.0 -0.8 -0.6 -0.4 -0.2 0.0 0.2 0.4 0.6 0.8 1.0
$\overline{Y}$

Figure 2-20.

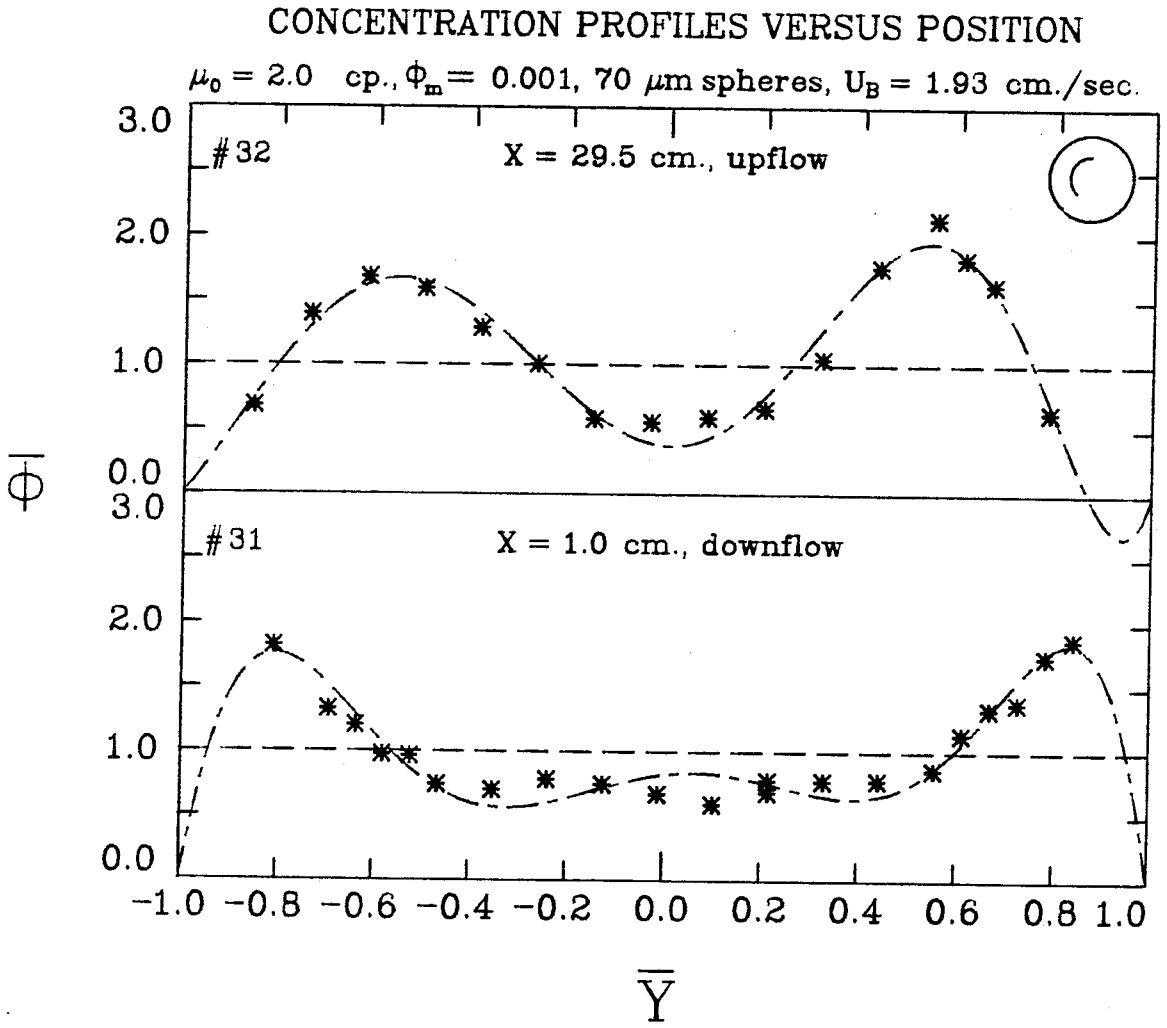
CONCENTRATION PROFILES VERSUS POSITION
μ_0 = 2.0 cp., Φ_m = 0.001, 70 μm spheres, U_B = 1.93 cm./sec.
#32
X = 29.5 cm., upflow
#31
X = 1.0 cm., downflow
3.0
2.0
1.0
0.0
$\overline{\Phi}$
-1.0 -0.8 -0.6 -0.4 -0.2 0.0 0.2 0.4 0.6 0.8 1.0
$\overline{Y}$

Figure 2-21.

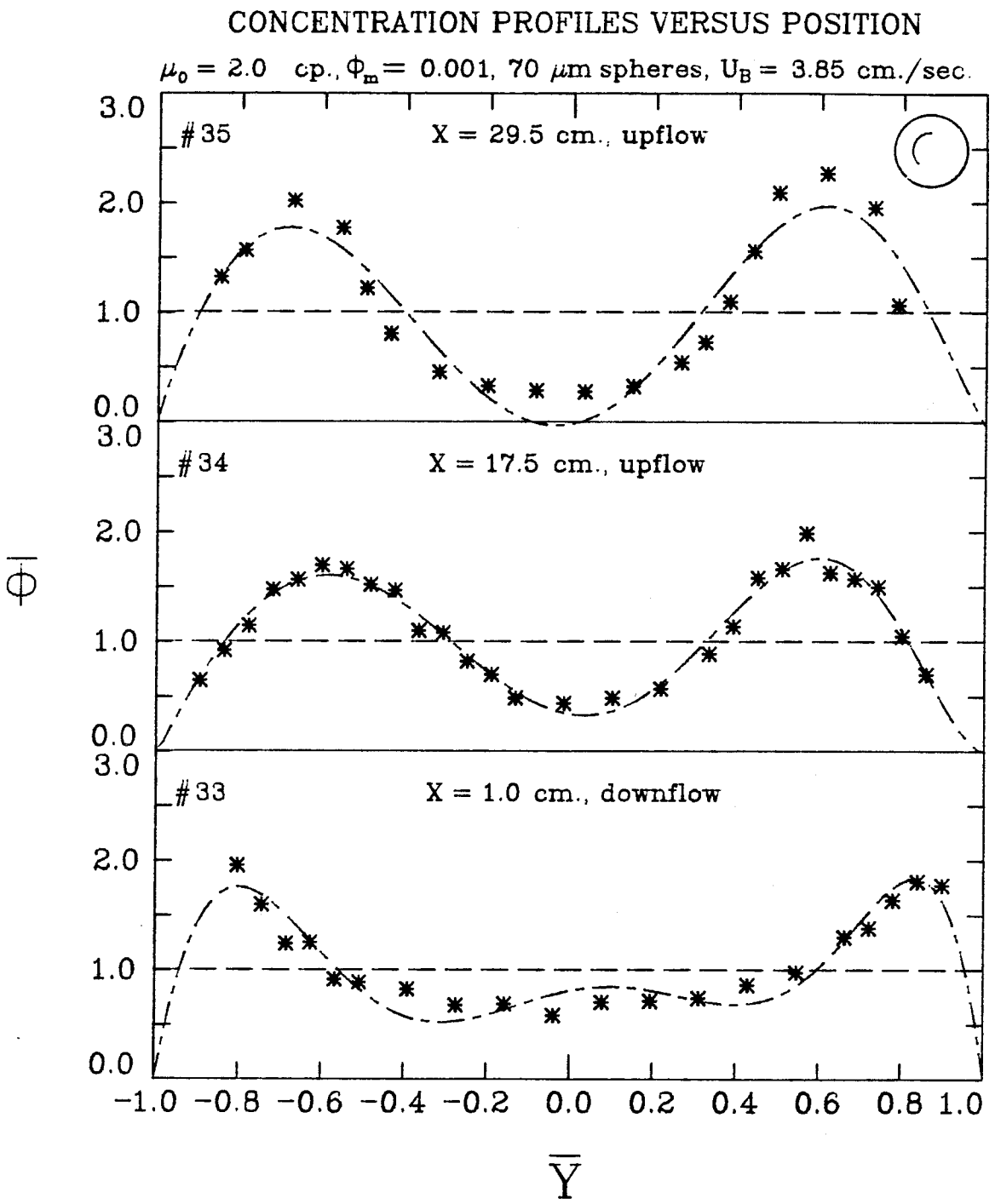
CONCENTRATION PROFILES VERSUS POSITION
μ_0 = 2.0 cp., Φ_m = 0.001, 70 μm spheres, U_B = 3.85 cm./sec.
#35
X = 29.5 cm., upflow
#34
X = 17.5 cm., upflow
#33
X = 1.0 cm., downflow
3.0
2.0
1.0
0.0
$\overline{\Phi}$
-1.0 -0.8 -0.6 -0.4 -0.2 0.0 0.2 0.4 0.6 0.8 1.0
$\overline{Y}$

Figure 2-22.

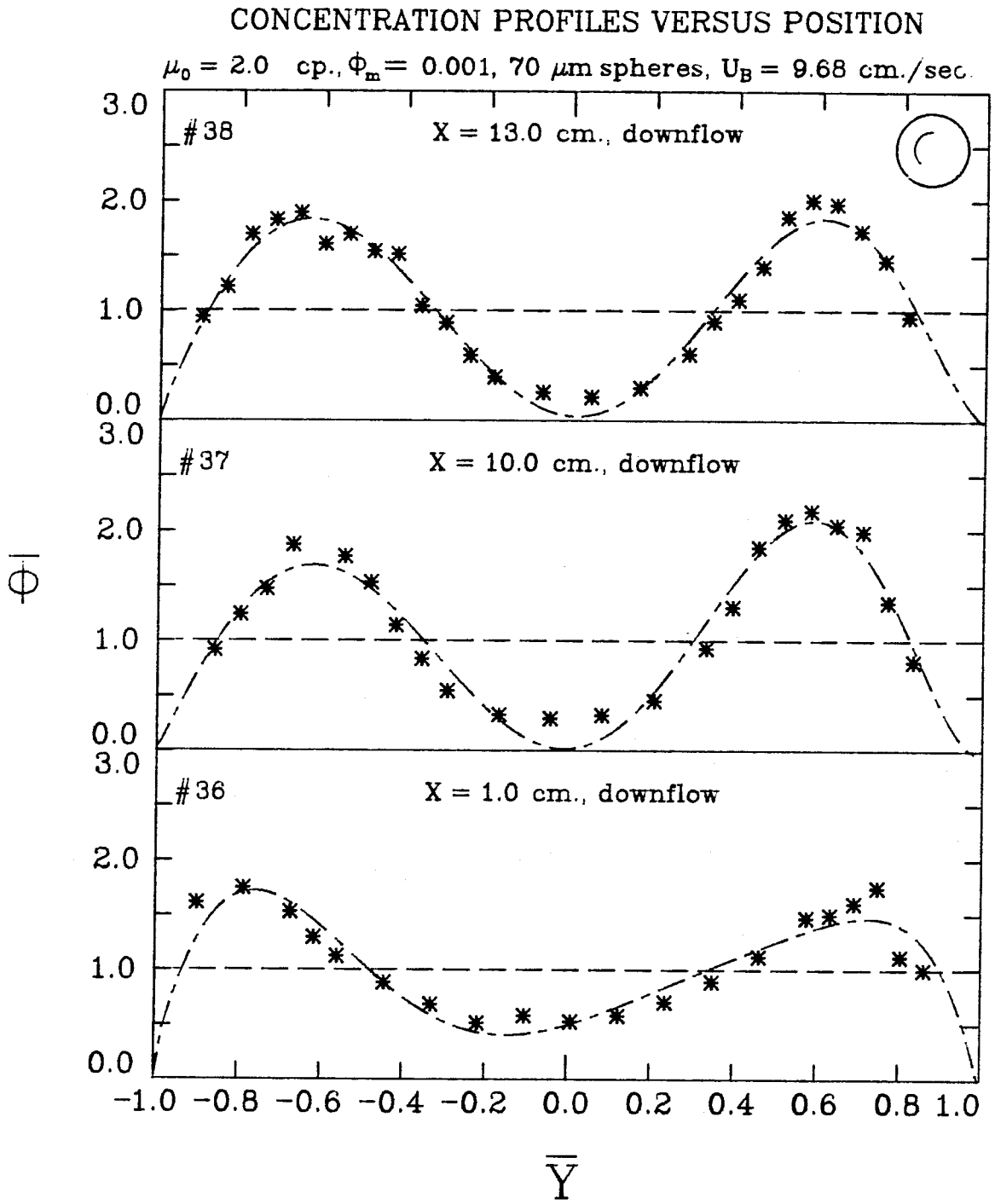
CONCENTRATION PROFILES VERSUS POSITION
μ_0 = 2.0 cp., Φ_m = 0.001, 70 μm spheres, U_B = 9.68 cm./sec.
#38
X = 13.0 cm., downflow
#37
X = 10.0 cm., downflow
#36
X = 1.0 cm., downflow
3.0
2.0
1.0
0.0
-1.0 -0.8 -0.6 -0.4 -0.2 0.0 0.2 0.4 0.6 0.8 1.0
$\overline{\Phi}$
$\overline{Y}$

Figure 2-23.

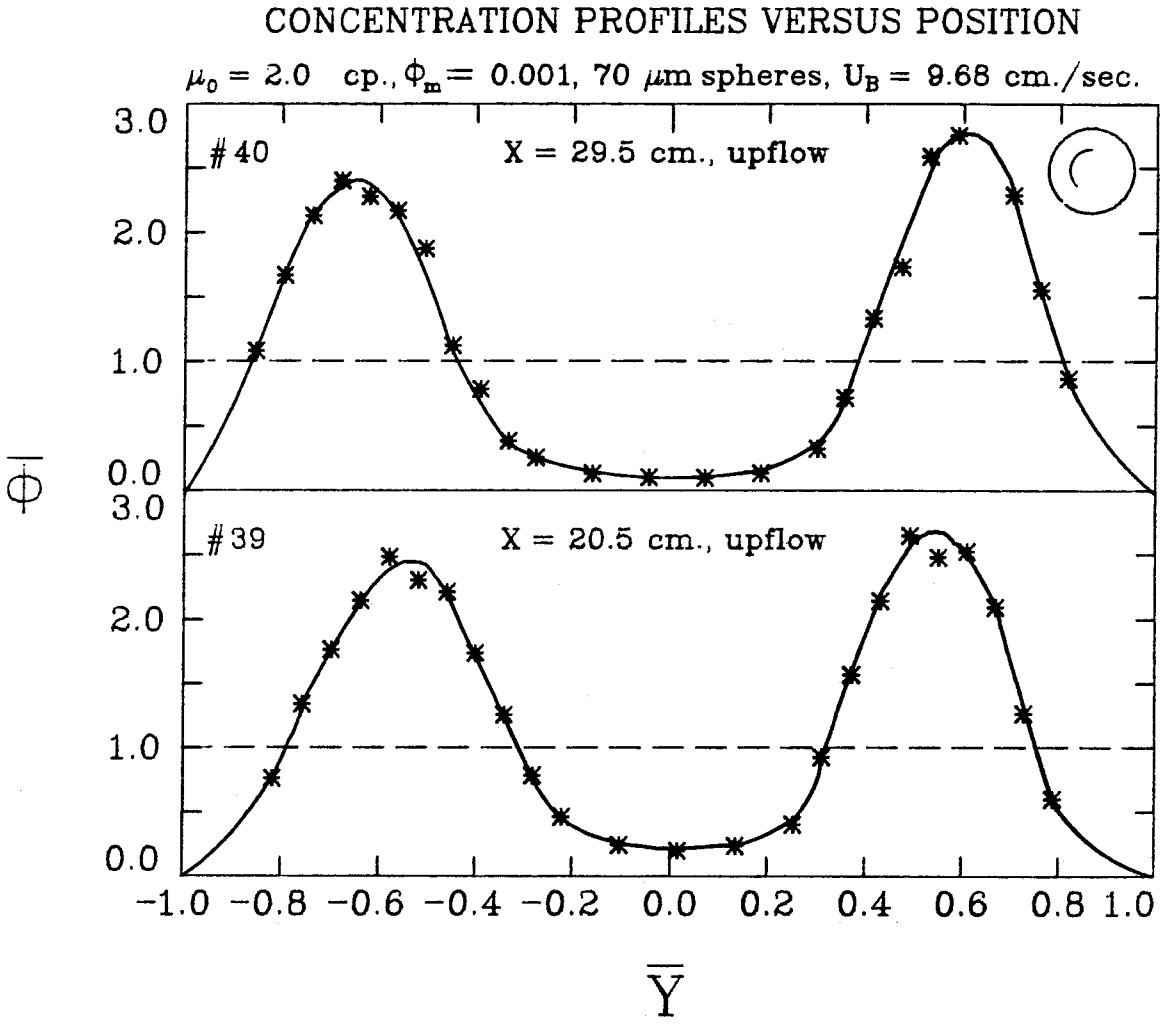
CONCENTRATION PROFILES VERSUS POSITION
μ_0 = 2.0 cp., Φ_m = 0.001, 70 μm spheres, U_B = 9.68 cm./sec.
#40
X = 29.5 cm., upflow
#39
X = 20.5 cm., upflow
3.0
2.0
1.0
0.0
-1.0 -0.8 -0.6 -0.4 -0.2 0.0 0.2 0.4 0.6 0.8 1.0
$\overline{\Phi}$
$\overline{Y}$

Figure 2-24.

from these results. First, data set 9, which was done with the same experimental conditions as set 1, except that the viscosity of the suspending fluid is lower, looks similar to data set 1. The reason for this will be discussed in the next section. At the far end of the channel for these conditions (x=29.5 cm., data set 12), there has been a slight amount of inward migration, as the inward shift of the peak shows.

Upon observing the remaining data, the following trends are evident. The concentration profiles become increasingly peaked about $\bar{Y} \approx +/-0.6$ as either the particle size, downstream position, or bulk velocity is increased. These trends are in agreement with what would be expected from theoretical particle trajectory calculations (Ho and Leal, 1974; Vasseur and Cox, 1976). Thus inward migration of particles due to inertia has been demonstrated. This phenomenon has been demonstrated previously for two-dimensional Poiseuille flow (Repetti and Leonard, 1966; and Tachibana, 1973). A quantitative comparison with theory will be presented in the next section.

2.5. THEORETICAL CONCENTRATION PROFILE CALCULATION

Theoretical concentration profiles were calculated for a number of the data sets represented in Table 2-1 using the theoretical particle trajectory result of Ho and Leal. Ho and Leal calculated the lateral migration velocity of a neutrally-buoyant sphere in two-dimensional Poiseuille flow for $Re_p << 1$ using the method of reflections. While this result was obtained for a single particle, the authors state that it is valid for a dilute suspension, as long as the following condition on the concentration of the suspension is met:

$$\Phi^2 \ll (a/d)^3 \quad . \tag{2.11}$$

If this condition is satisfied, then "it may be assumed that the lateral force on a particle in a suspension is equal to that on a single sphere immersed in the fluid." This condition was approximately satisfied for the suspensions used in

this study. The theoretical method of solution also required that $(a/d) \ll 1$, which probably is questionable for the larger spheres.

The method used to calculate the theoretical concentration profiles was as follows: An initially uniform concentration distribution at the entry was assumed for the low Reynolds number cases. For a given initial position of a sphere $\bar{Y}_i$ at the entry, the final lateral position at a downstream position X was calculated using the particle trajectory result of Ho and Leal:

$$X - X_0 = \frac{36\pi\mu_0}{\rho_0 U_B (a/d)^3} \int_{s_0}^{s} \frac{s'(1-s')}{G(s')} ds' \quad , \tag{2.12}$$

where x_0 is the initial downstream position, $s=(1+\bar{Y})/2$ is a dimensionless lateral position, and s_0 is the initial lateral position of the particle. Since G(s) is a complicated function, it was necessary to evaluate the integral numerically. The concentration profile was calculated numerically for half of the channel (since it is symmetrical about $\bar{Y}=0$) by dividing half of the channel into 200 intervals Δy_i. Within each interval, a Gaussian distribution of particle sizes was assumed, using the measured mean radius a and standard deviation σ for each particle size. The size distribution for each mean particle size was divided into 128 intervals Δa_i for calculation purposes. The fraction of particles in interval i of size j initially (at x=0) $\bar{n}_{ij,I}$ was given by the Gaussian distribution function:

$$\bar{n}_{ij,I} = \frac{\displaystyle\int_{a_1}^{a_1+\Delta a_1} \exp\left[-\frac{(a'-a)}{2\sigma^2}\right] da'}{\displaystyle\int_{a_1}^{a_{128}} \exp\left[-\frac{(a'-a)}{2\sigma^2}\right] da'} \quad , \tag{2.13}$$

where $a_1=-4.5\sigma$, $a_{128}=4.5\sigma$, $\Delta a_i=0.0703\sigma$, $\left(\sum_{j=1}^{128} \bar{n}_{ij,I}=1, \sum_{i=1}^{200}\sum_{j=1}^{128} \bar{n}_{ij,I}=200\right)$.

The final lateral position of each particle size in each starting interval was then computed (a total of 25,600 computations) for a given X, U_B, μ_0, and a. The total concentration of particles Φ_i in interval i at the downstream position X being examined was then the sum of all the particles that had that interval as their final one:

$$\Phi_i = \frac{\sum_{j=1}^{128} \bar{n}_{ij,F}}{\sum_{i=1}^{200} \sum_{j=1}^{128} \bar{n}_{ij,F}} \quad , \tag{2.14}$$

where $\bar{n}_{ij,F}$ is the fraction of particles in interval i of size j finally (at the downstream position X).

The above calculations were duplicated for a few cases using the particle trajectory results of Vasseur and Cox (1976). Vasseur and Cox solved the same particle migration problem as Ho and Leal and obtained similar results, except near the walls. Thus the calculations were duplicated using their results to determine if the differences between the two theoretical results affected the calculated concentration profiles substantially. The results of the duplicate calculations were similar to those shown below.

The computed concentration distributions, along with the corresponding experimental data, appear in Figures 2-25 to 2-38. The solid line in these figures is the calculated concentration distribution, and the polynomial curve-fit has been omitted. If the calculated concentration distribution at any point exceeded $\bar{\Phi}(y_i)$=5.0, it was given a value of 5.0 for plotting purposes (the peaks were truncated so that they would fit onto the figure).

For the low Re_p (high viscosity) data sets 1 and 5 (Figures 2-25 and 2-26), the calculated concentration distributions were nearly flat. The peaks near the

wall were too close to the wall to have been measured experimentally. These results demonstrate that no measurable migration should occur under these conditions, and that the shapes of the measured concentration distributions were apparently determined by an entrance effect.

Since from the above it is apparent that the concentration distributions were not flat at the channel entry, initially flat concentration distributions were not assumed when calculating the theoretical concentration profiles for the higher Re_p cases. Rather, the measured concentration profile for the low Re_p case of the appropriate sphere size was used, since this presumably corresponded to the initial concentration profile shape. Thus, for example, for the 27 μm diameter spheres, the polynomial curve-fit to the concentration data of data set 1 was used as the concentration distribution at the flow channel inlet. Where little migration was expected (due to small a, U_B, and X), as in data set 9, this change to a non-uniform initial distribution had a significant effect. For this case the theoretical and measured concentration profiles are similar. Conversely, when a large amount of migration occurred (e.g., data set 40), the final concentration distribution was not affected significantly by this change.

It is apparent from observing the high Re_p (high viscosity) data sets in Figures 2-27 to 2-38 that the experimental and theoretical concentration distributions have some similarities, mainly in the lateral positions of the peaks, but the calculated concentration distributions are in general more sharply peaked than the measured concentration profiles. This discrepancy is due in part to the fact that the theoretical method assumes that the particle is very small with respect to the channel spacing, which is not a good assumption for the largest particle size (e.g., data set 40, Figure 2-38). For this data set the theory essentially predicts that all of the particles would be aligned at the equilibrium position of

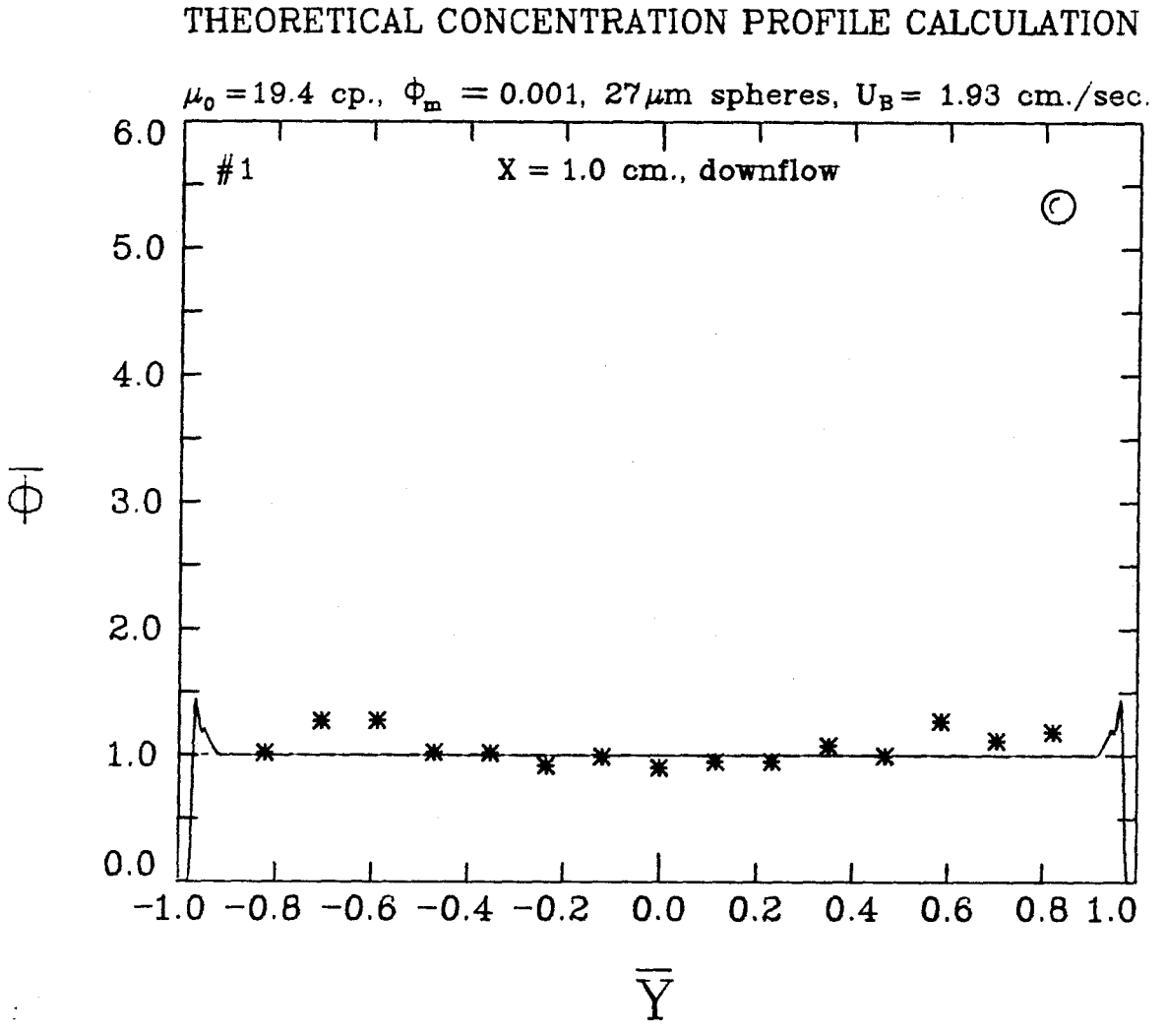
THEORETICAL CONCENTRATION PROFILE CALCULATION
μ_0 = 19.4 cp., Φ_m = 0.001, 27μm spheres, U_B = 1.93 cm./sec.
#1
X = 1.0 cm., downflow
6.0
5.0
4.0
3.0
2.0
1.0
0.0
$\overline{\Phi}$
-1.0 -0.8 -0.6 -0.4 -0.2 0.0 0.2 0.4 0.6 0.8 1.0
$\overline{Y}$

Figure 2-25.

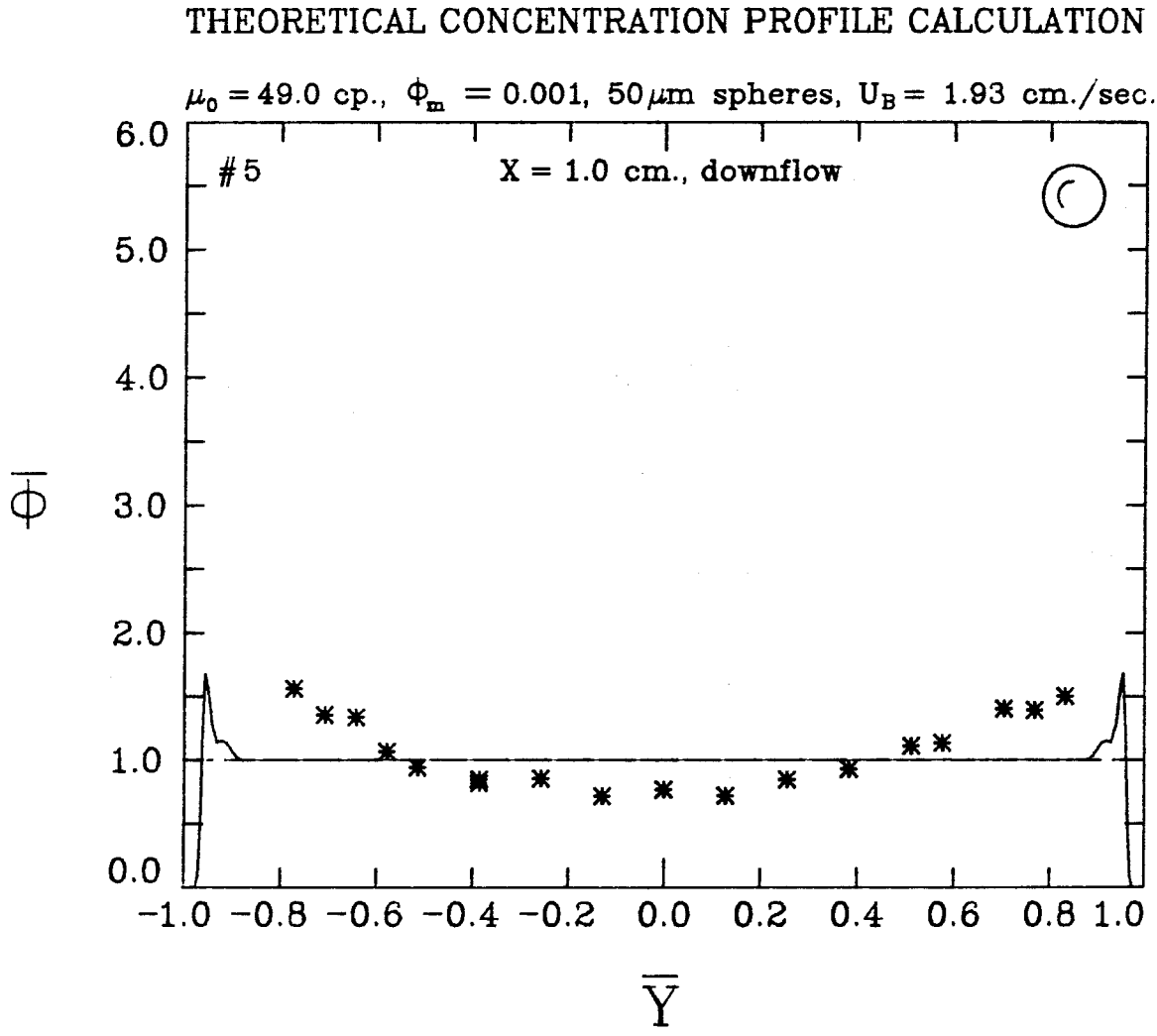
THEORETICAL CONCENTRATION PROFILE CALCULATION
$\mu_0 = 49.0$ cp., $\Phi_m = 0.001$, 50 μm spheres, $U_B = 1.93$ cm./sec.
#5
X = 1.0 cm., downflow
6.0
5.0
4.0
3.0
2.0
1.0
0.0
$\overline{\Phi}$
-1.0 -0.8 -0.6 -0.4 -0.2 0.0 0.2 0.4 0.6 0.8 1.0
$\overline{Y}$

Figure 2-26.

$\bar{Y}$=+/ − 0.6, with the peak width in the concentration profile equalling one particle diameter. The measured peaks are still somewhat broader than one sphere diameter, however.

A possible explanation for the broadening of concentration peaks is that, despite the overall diluteness of the suspensions, when the particles approach the equilibrium position, the local concentration is sufficiently high that substantial particle-particle interactions occur, spreading out the distributions. Also, if the local concentration is much higher than the bulk concentration, the condition (2.10) might not be satisfied in that region. Since the theory does not take particle interactions into account, it would not be valid in that region. This idea is supported by the data in that the best agreement between theory and experiment occurs when relatively little migration has occurred (e.g. data set 21), and hence less local crowding and interaction of particles should occur. Conversely, the worst agreement occurs when the particles should be at the equilibrium position in theory (set 40), and the greatest local crowding and hence the greatest particle interaction should occur.

2.6. CONCLUSIONS

A velocity and concentration distribution measurement technique was discussed and was shown experimentally to give reasonable results for dilute suspensions in a quasi-two-dimensional flow. The measured concentration distributions in the regime where inertial effects were important demonstrated the effects of the expected lateral migration of particles. Where inertial effects were unimportant, the concentration distributions showed a small peak near the wall, which was presumably due to an entrance effect. Theoretically calculated concentration profiles agreed qualitatively with experimental profiles, but were less sharply peaked as particle migration increased, apparently due to particle-particle interactions.

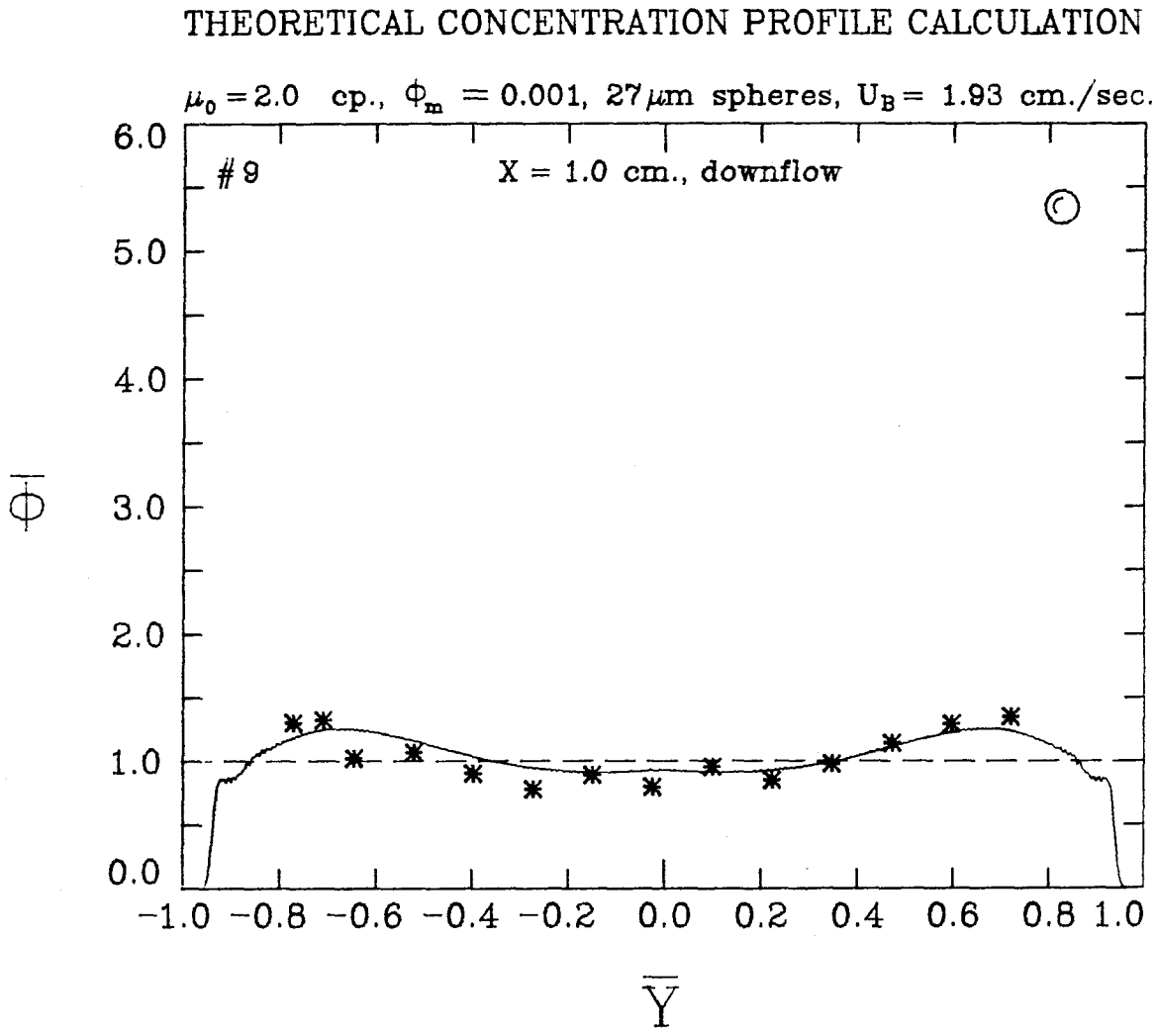
THEORETICAL CONCENTRATION PROFILE CALCULATION
$\mu_0 = 2.0$ cp., $\Phi_m = 0.001$, 27μm spheres, $U_B = 1.93$ cm./sec.
# 9
X = 1.0 cm., downflow
6.0
5.0
4.0
3.0
2.0
1.0
0.0
$\overline{\Phi}$
-1.0 -0.8 -0.6 -0.4 -0.2 0.0 0.2 0.4 0.6 0.8 1.0
$\overline{Y}$

Figure 2-27.

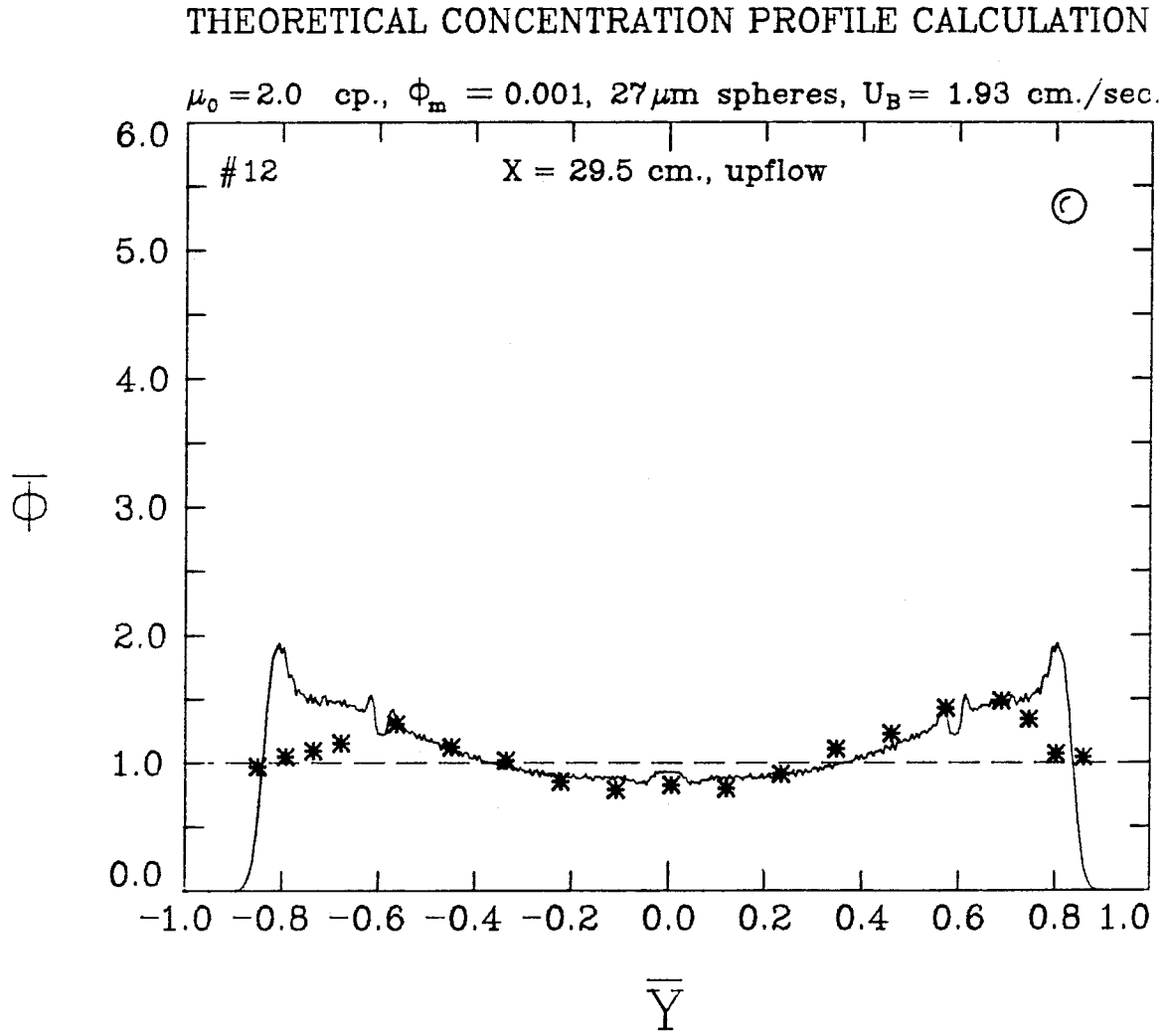
THEORETICAL CONCENTRATION PROFILE CALCULATION
$\mu_0 = 2.0$ cp., $\Phi_m = 0.001$, 27μm spheres, $U_B = 1.93$ cm./sec.
#12
X = 29.5 cm., upflow
6.0
5.0
4.0
3.0
2.0
1.0
0.0
$\overline{\Phi}$
-1.0 -0.8 -0.6 -0.4 -0.2 0.0 0.2 0.4 0.6 0.8 1.0
$\overline{Y}$

Figure 2-28.

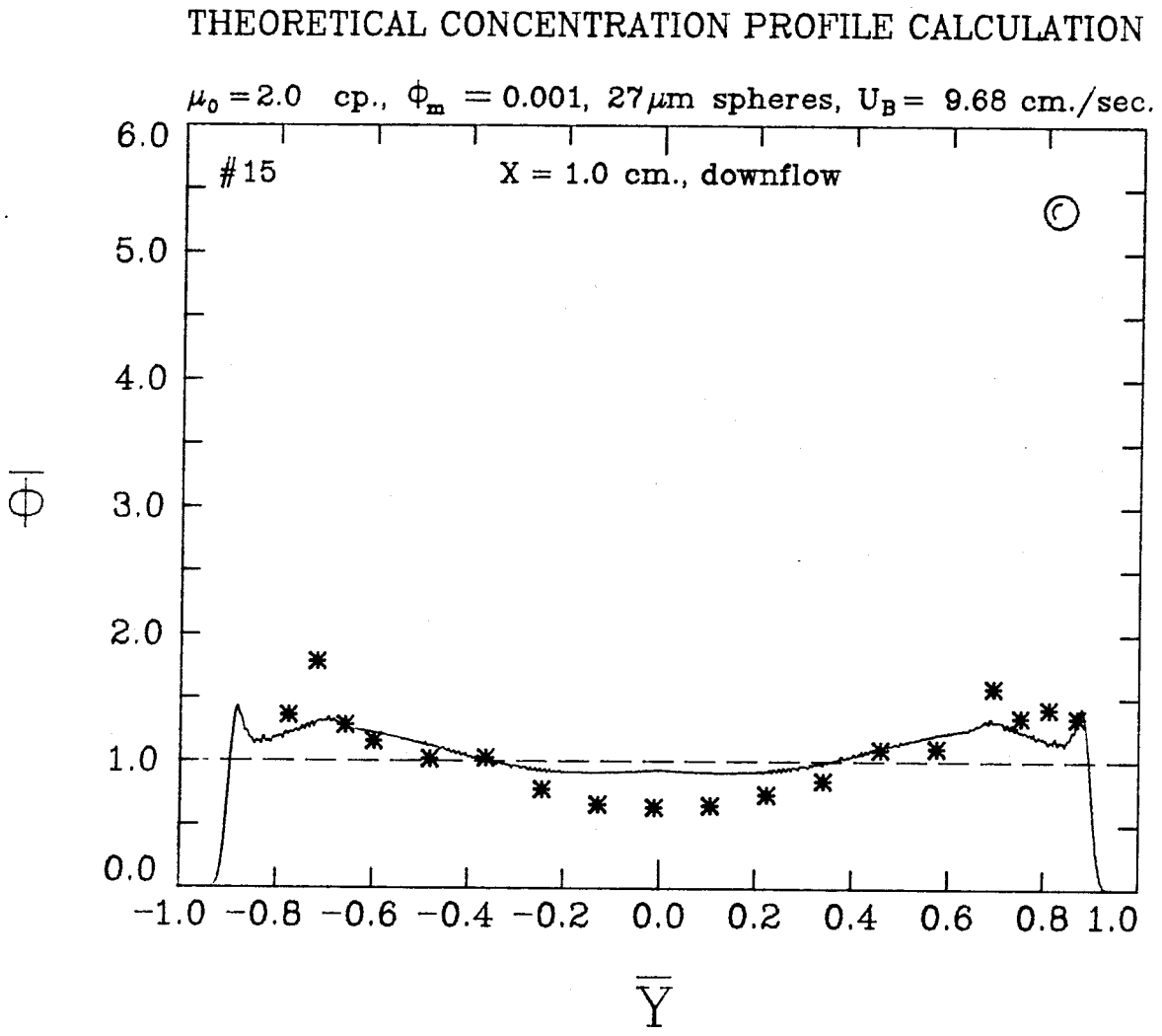
THEORETICAL CONCENTRATION PROFILE CALCULATION
$\mu_0 = 2.0$ cp., $\Phi_m = 0.001$, 27μm spheres, $U_B = 9.68$ cm./sec.
#15
X = 1.0 cm., downflow
6.0
5.0
4.0
3.0
2.0
1.0
0.0
$\overline{\Phi}$
-1.0 -0.8 -0.6 -0.4 -0.2 0.0 0.2 0.4 0.6 0.8 1.0
$\overline{Y}$

Figure 2-29.

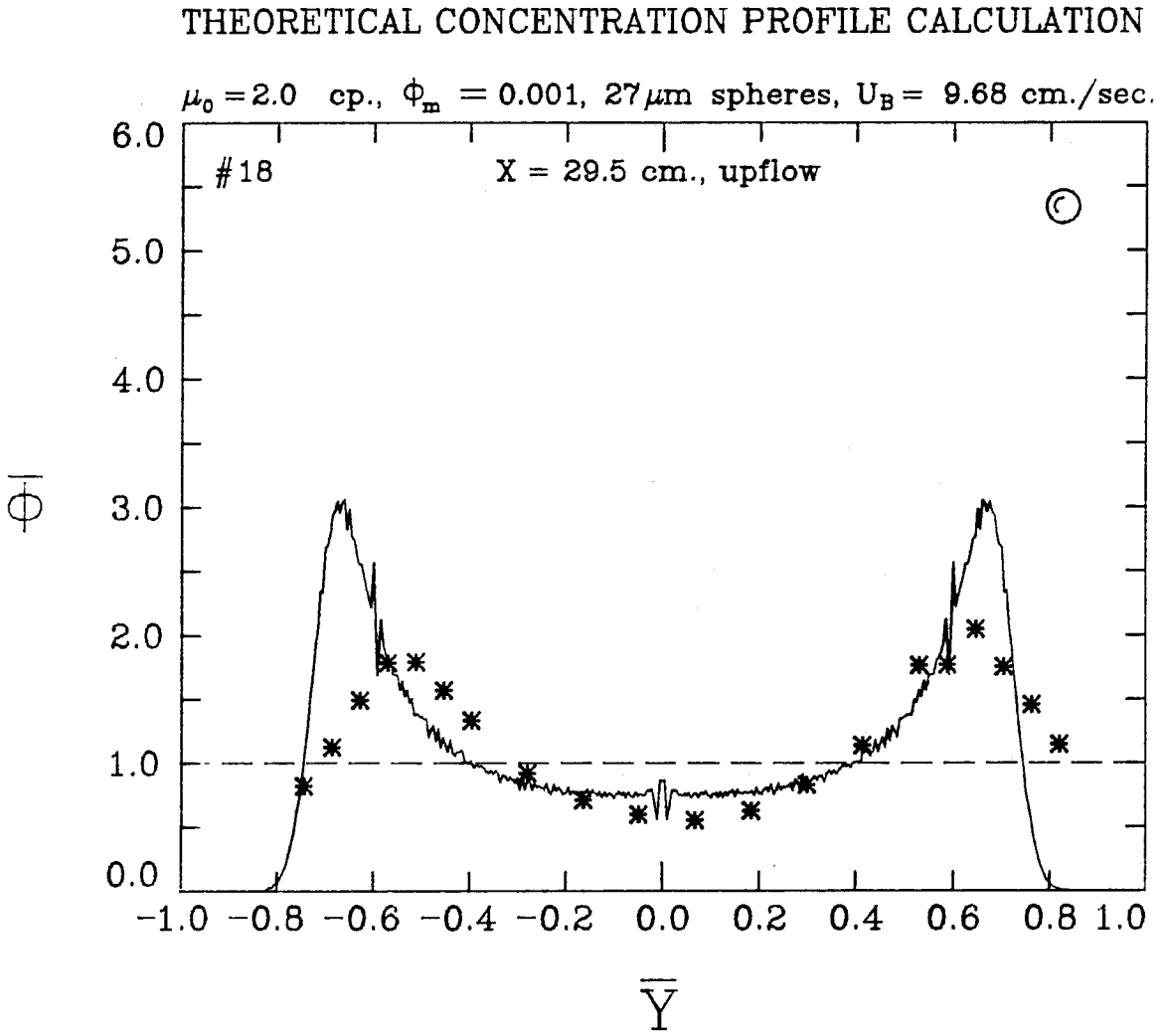
THEORETICAL CONCENTRATION PROFILE CALCULATION
$\mu_0 = 2.0$ cp., $\Phi_m = 0.001$, 27μm spheres, $U_B = 9.68$ cm./sec.
#18
X = 29.5 cm., upflow
6.0
5.0
4.0
3.0
2.0
1.0
0.0
$\overline{\Phi}$
-1.0 -0.8 -0.6 -0.4 -0.2 0.0 0.2 0.4 0.6 0.8 1.0
$\overline{Y}$

Figure 2-30.

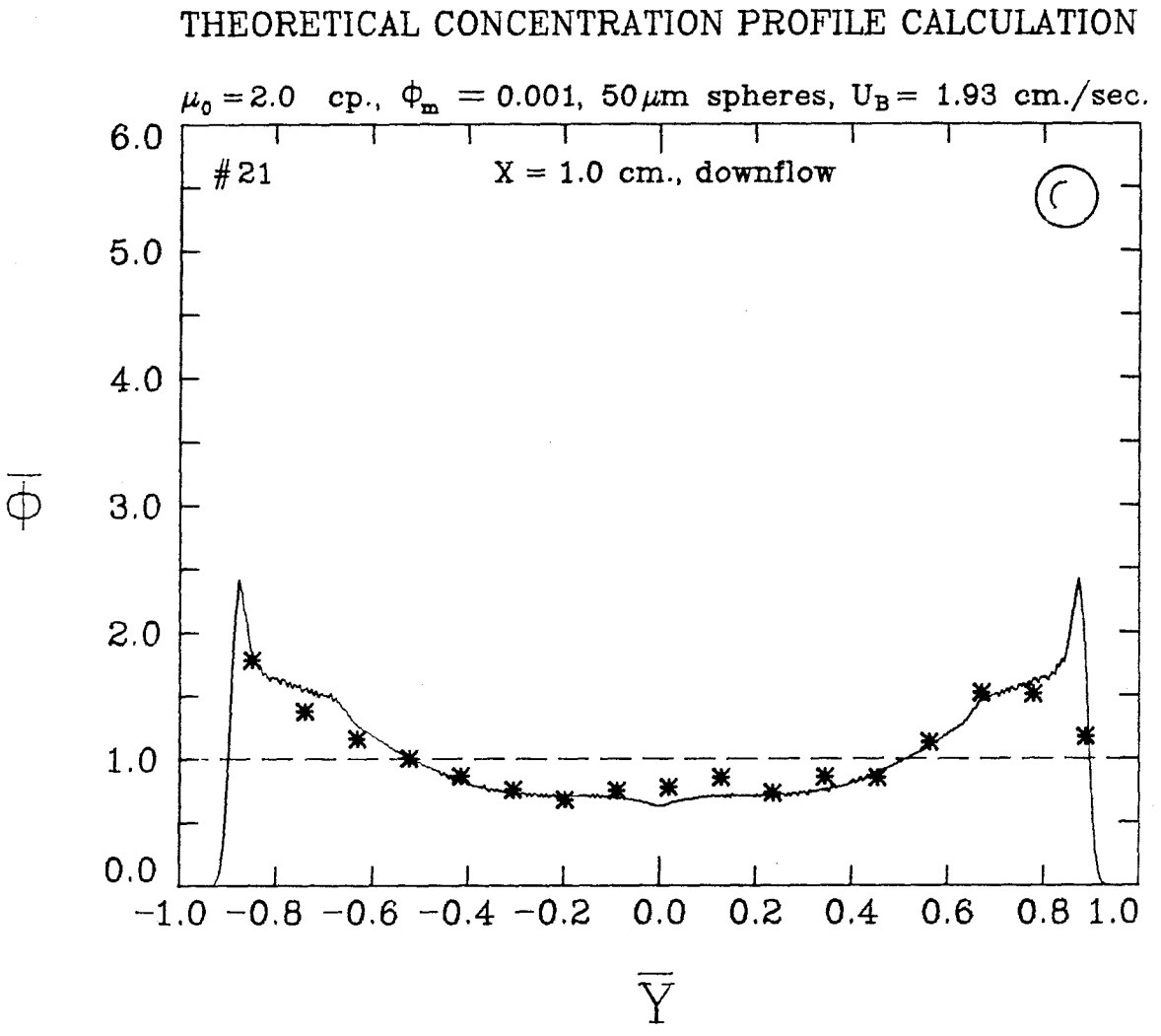
THEORETICAL CONCENTRATION PROFILE CALCULATION
$\mu_0 = 2.0$ cp., $\Phi_m = 0.001$, 50μm spheres, $U_B = 1.93$ cm./sec.
#21
X = 1.0 cm., downflow
6.0
5.0
4.0
3.0
2.0
1.0
0.0
$\overline{\Phi}$
-1.0 -0.8 -0.6 -0.4 -0.2 0.0 0.2 0.4 0.6 0.8 1.0
$\overline{Y}$

Figure 2-31.

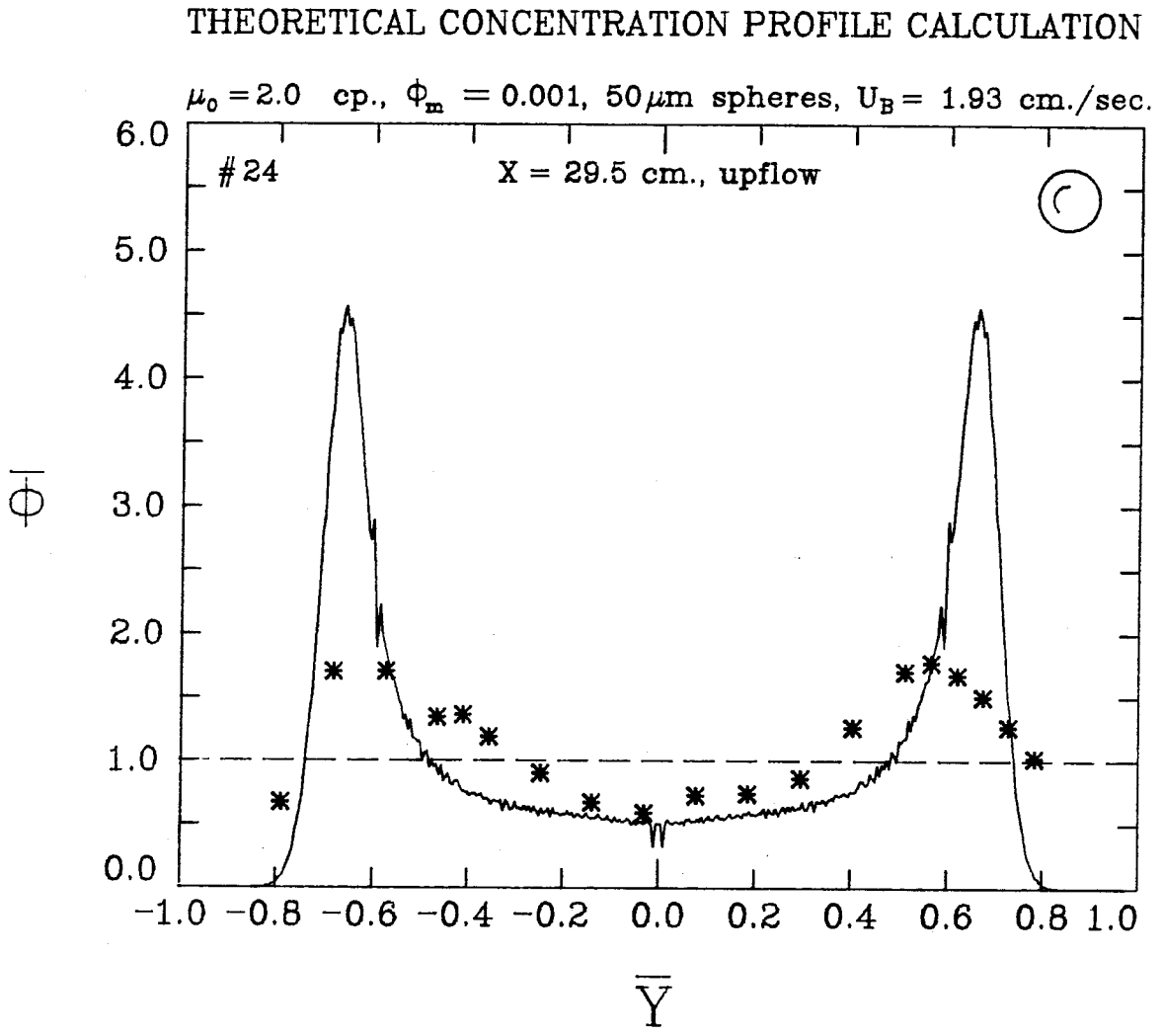
THEORETICAL CONCENTRATION PROFILE CALCULATION
$\mu_0 = 2.0$ cp., $\Phi_m = 0.001$, 50μm spheres, $U_B = 1.93$ cm./sec.
# 24
X = 29.5 cm., upflow
6.0
5.0
4.0
3.0
2.0
1.0
0.0
$\overline{\Phi}$
-1.0 -0.8 -0.6 -0.4 -0.2 0.0 0.2 0.4 0.6 0.8 1.0
$\overline{Y}$

Figure 2-32.

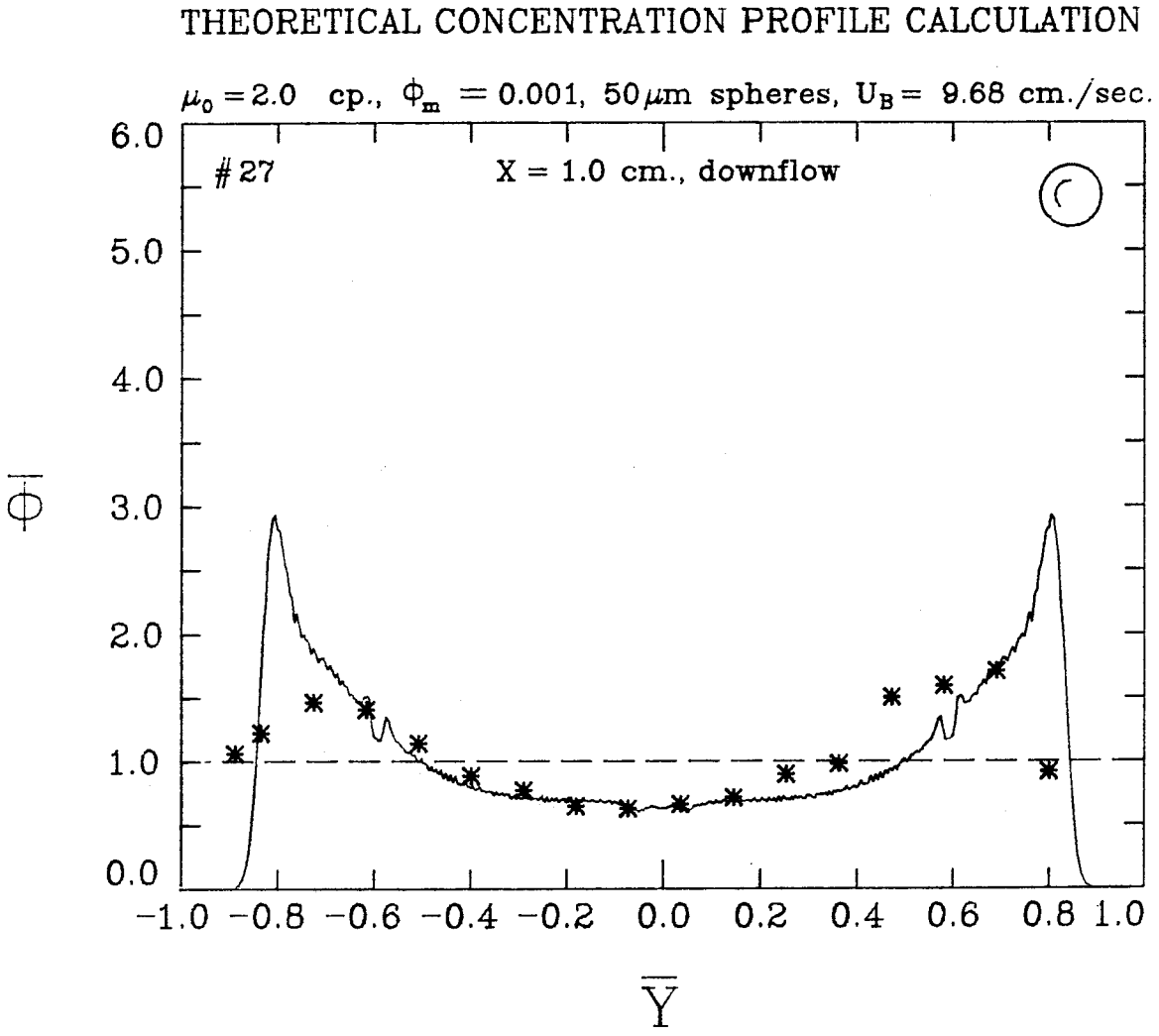
THEORETICAL CONCENTRATION PROFILE CALCULATION
$\mu_0 = 2.0$ cp., $\Phi_m = 0.001$, 50μm spheres, $U_B = 9.68$ cm./sec.
#27
X = 1.0 cm., downflow
6.0
5.0
4.0
3.0
2.0
1.0
0.0
$\overline{\Phi}$
-1.0 -0.8 -0.6 -0.4 -0.2 0.0 0.2 0.4 0.6 0.8 1.0
$\overline{Y}$

Figure 2-33.

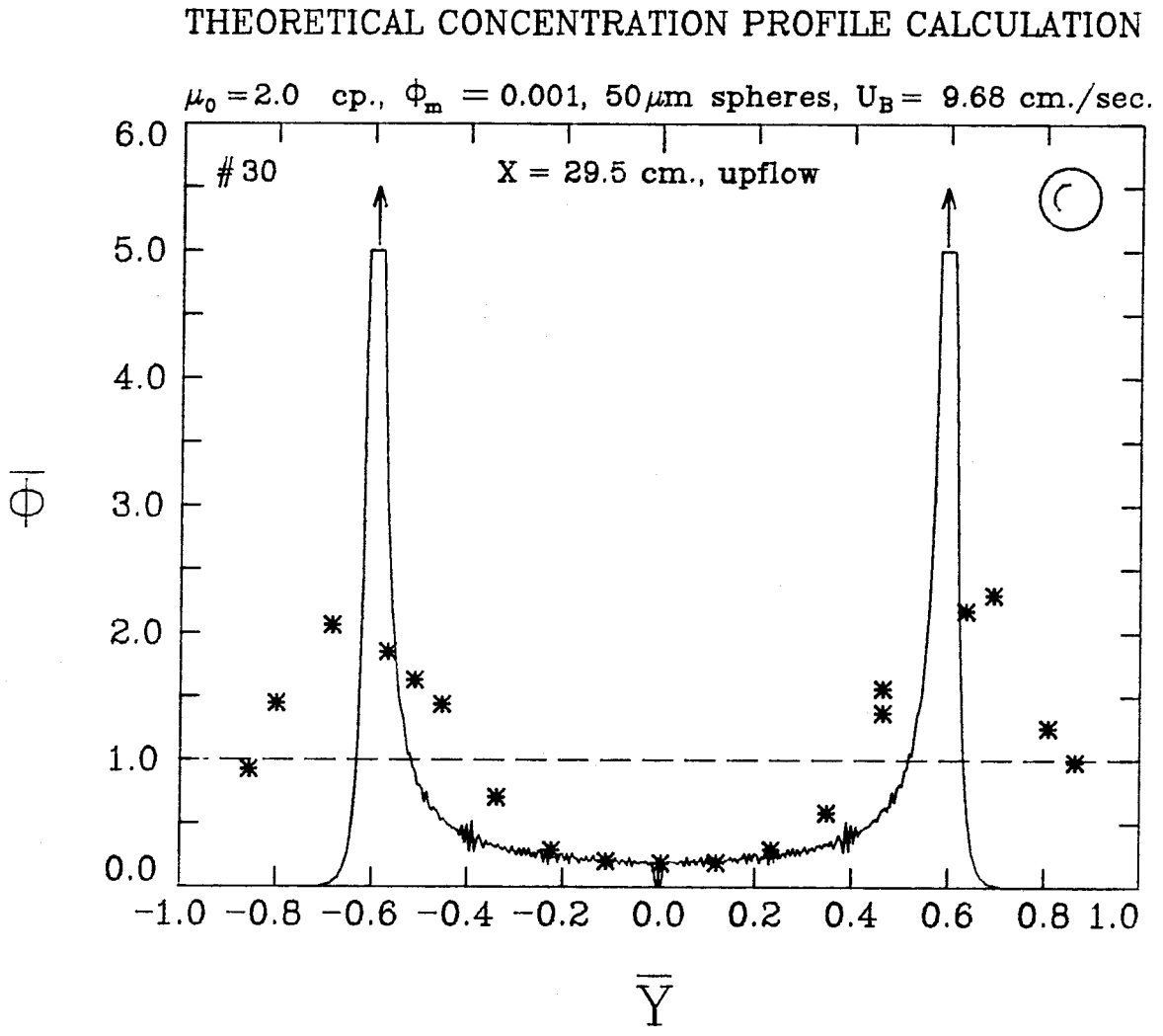
THEORETICAL CONCENTRATION PROFILE CALCULATION
$\mu_0 = 2.0$ cp., $\Phi_m = 0.001$, 50 μm spheres, $U_B = 9.68$ cm./sec.
# 30
X = 29.5 cm., upflow
C
6.0
5.0
4.0
3.0
2.0
1.0
0.0
$\overline{\Phi}$
-1.0 -0.8 -0.6 -0.4 -0.2 0.0 0.2 0.4 0.6 0.8 1.0
$\overline{Y}$

Figure 2-34.

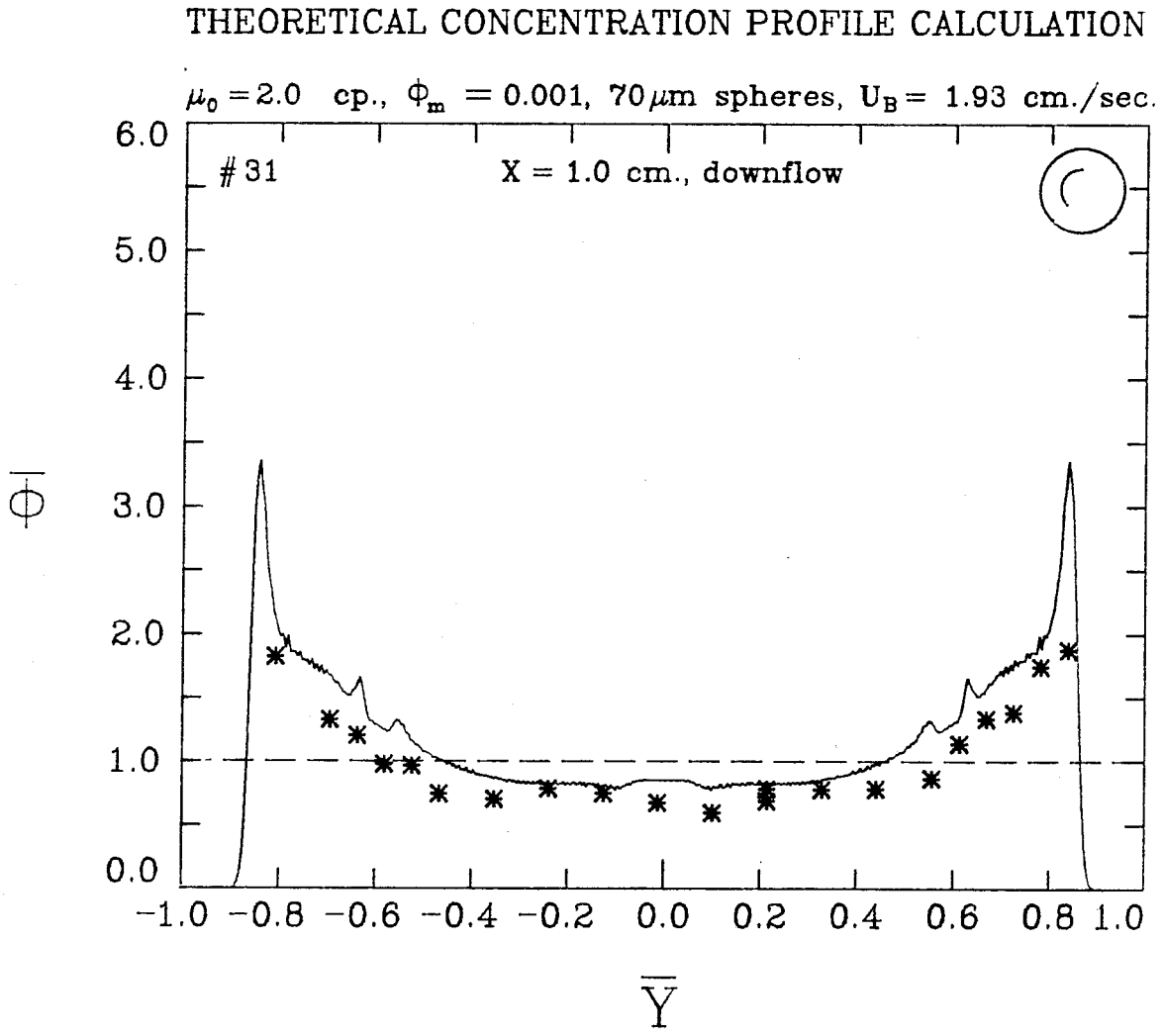
THEORETICAL CONCENTRATION PROFILE CALCULATION
$\mu_0 = 2.0$ cp., $\Phi_m = 0.001$, 70μm spheres, $U_B = 1.93$ cm./sec.
#31
X = 1.0 cm., downflow
6.0
5.0
4.0
3.0
2.0
1.0
0.0
$\overline{\Phi}$
-1.0 -0.8 -0.6 -0.4 -0.2 0.0 0.2 0.4 0.6 0.8 1.0
$\overline{Y}$

Figure 2-35.

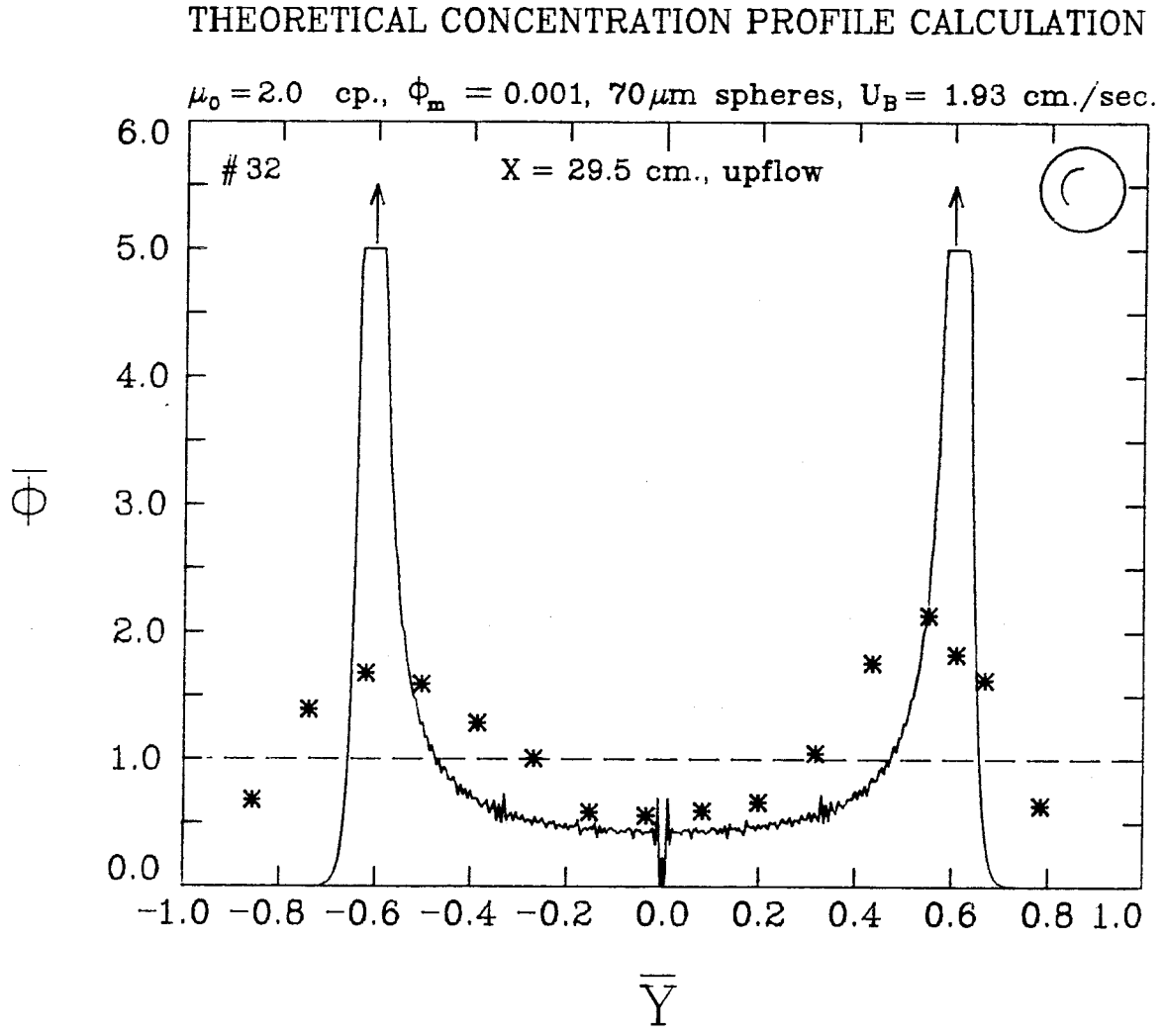
THEORETICAL CONCENTRATION PROFILE CALCULATION
$\mu_0 = 2.0$ cp., $\phi_m = 0.001$, 70μm spheres, $U_B = 1.93$ cm./sec.
# 32
X = 29.5 cm., upflow
6.0
5.0
4.0
3.0
2.0
1.0
0.0
$\overline{\Phi}$
-1.0 -0.8 -0.6 -0.4 -0.2 0.0 0.2 0.4 0.6 0.8 1.0
$\overline{Y}$

Figure 2-36.

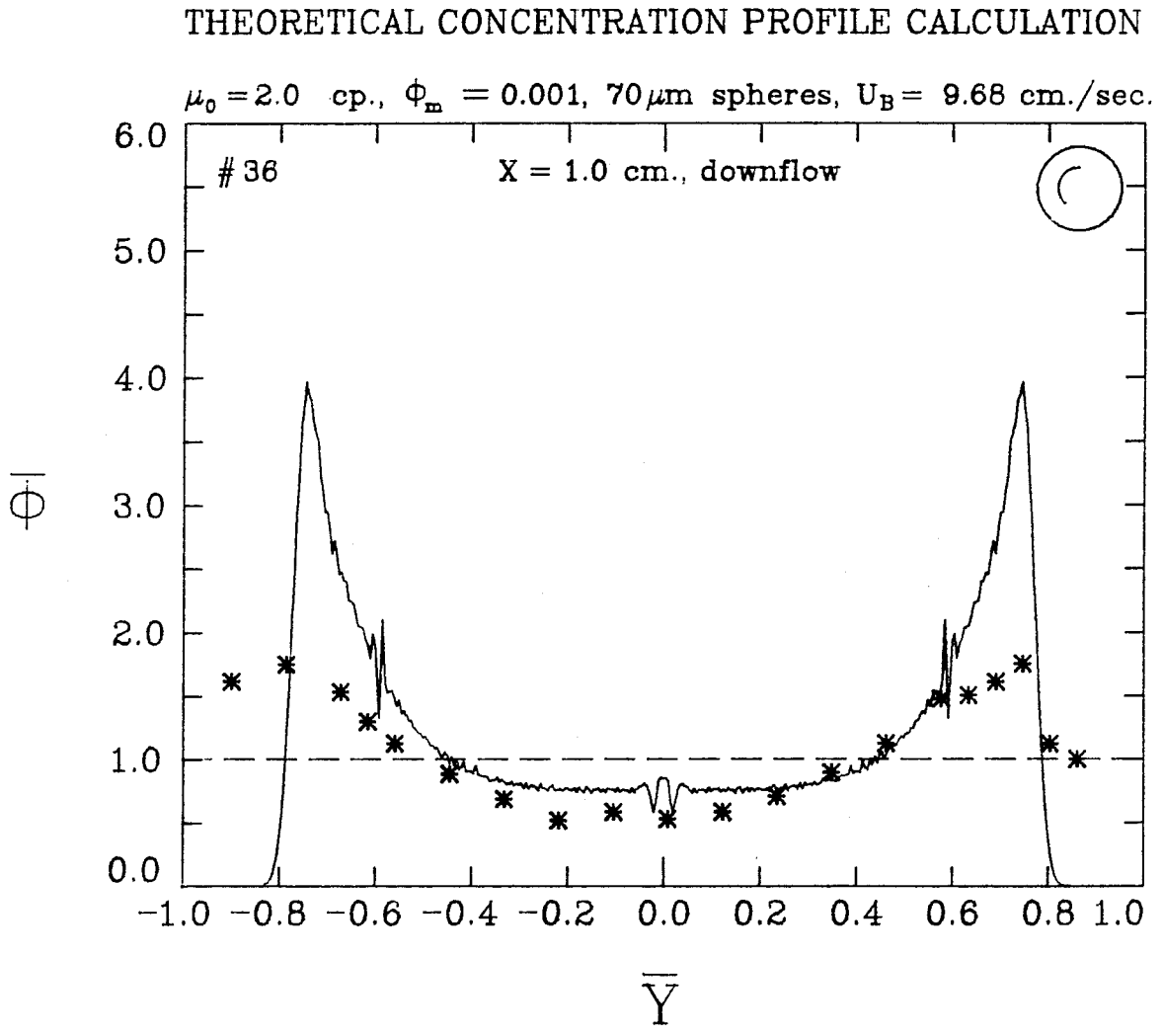
THEORETICAL CONCENTRATION PROFILE CALCULATION
$\mu_0 = 2.0$ cp., $\Phi_m = 0.001$, 70μm spheres, $U_B = 9.68$ cm./sec.
# 36
X = 1.0 cm., downflow
6.0
5.0
4.0
3.0
2.0
1.0
0.0
$\overline{\Phi}$
-1.0 -0.8 -0.6 -0.4 -0.2 0.0 0.2 0.4 0.6 0.8 1.0
$\overline{Y}$

Figure 2-37.

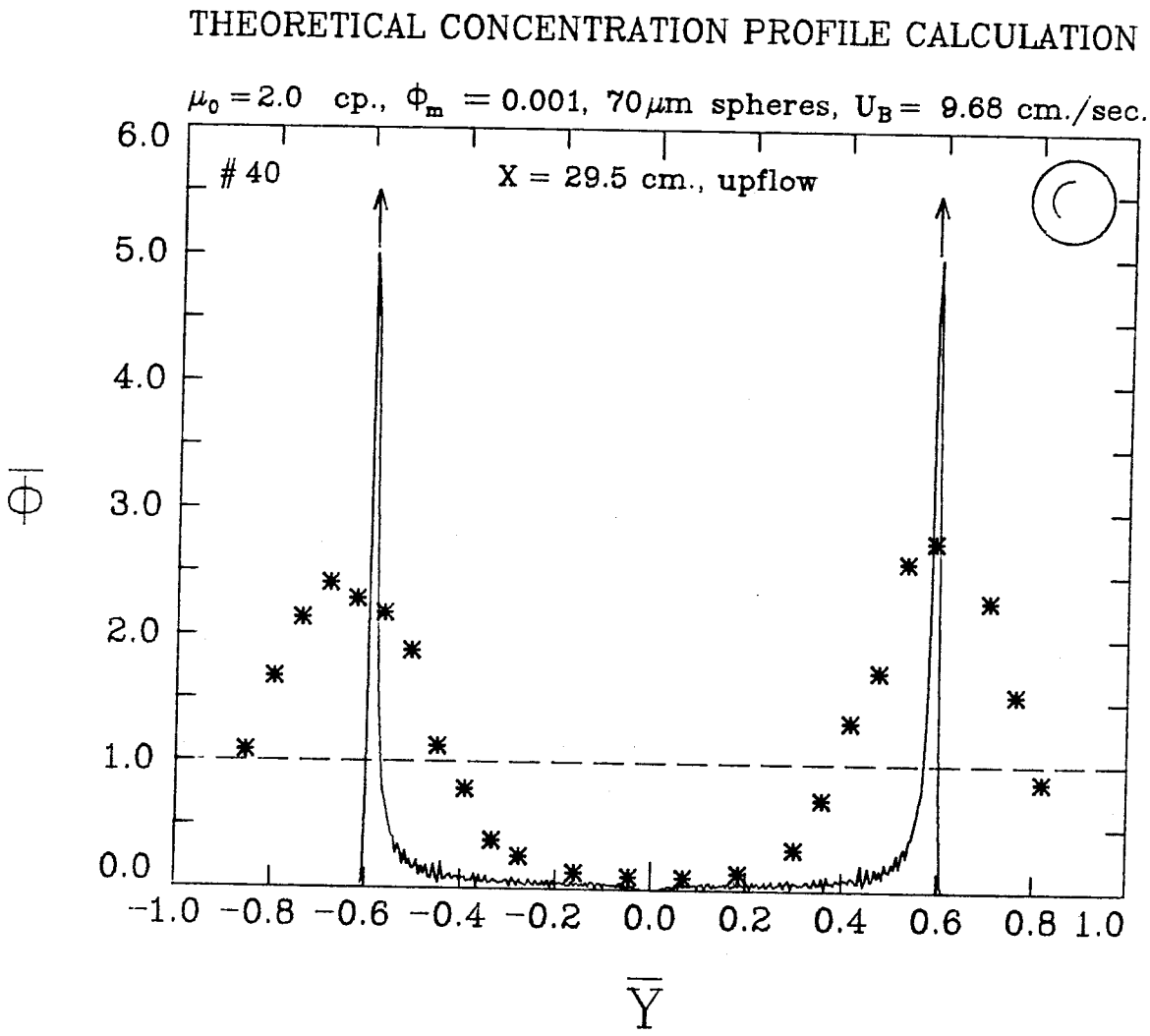
THEORETICAL CONCENTRATION PROFILE CALCULATION
$\mu_0 = 2.0$ cp., $\Phi_m = 0.001$, 70 μm spheres, $U_B = 9.68$ cm./sec.
# 40
X = 29.5 cm., upflow
$\overline{\Phi}$
6.0
5.0
4.0
3.0
2.0
1.0
0.0
-1.0 -0.8 -0.6 -0.4 -0.2 0.0 0.2 0.4 0.6 0.8 1.0
$\overline{Y}$

Figure 2-38.

2.7. REFERENCES

Adrian, R. J. 1980 *Laser Velocimetry*. Department of Theoretical and Applied Mechanics Report No. 442, University of Illinois, Urbana.

Bitbol, M. and D. Quemada 1981 *Revue Phys. Appl.* **16** , 663.

Bretherton, F. P. 1962 *J. Fluid Mech.* **14** , 284.

Chung, E. Y.-C. 1980 *Ph.D. Thesis*. California Institute of Technology.

Drain, L. E. 1980 *The Laser Doppler Technique*. John Wiley & Sons.

Durrani, T. S. and C. A. Greated 1977 *Laser Systems in Flow Measurement*. Plenum Press.

Durst, F., A. Melling, and J. H. Whitelaw 1976 *Principles and Practice of Laser-Doppler Anemometry*. Academic Press.

Ho, B. P. and L. G. Leal 1974 *J. Fluid Mech.* **65** , 365.

Lee, S. L. and J. Srinivasan 1978 *Int. J. Multiphase Flow* **4** , 141.

Maude, A. D. and J. A. Yearn 1967 *J. Fluid Mech.* **30** , 601.

Perry, R. H. 1973 *Chemical Engineers' Handbook*. McGraw-Hill.

Repetti, R. V. and E. F. Leonard 1966 *Chem. Eng. Prog. Symp. Ser.* **62** , 80.

TSI Inc. 1982 *Model 1980B Counter Type Signal Processor Instruction Manual*. Thermosystems Inc.

Schlichting, H. 1955 *Boundary Layer Theory*. McGraw-Hill.

Tachibana, M. 1973 *Rheol. Acta*, **12** , 58.

Vasseur, P. and R. G. Cox 1976 *J. Fluid Mech.* **78** , 385.

3. CONCENTRATED SUSPENSIONS

3.1. INTRODUCTION

This chapter contains experimental velocity and concentration profiles for concentrated suspensions of 27, 50, and 70 μm diameter neutrally-buoyant polystyrene spheres flowing in a rectangular channel. Experimental methods and apparatus are discussed only as they differ from the dilute-suspension experiments (the differences are minor). The experimental results are presented and discussed, and then compared to a model velocity profile calculation and previous experimental data.

3.2. EXPERIMENTAL METHODS AND APPARATUS

3.2.1. EXPERIMENTAL METHODS

The main change in experimental method necessary for making measurements in concentrated suspensions was matching the refractive indices of the spheres and the suspending fluid. This match was needed to improve the transmission of the incident and scattered laser light through the suspension. It was not possible to make the suspensions completely transparent by this matching (although they were nearly so). The match was good enough that adequate Doppler signals could be obtained at moderate concentrations ($\Phi_m \approx 0.10-0.25$), however.

Figure 3-1 shows the visual effect of the refractive index matching on a suspension of polystyrene spheres. In Figure 3-1a, a photomicrograph of the spheres suspended in a fluid with refractive index $n_D^{20}=1.5873$ is shown, and in Figure 3-1b the spheres are shown suspended in a fluid with $n_D^{20}=1.5903$, which very nearly matches the refractive index of the spheres. (These photomicrographs may be compared with a photomicrograph of the dry spheres, Figure 2-8.) The change in refractive index of the fluid from 3-1a to 3-1b is only 0.2%, but

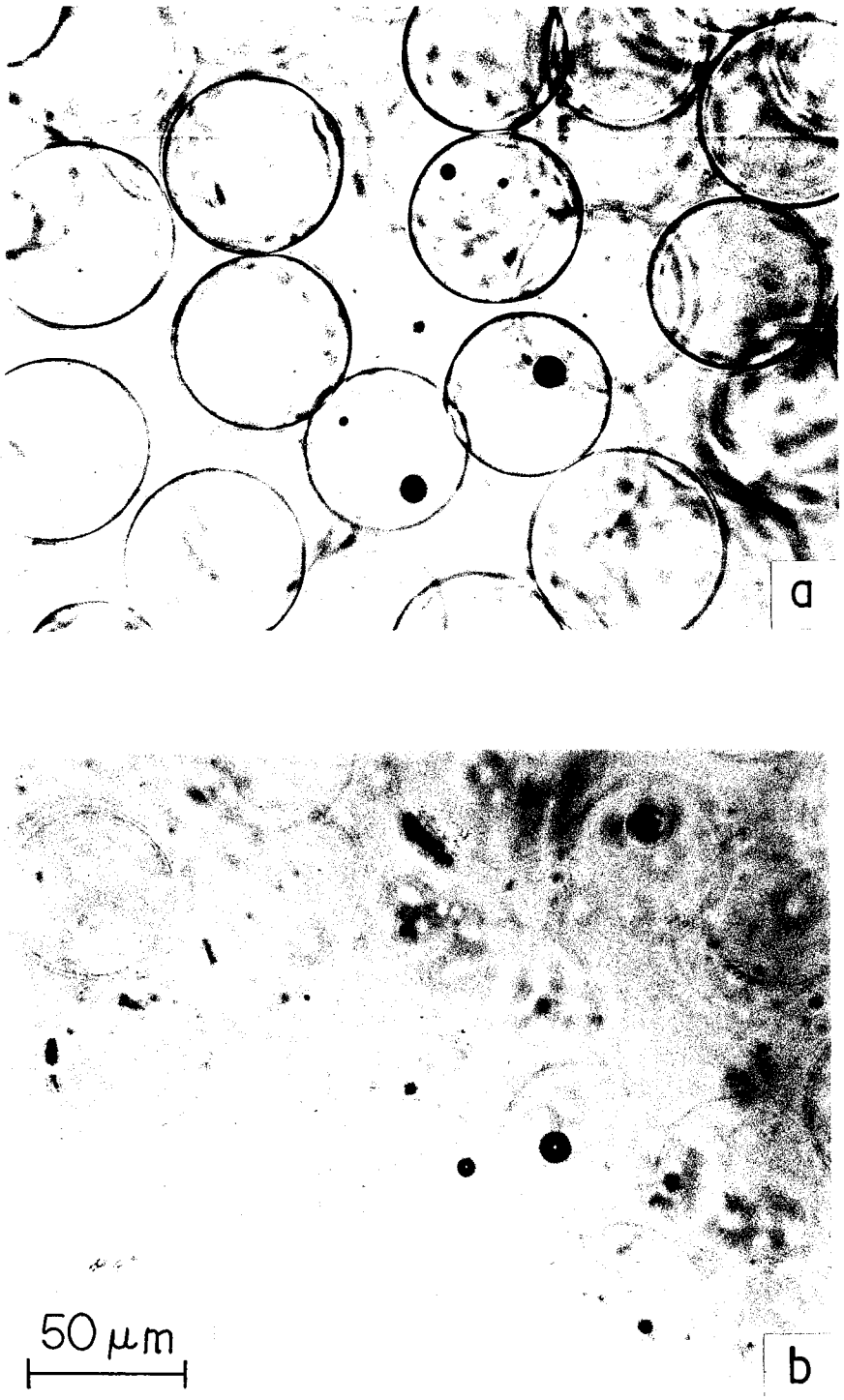

Figure 3-1. Photomicrographs of 50 micron diameter spheres suspended in a fluid with: a. n_D=1.5873, b. n_D=1.5903.

the change causes the spheres to change from being clearly visible to nearly invisible. This figure qualitatively illustrates the accuracy of matching necessary to produce a transparent suspension.

Another change in experimental method for the concentrated-suspension experiments was that the amplitude threshold for discrimination of the bursts to be counted (see section 2.2.2) was raised somewhat, so that the signals from only a small fraction of the particles were used for velocity measurement. This change was required because in the concentrated suspensions, even with the refractive index match the scattered light from the particles passing through the measurement volume was frequently rescattered by other particles on its way out of the flow channel. By using amplitude discrimination, and also by requiring a minimum number of cycles per signal, only signals with a relatively high signal-to-noise ratio (S/N) that had not been rescattered were used to measure the velocities (see Durst et al., 1976; p. 252).

3.2.2. EXPERIMENTAL APPARATUS

The only difference in the laser-Doppler system for the concentrated-suspension experiments was the use of a narrower slit in front of the photomultiplier tube. A narrower slit was needed because the laser beam intersection image was smaller for the concentrated-suspension experiments, due to the higher refractive index of the fluid used for the these experiments. This change in n_D^{20} caused a smaller change in angle when the scattered light crossed the liquid/glass interface at the flow channel wall, thus reducing the size of the beam intersection image, see Figure 3-2. This figure is a ray-tracing diagram which shows how the size of the image of the beam intersection outside of the flow channel changed when the concentrated-suspension fluid (new) was used instead of the dilute-suspension fluid (old). (This figure is an enlarged top view of part of Figure 2-1.) The new slit width was 0.11 mm. The ratio of the slit

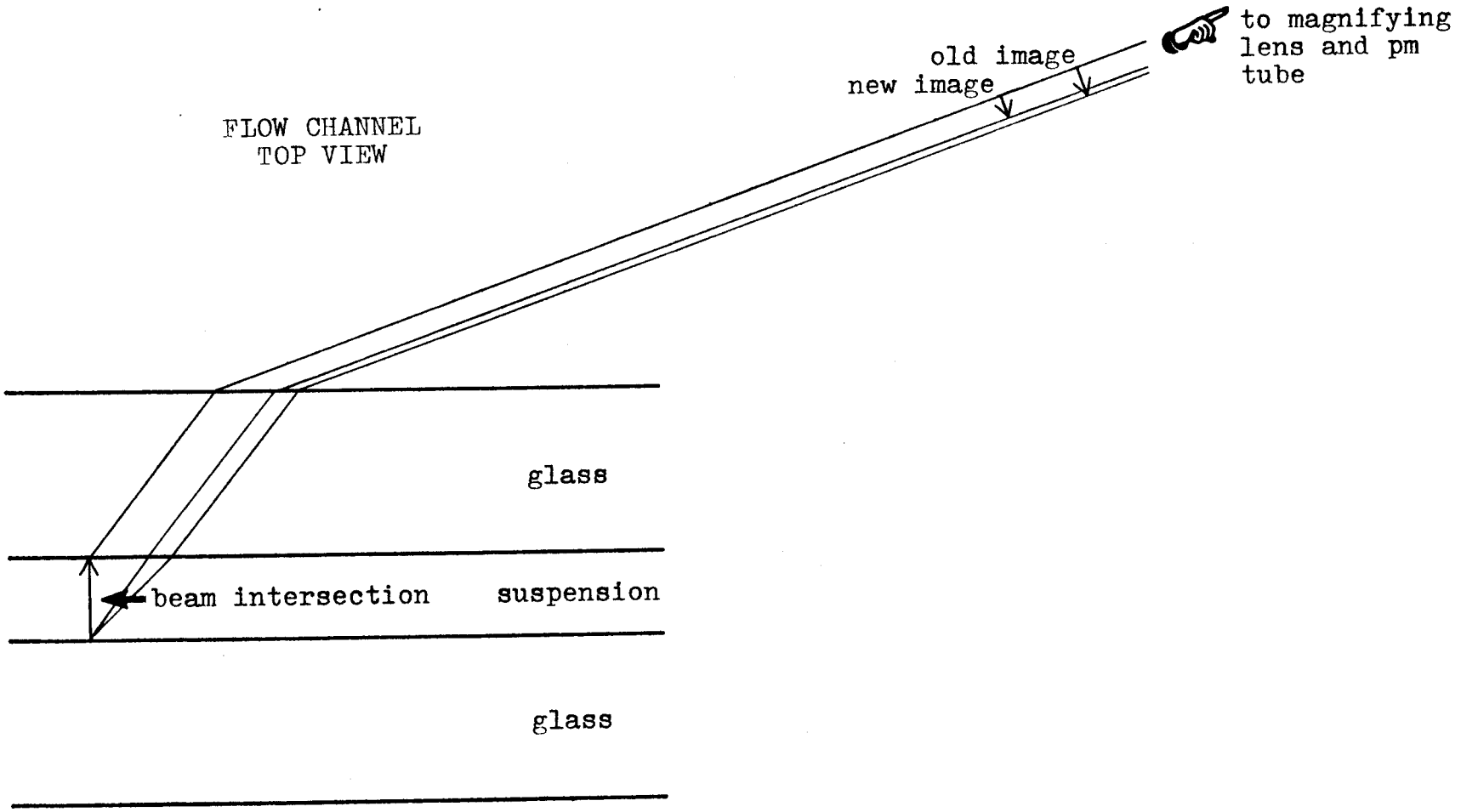

Figure 3-2. Illustration of change in beam intersection size with change in fluid refractive index (not to scale).

width to the beam intersection width was 0.041. Thus each measurement was an average taken over 4.1% of the channel spacing d.

The spacing between the flow channel walls was changed slightly to 0.0725 cm. from the 0.0798 cm. spacing used for the dilute-suspension experiments. This change (unintentionally) occurred when the flow system was re-glued to repair leaks. The rubber gaskets in the flow system were replaced with Viton seals, which did not absorb the suspending fluid appreciably, as the rubber seals did.

One experiment was done with a modified flow channel entry section. This modification is shown in Figure 3-3, a scale drawing of the entry section. The entry was modified by cutting along the dashed lines, thus producing a 45 degree angle at the channel entry, instead of an angle of almost 90 degrees in the unmodified entry.

Concentrated suspensions were made using the same 26.7 +/- 4.4 μm and 50.1 +/- 8.7 μm diameter spheres used for the dilute suspensions. A different larger particle size was used for the concentrated suspensions, however. These larger spheres were also made of polystyrene-divinylbenzene and were sized by sieving between 150 and 200 mesh. The approximate average diameter of these spheres, as determined by microscopy, was 70 +/- 17 μm. A photomicrograph of these larger spheres appears in Figure 3-4, which is on page 25. The fluorescent tracer spheres used for the concentrated 70 μm sphere suspensions were the same as the 70 μm diameter spheres used for the dilute suspension experiments, however (70 +/- 7 μm). These spheres were used as tracers because their more narrow size distribution yielded more accurate concentration measurements than tracers with a broad size distribution.

The suspending fluid was a mixture of 69.3% 1-methylnapthalene, 12.2% 1-chloronapthalene, and 18.5% Union Carbide UCON oil 75-H-90,000. The compo-

CUTAWAY SIDE VIEW
4x actual size

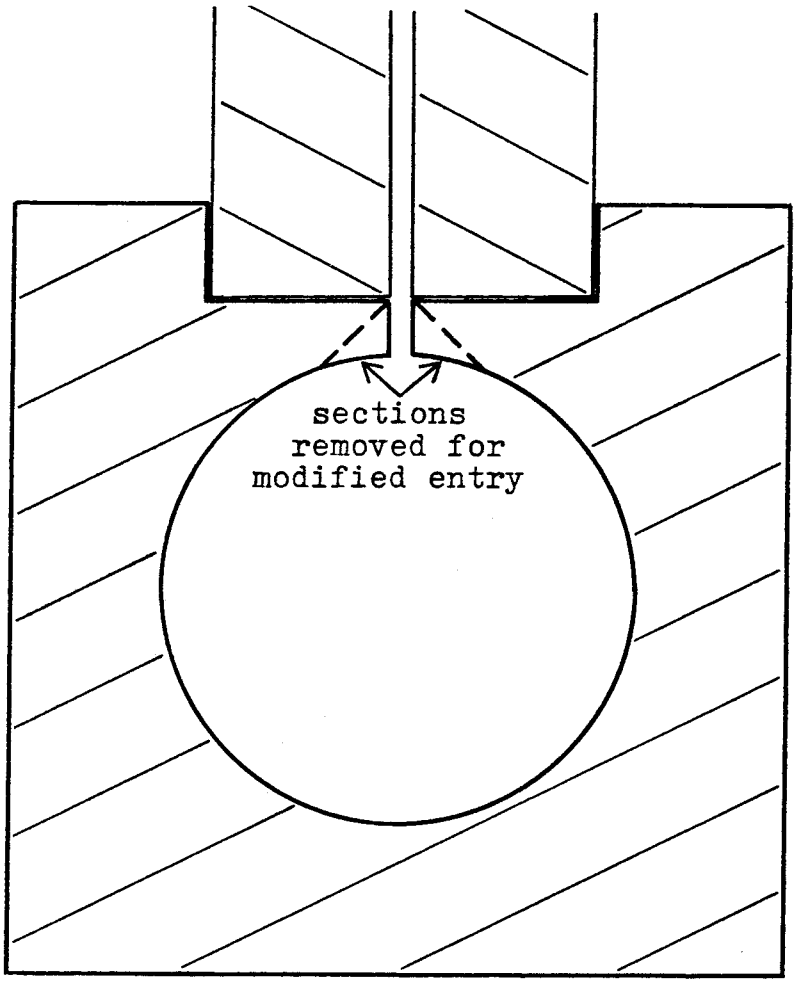

Figure 3-3. Modified flow channel entry section.

sition of the fluid was such that it matched the sphere density of 1.052 g./cm.^{3} and the sphere refractive index n_D^{20} of 1.590. The approximate composition of a fluid which had the above properties was calculated by assuming that the individual densities and refractive indices of the component fluids combined in a linear manner to form the density and refractive index of the mixture. The fluid composition was then adjusted until the appropriate density and refractive index were obtained. The viscosity μ_0 of the fluid was 92.9 centipoise at 21.0 degrees Centigrade.

The procedure for preparing the suspensions was as follows. A 140 ml. sample of the suspending fluid was first measured into a beaker on an magnetic stirrer. Then a weighed amount of particles, including 0.2 g. of the fluorescent dyed spheres, was added slowly to the fluid with constant stirring. The fluorescent particles comprised 0.14% of the total suspension volume. After all of the spheres had been added, the mixture was stirred until it was well mixed, about 10 minutes. The suspension was then allowed to stand for 10-15 minutes, so that any air bubbles present in the mixture would rise to the top. Following this, the suspension was restirred briefly and introduced into the flow system. The fluorescent dye was not found to dissolve significantly in the suspending fluid over the length of time needed to perform an experiment, which was about 3 hours. The experiments were usually done on the same day that the suspensions were prepared.

3.3. EXPERIMENTAL RESULTS AND DISCUSSION

Table 3-1 is a list of all experiments that were done in the concentrated-suspension regime, along with the conditions for each experiment. The variables are as defined in section 2.3. For all experiments, μ_0 was 92.9 centipoise, and U_B was 2.1 cm./sec. Only one U_B was used since the measurements were expected to be independent of U_B in the low Reynolds number regime being

examined.

Table 3-1

Number	2a (cm.×10^4)	2a/d	Φ_m	X (cm.)	Flow Direction	Re_p
41	27	0.037	0.02	29.5	up	8.9×10^{-5}
42	27	0.037	0.05	29.5	up	8.9×10^{-5}
43	27	0.037	0.10	29.5	up	8.9×10^{-5}
44	50	0.069	0.02	1.0	down	3.0×10^{-4}
45	50	0.069	0.02	29.5	up	3.0×10^{-4}
46	50	0.069	0.05	29.5	up	3.0×10^{-4}
47	50	0.069	0.10	29.5	up	3.0×10^{-4}
48	50	0.069	0.15	29.5	up	3.0×10^{-4}
49	50	0.069	0.20	1.0	down	3.0×10^{-4}
50	50	0.069	0.20	29.5	up	3.0×10^{-4}
51*	50	0.069	0.20	29.5	up	3.0×10^{-4}
52	50	0.069	0.25	29.5	up	3.0×10^{-4}
53	70	0.097	0.10	29.5	up	6.0×10^{-4}
54	70	0.097	0.25	29.5	up	6.0×10^{-4}

* (Modified flow channel entry was used)

The maximum values of Φ_m listed (0.10 for the 27 μm spheres and 0.25 for the 50 and 70 μm spheres) were the highest concentrations at which acceptable data were obtained. Above these concentrations, the standard deviations of the

individual velocity data points were judged to be too large for the data to be reliable. A higher maximum concentration was attainable for the larger spheres, because at a given Φ_m the number density of the larger spheres was much less than the number density of the smaler spheres. Thus the chance that the scattered light from a particle passing through the measurement volume would have been rescattered was less for the larger spheres at a given Φ_m, and for a given signal-to-noise ratio a higher maximum Φ_m was attainable.

Figures 3-5 to 3-18 are plots of normalized velocity ($\overline{U}$) and concentration ($\overline{\Phi}$) versus lateral position $\overline{Y}$. The format of the figures is as described in section 2.3.

Sample concentration error bars were calculated for one case, data set 54 (Figure 3-18) using the method described in section 2.4. For this data set, error bars are shown at $\overline{Y}\approx+/-0.6$ and $\overline{Y}\approx-0.1$. The data used to calculate these error bars were taken at the same time as the rest of the data for set 54.

In some cases, it was not possible to obtain an accurate polynomial curve-fit to the velocity data. For most of these cases, the curve-fit and the parabola are superimposed on the figures. Thus the shape of the velocity profiles should be determined by observing the velocity data points, rather than the curve-fit.

The velocity profiles for the 27 μm sphere suspensions are all basically parabolic, although there is some scatter in the data for the Φ_m=0.10 data set 43. The scatter in the velocity data points is apparently due to experimental scatter, and thus is not meaningful (note the relatively large error bars for this data set). The fact that parabolic velocity profiles were measured for these cases is in agreement with the results of Karnis et al. (1966), who found that for tube flow of neutrally-buoyant suspensions of spheres at low Re, the velocity profiles were parabolic for a/R=0.039 (almost the same as 2a/d=0.037 for the present experiments) and $\Phi_m<0.17$.

VELOCITY AND CONCENTRATION PROFILES

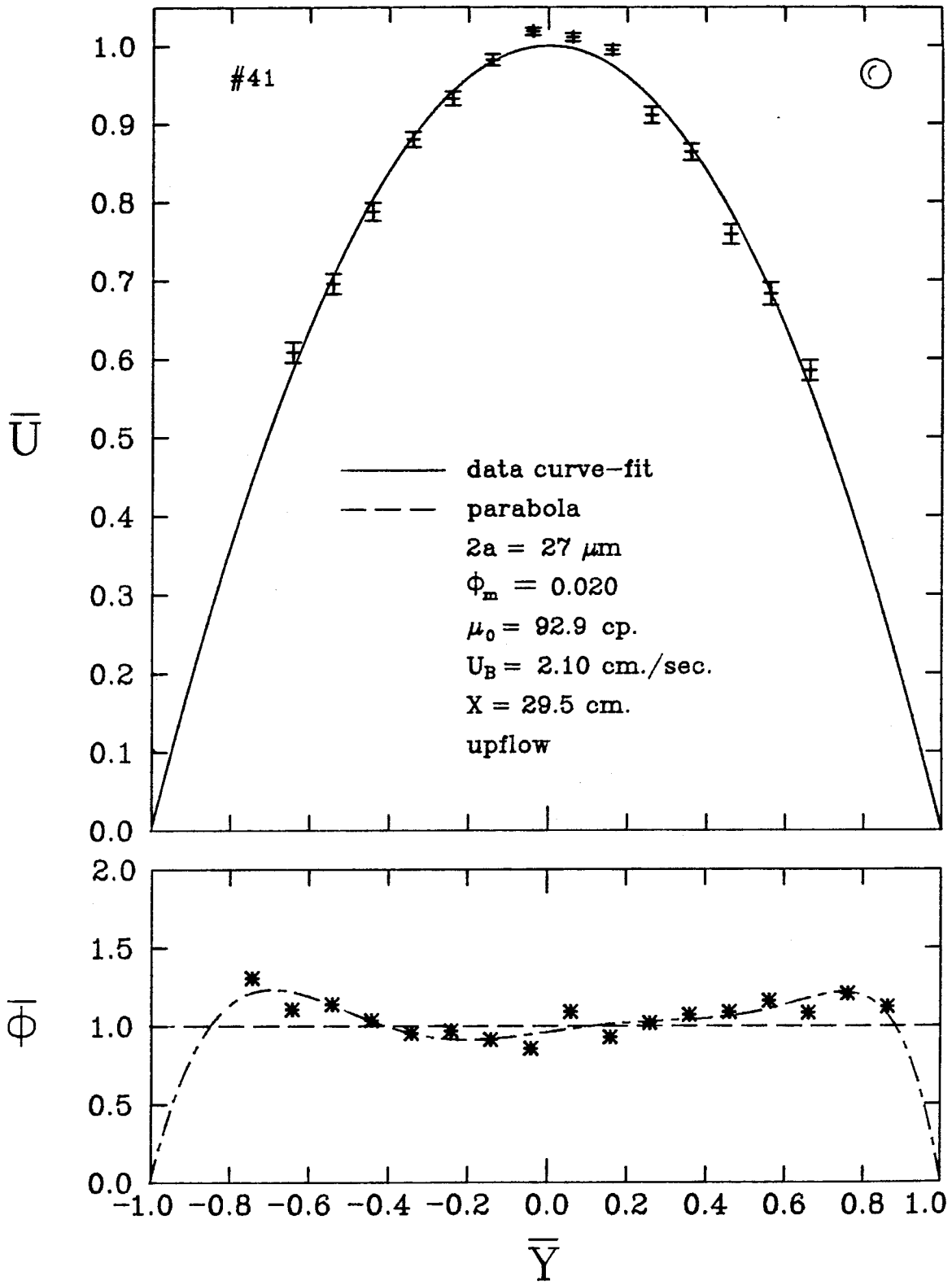

Figure 3-5.

VELOCITY AND CONCENTRATION PROFILES

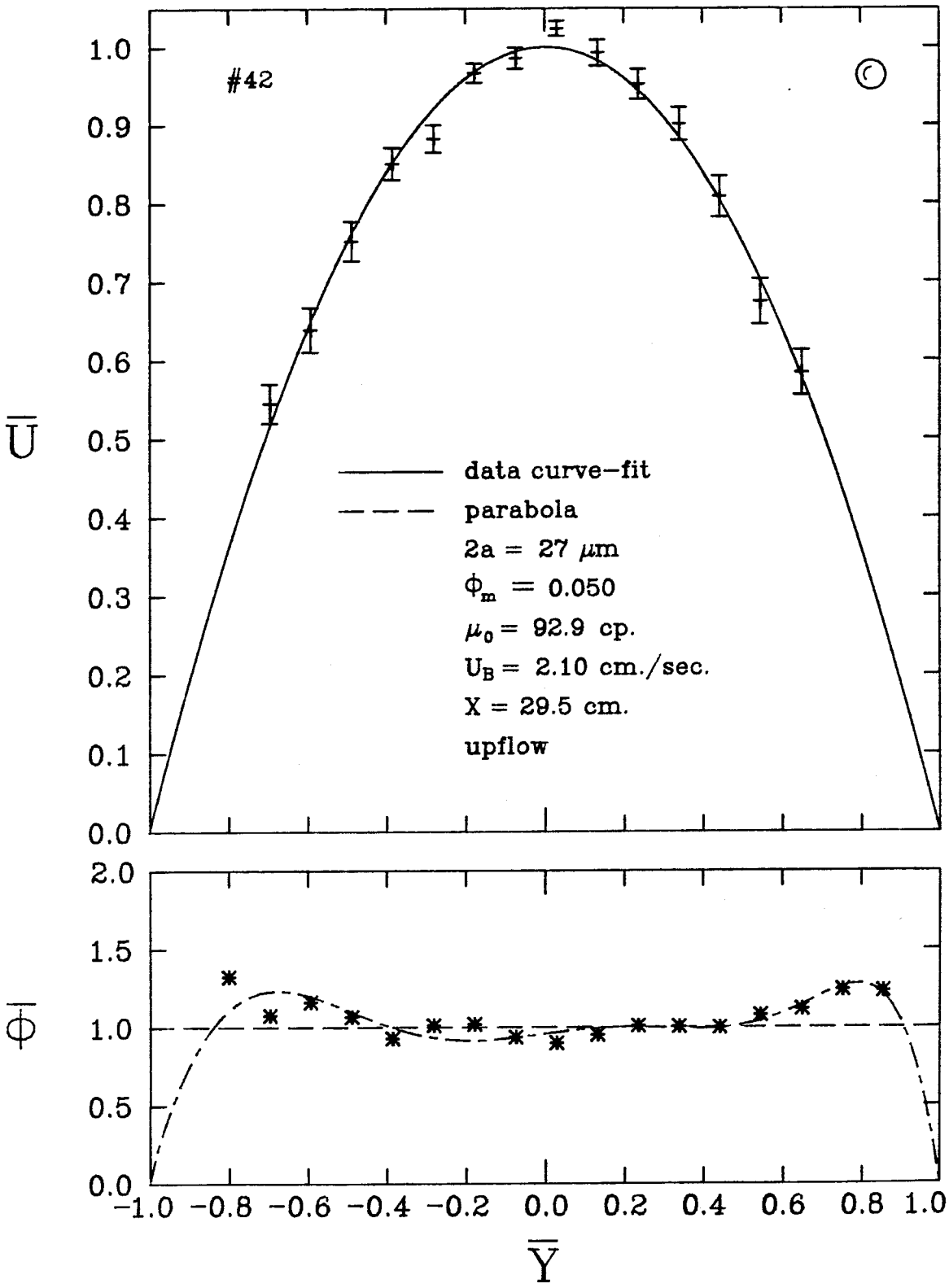

Figure 3-6.

VELOCITY AND CONCENTRATION PROFILES

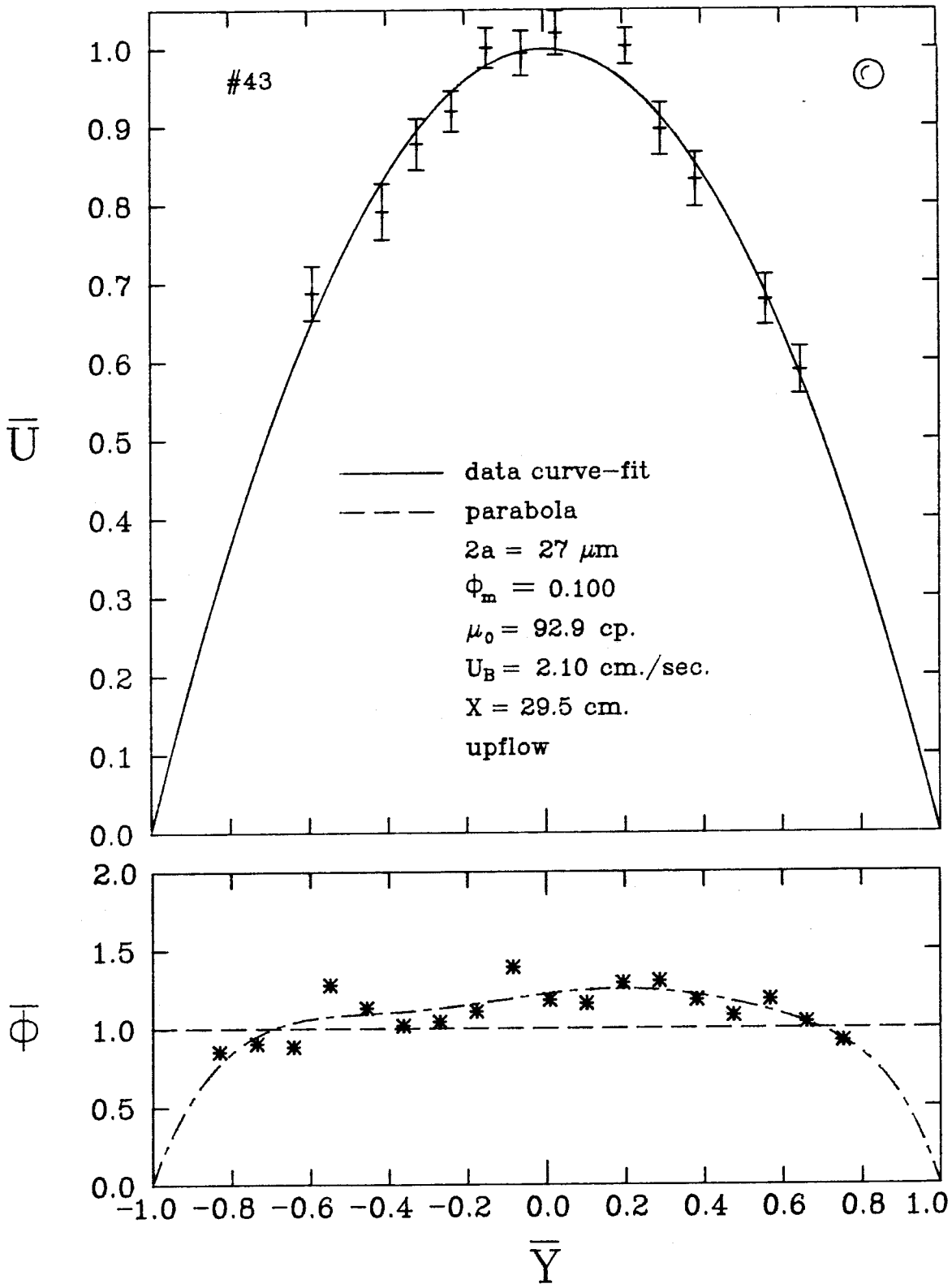

Figure 3-7.

VELOCITY AND CONCENTRATION PROFILES

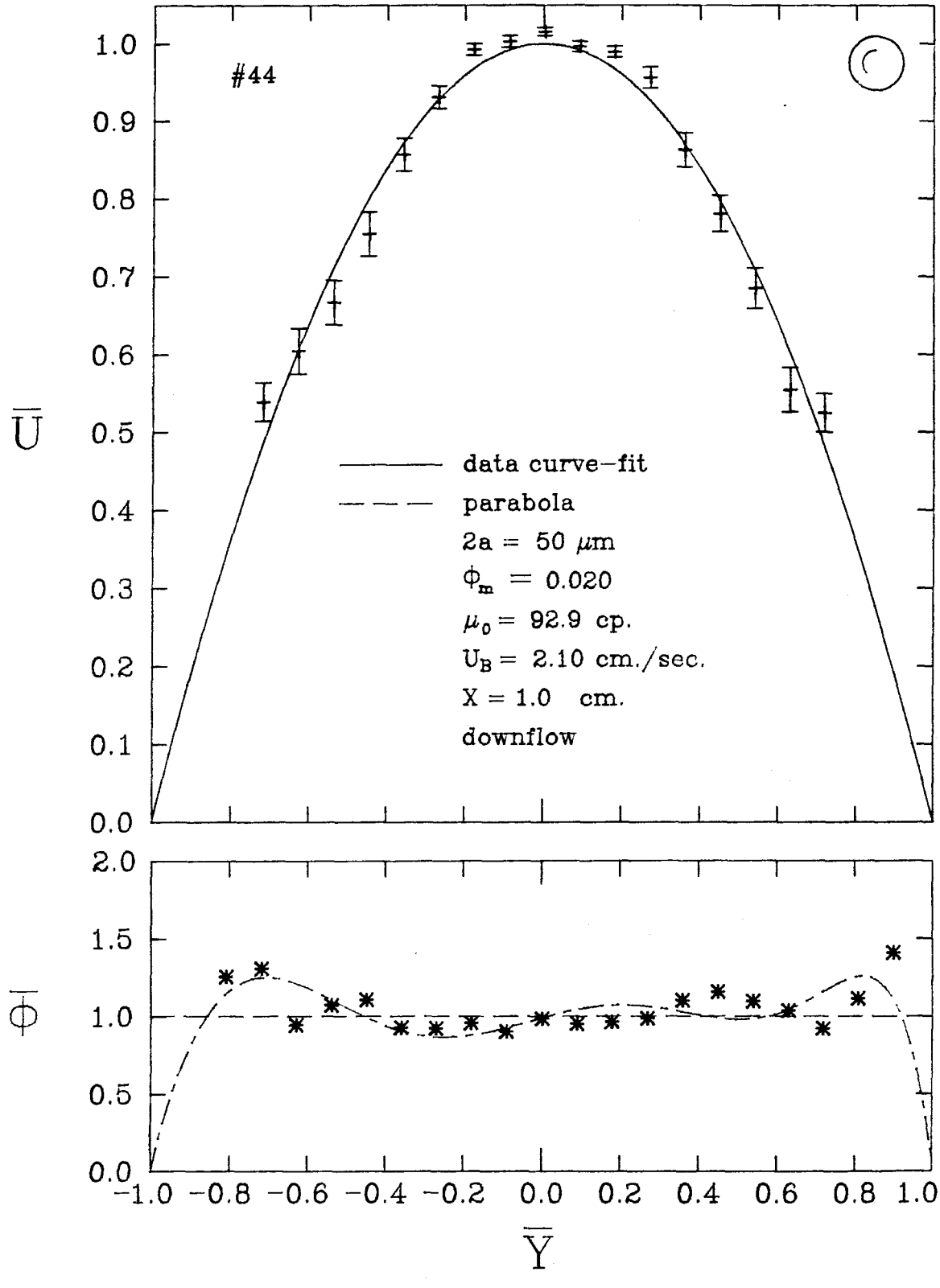

Figure 3-8.

VELOCITY AND CONCENTRATION PROFILES

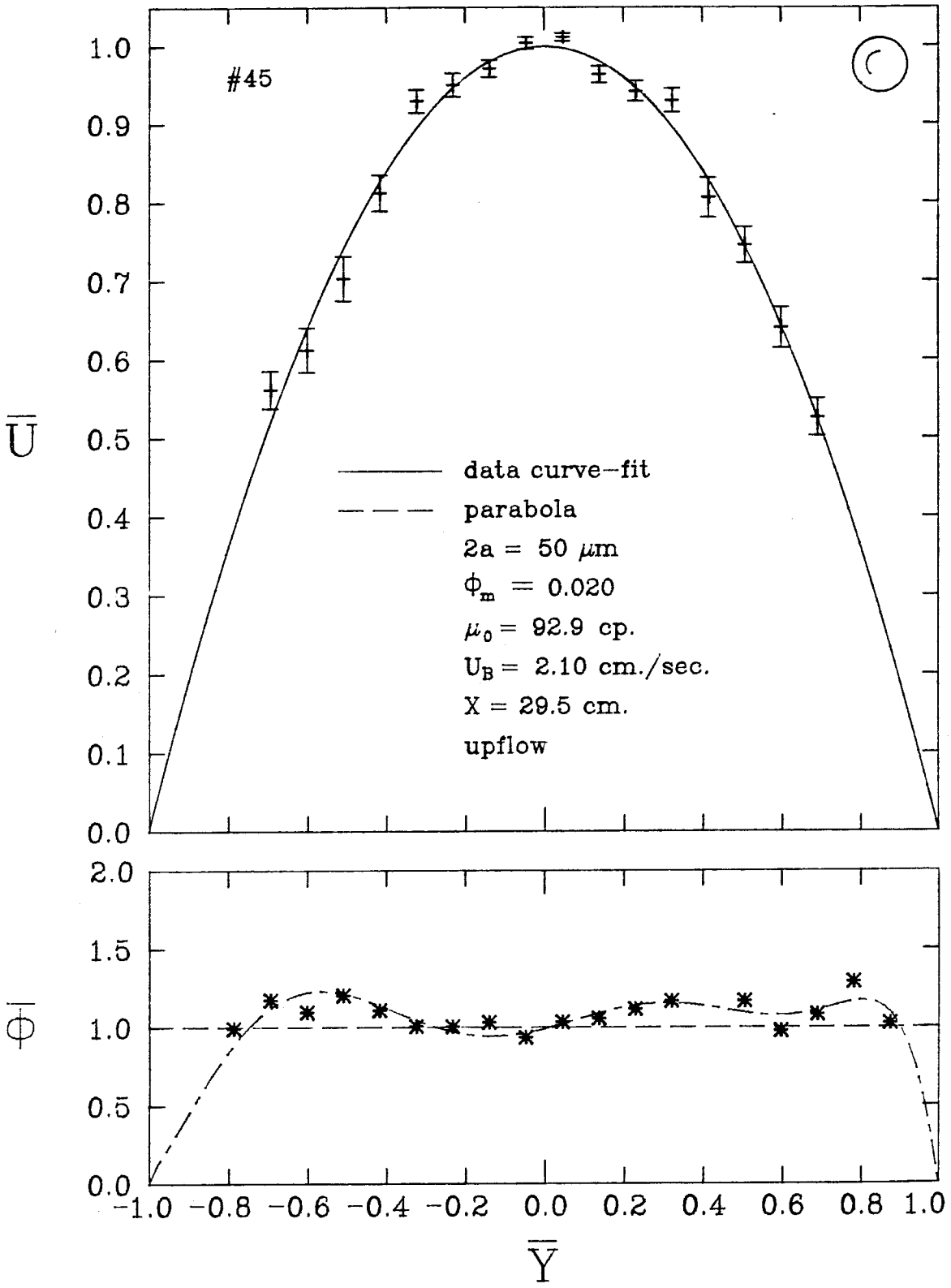

Figure 3-9.

VELOCITY AND CONCENTRATION PROFILES

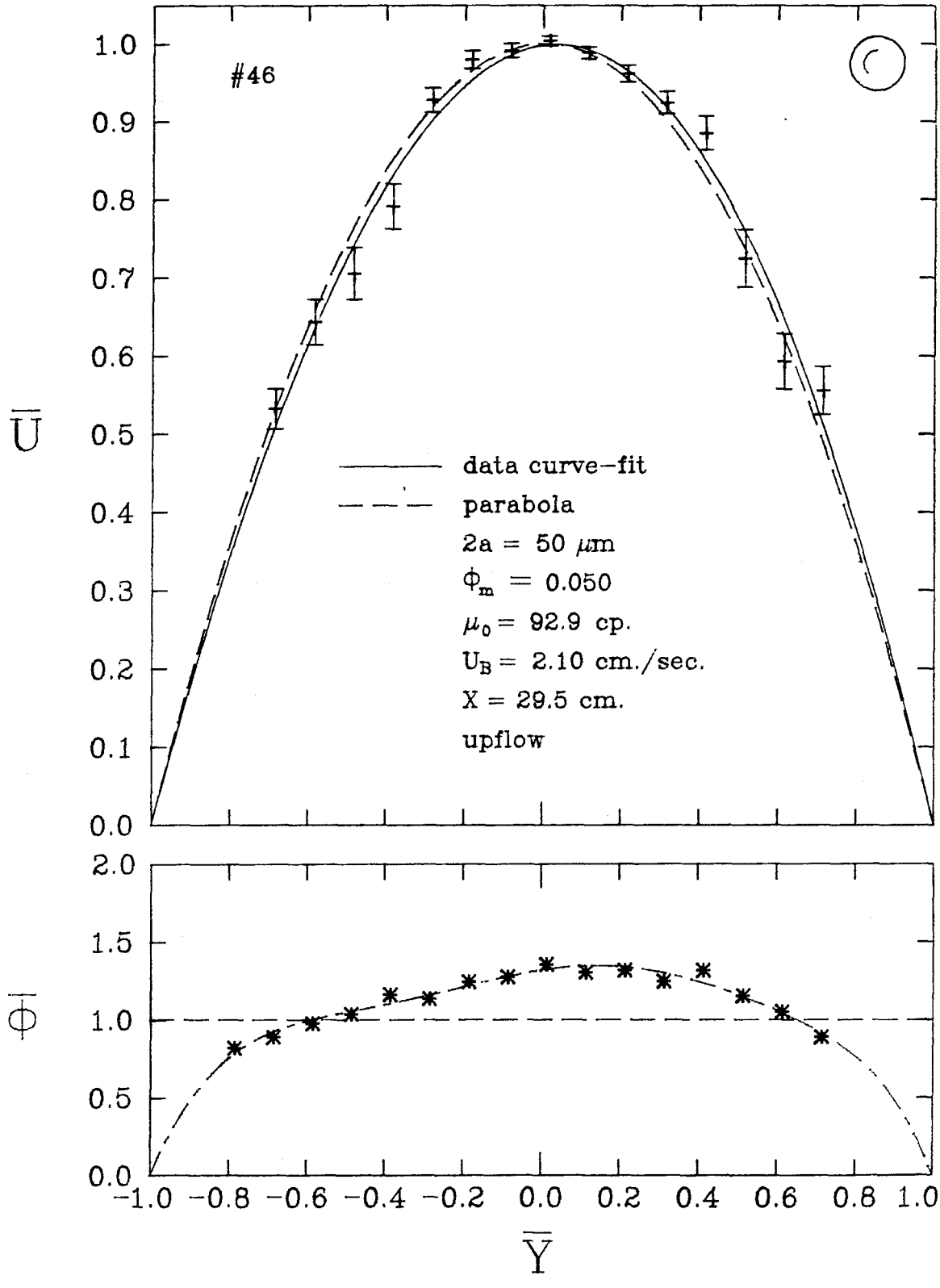

Figure 3-10.

VELOCITY AND CONCENTRATION PROFILES

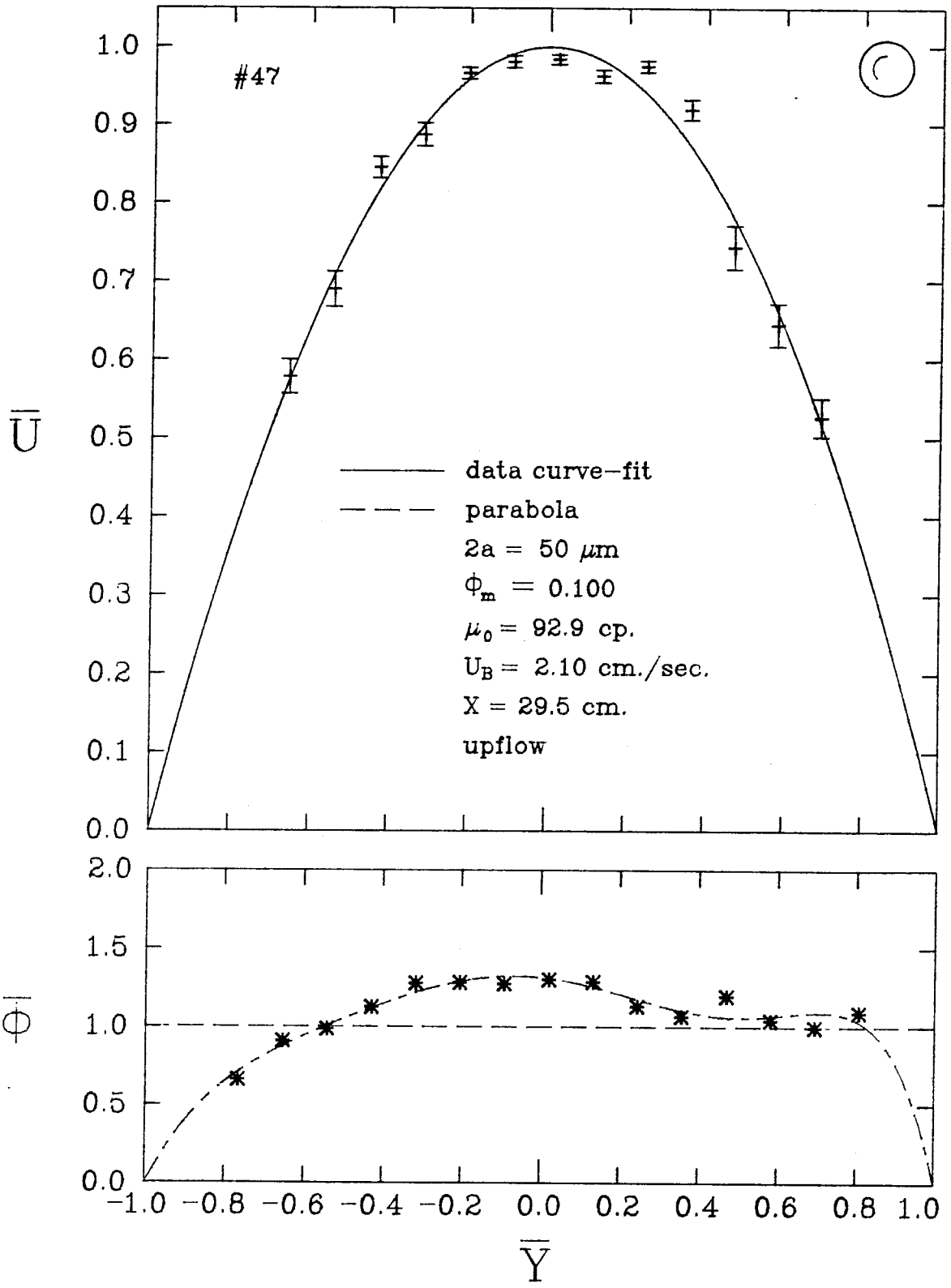

Figure 3-11.

VELOCITY AND CONCENTRATION PROFILES

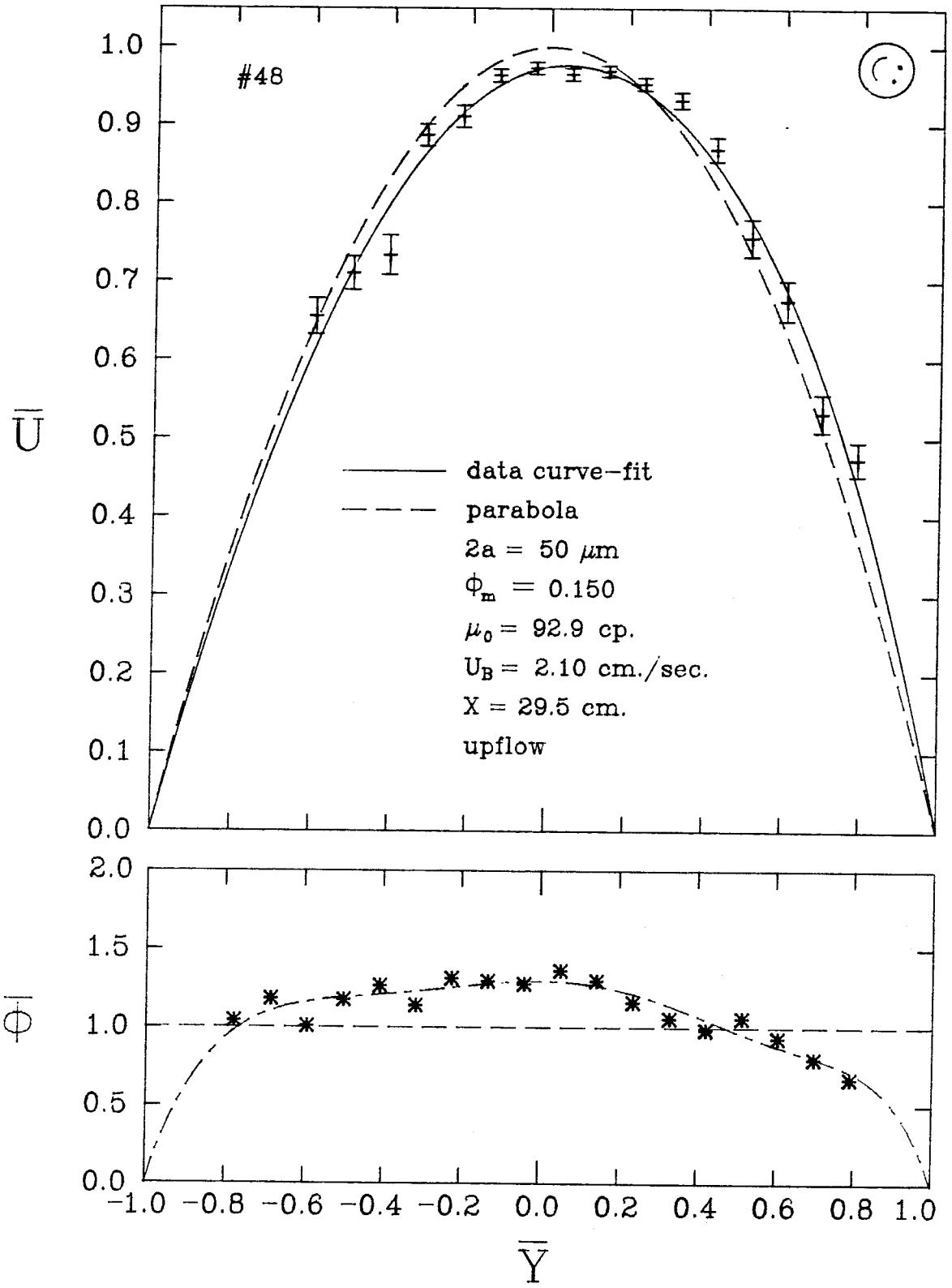

Figure 3-12.

VELOCITY AND CONCENTRATION PROFILES

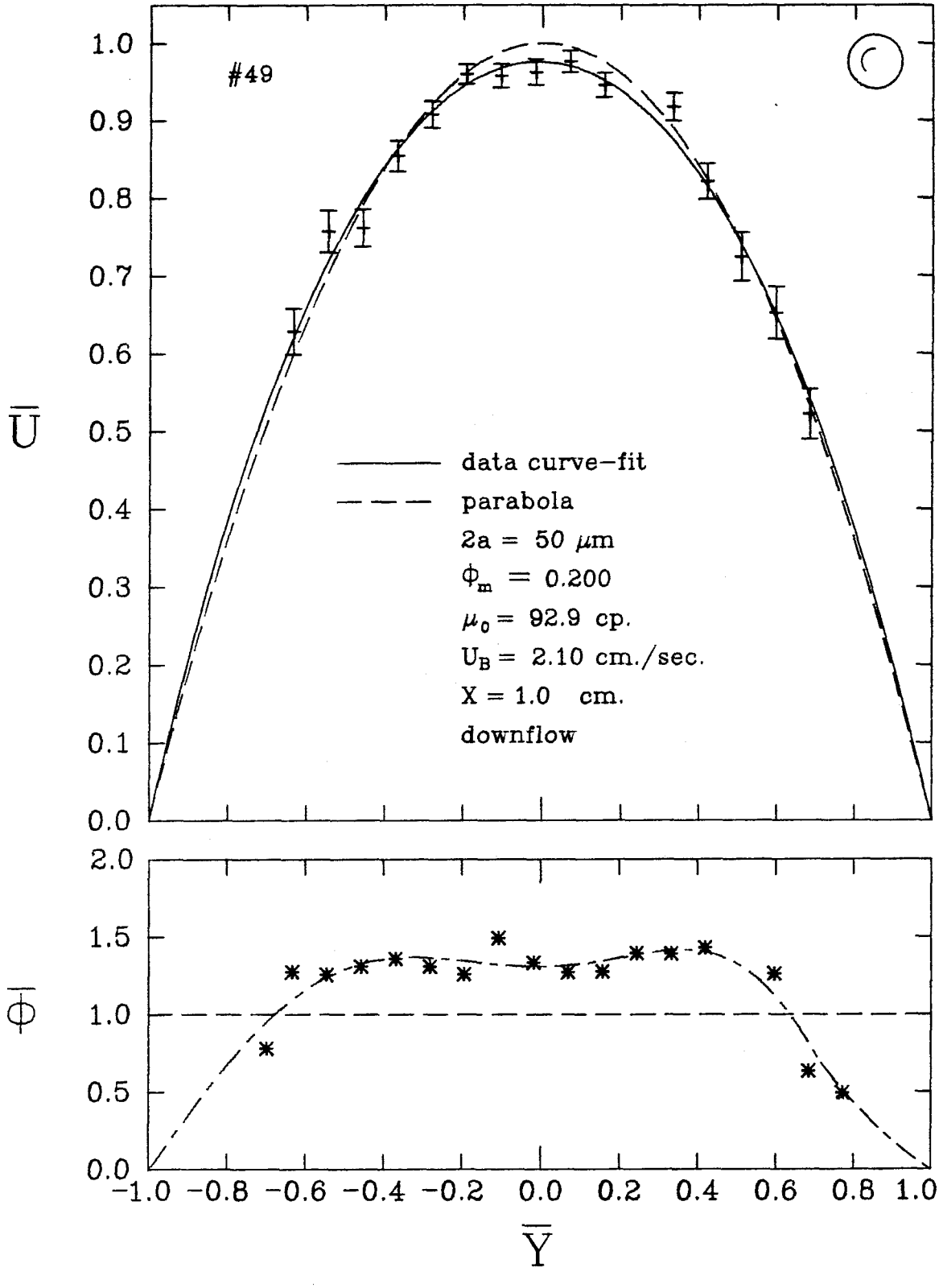

Figure 3-13.

VELOCITY AND CONCENTRATION PROFILES

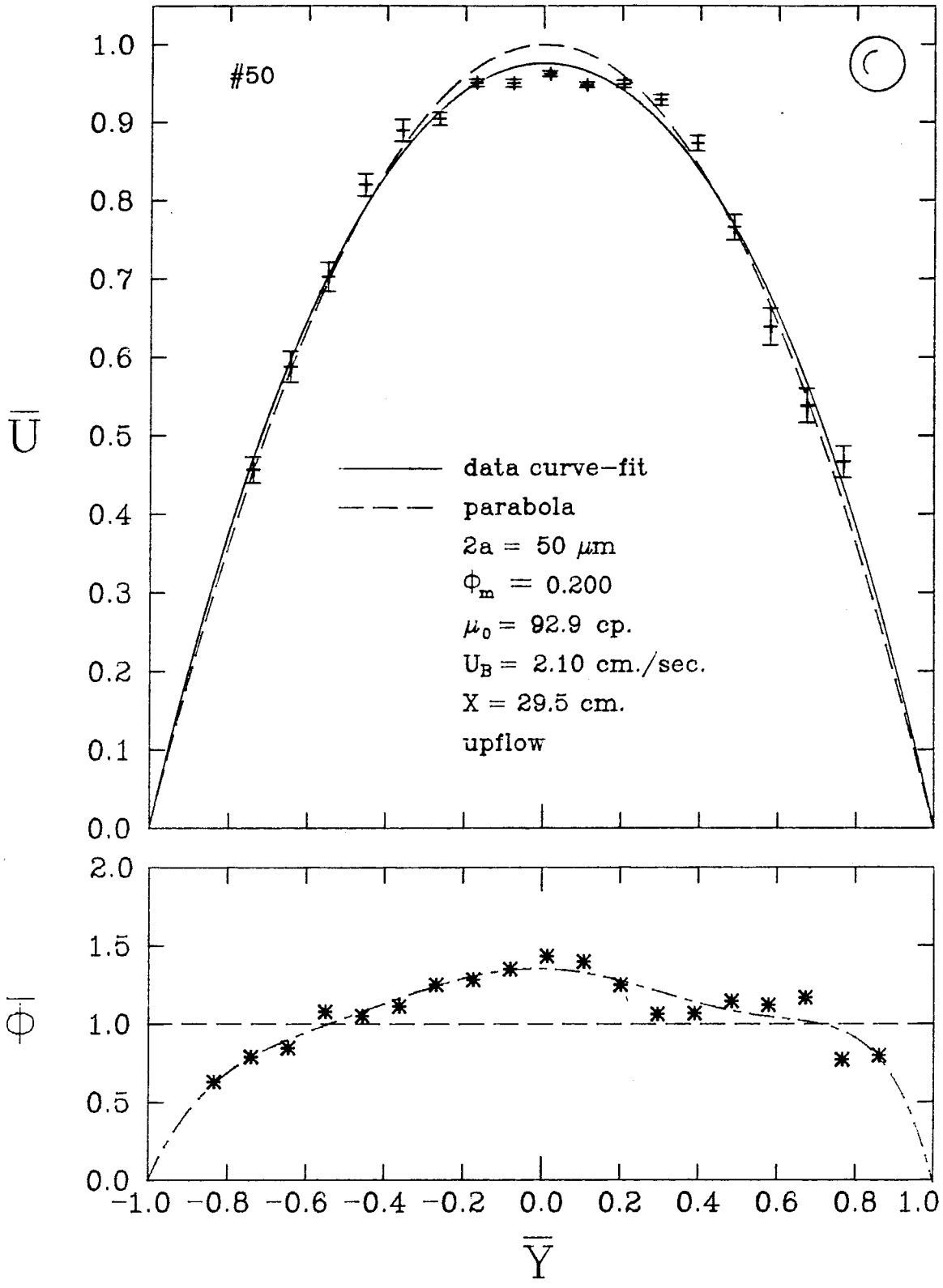

Figure 3-14.

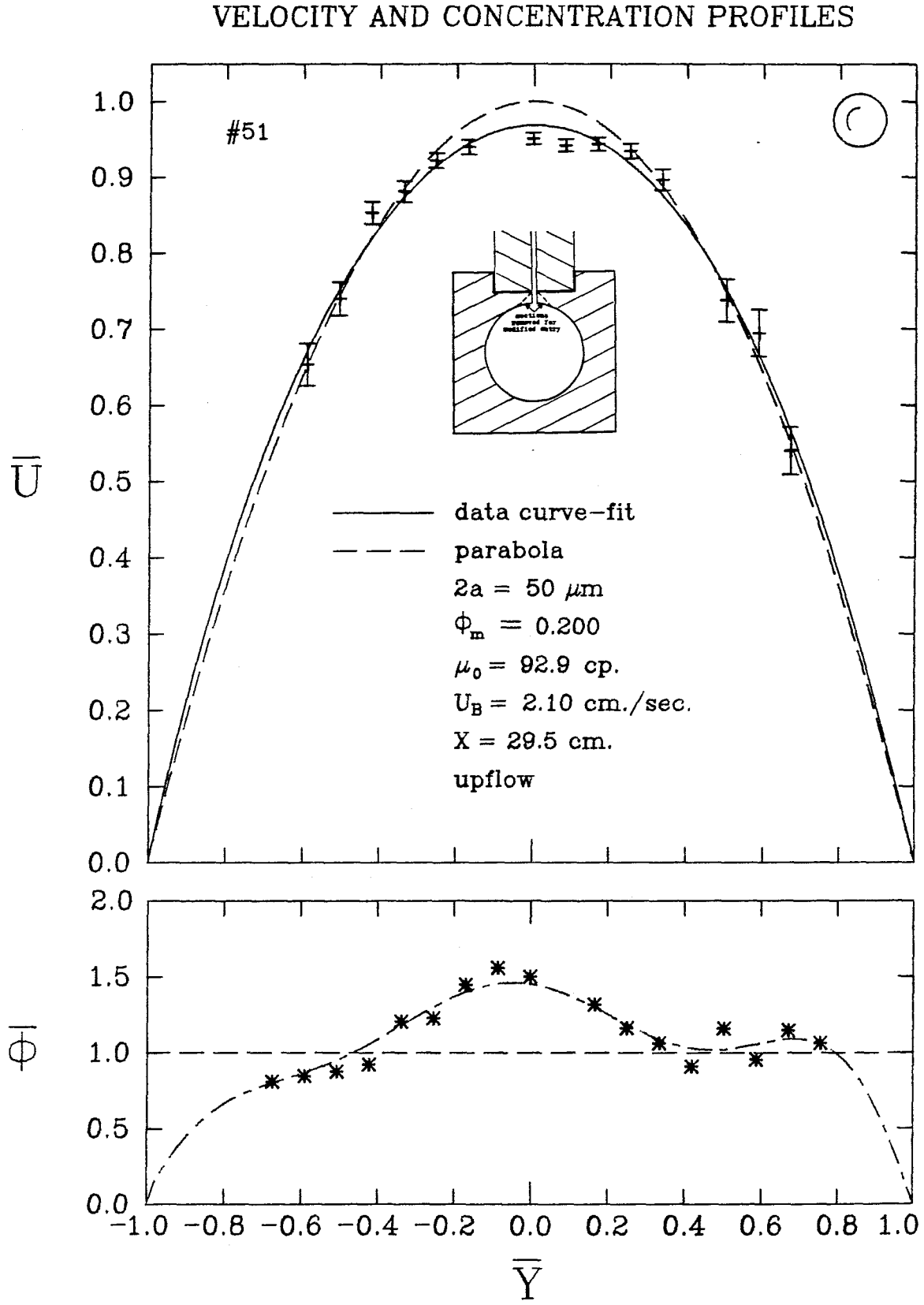

Figure 3-15. Velocity and concentration profiles for modified flow channel entry.

VELOCITY AND CONCENTRATION PROFILES

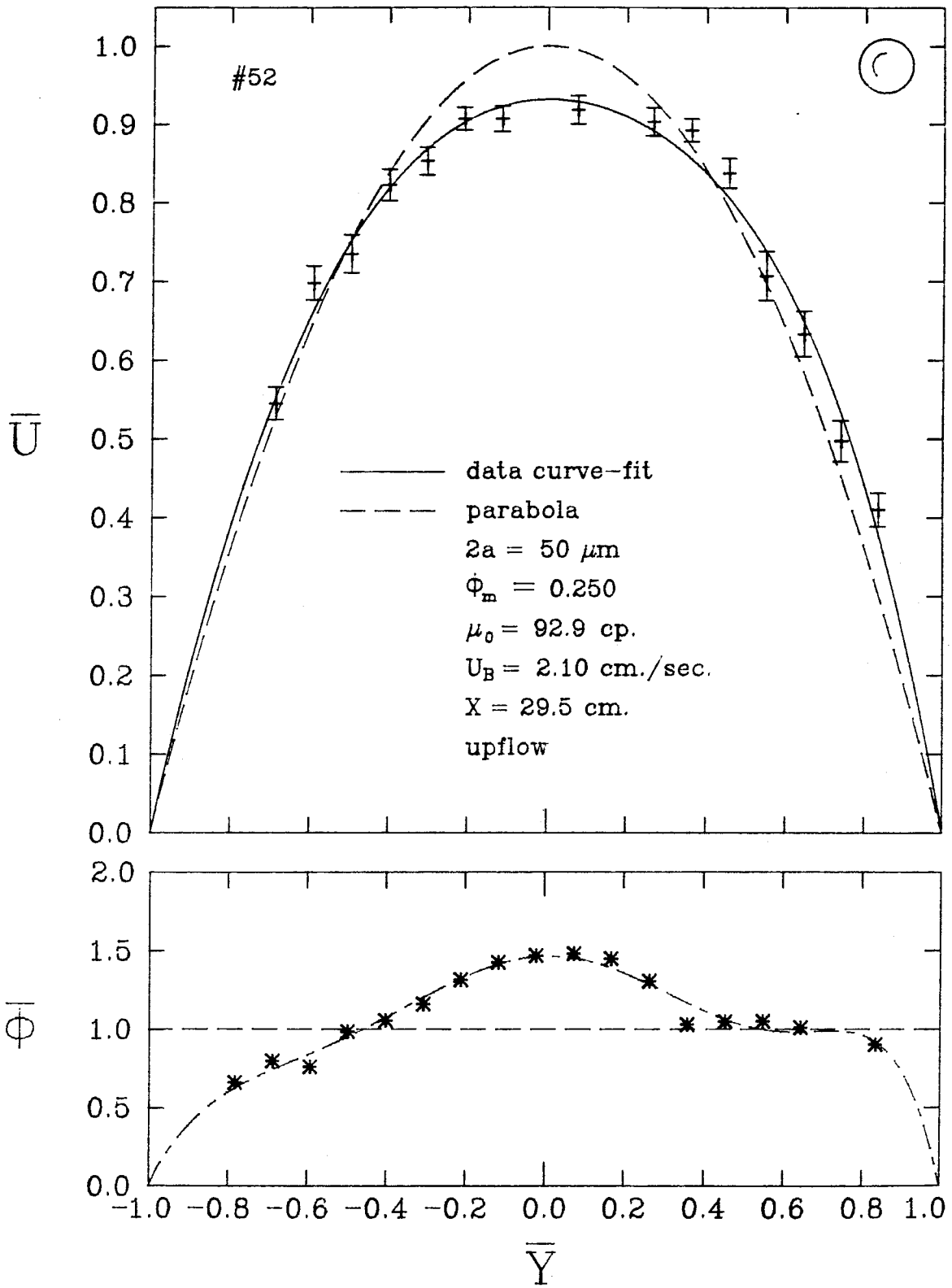

Figure 3-16.

VELOCITY AND CONCENTRATION PROFILES

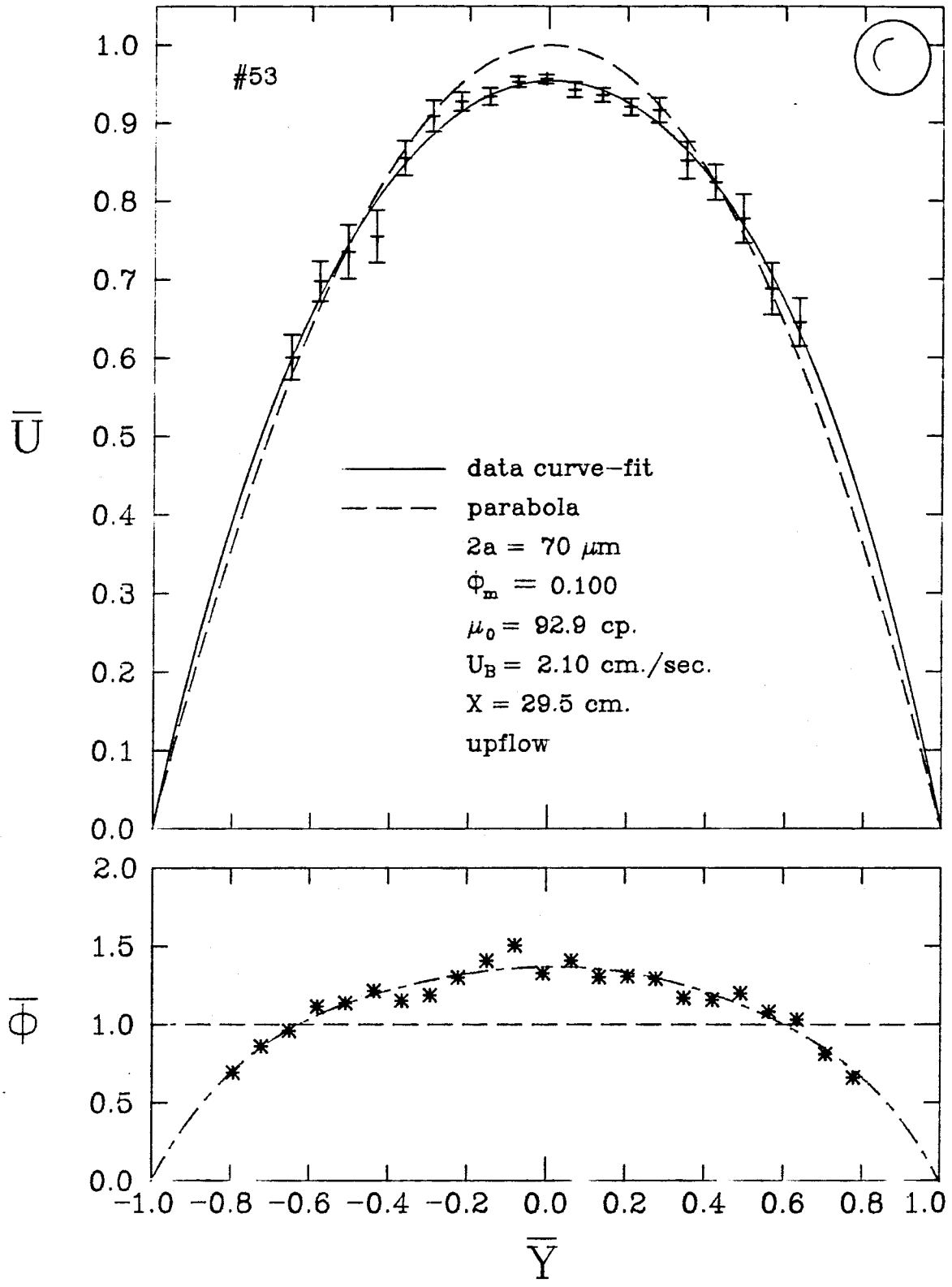

Figure 3-17.

VELOCITY AND CONCENTRATION PROFILES

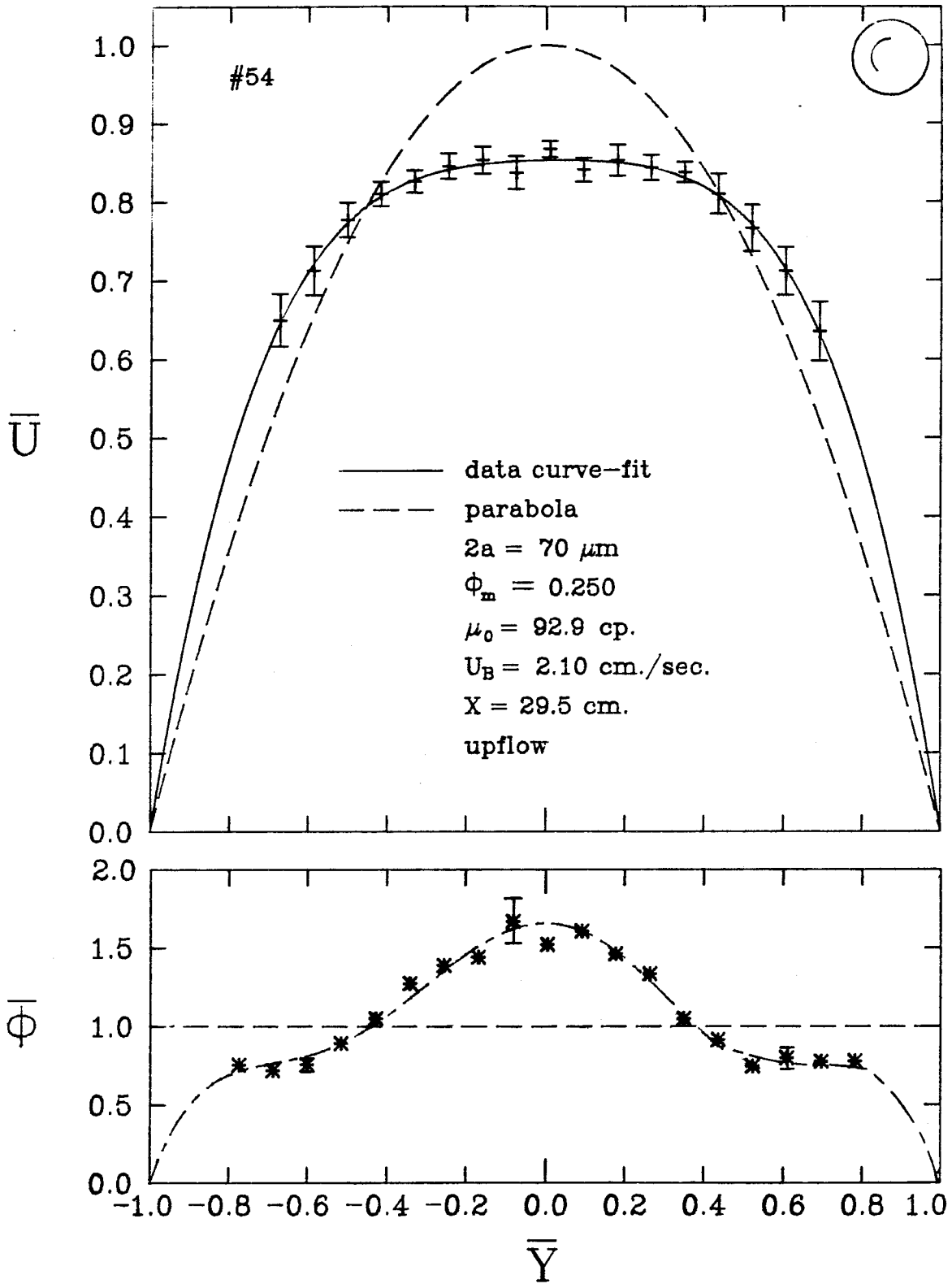

Figure 3-18.

The concentration profiles for the 27 μm diameter spheres are summarized in Figure 3-19. The profiles for Φ_m=0.02 and Φ_m=0.05 look like the corresponding dilute-suspension concentration profile (data set 1, Figure 2-15). As Φ_m was increased to 0.10, however, the small concentration peaks near the wall disappeared and the concentration profile became slightly peaked in the center of the channel. Karnis et al. also measured the concentration profile for the conditions noted above (a/R=0.039 and Φ_m=0.17), and found it to be flat, within experimental error. As noted in Chapter 1, however, their technique was subject to a relatively large statistical error.

The velocity profiles for the 50 μm diameter sphere suspensions were parabolic up to $\Phi_m \approx 0.05$. As the concentration was increased beyond that point, the velocity profiles became increasingly blunted in the center of the channel. At the maximum concentration of Φ_m=0.25, the maximum velocity was about 10% less than the maximum velocity that a Newtonian fluid would have for the same conditions. Karnis et al. observed blunting for a/R=0.070 and Φ_m=0.27, which is close to the conditions for data set 52. They observed a central plug flow core in the velocity profile with no measurable velocity gradient, and with a radius equal to 0.26 times the tube radius. While the velocity profiles measured in the present experiments are not totally flat in the center of the channel, the shape of the velocity profile for data set 52 is similar to the shape observed by Karnis et al. for similar conditions.

The concentration profiles for the 50 μm diameter spheres are summarized in Figures 3-20 and 3-21. For Φ_m=0.02, the concentration profile is similar to the corresponding dilute-suspension data set (5), except that the peaks near the wall are somewhat smaller for Φ_m=0.02. As Φ_m was increased beyond Φ_m=0.02, the concentration profiles became increasingly peaked in the center of the channel. The height of the concentration peak in the center of the channel

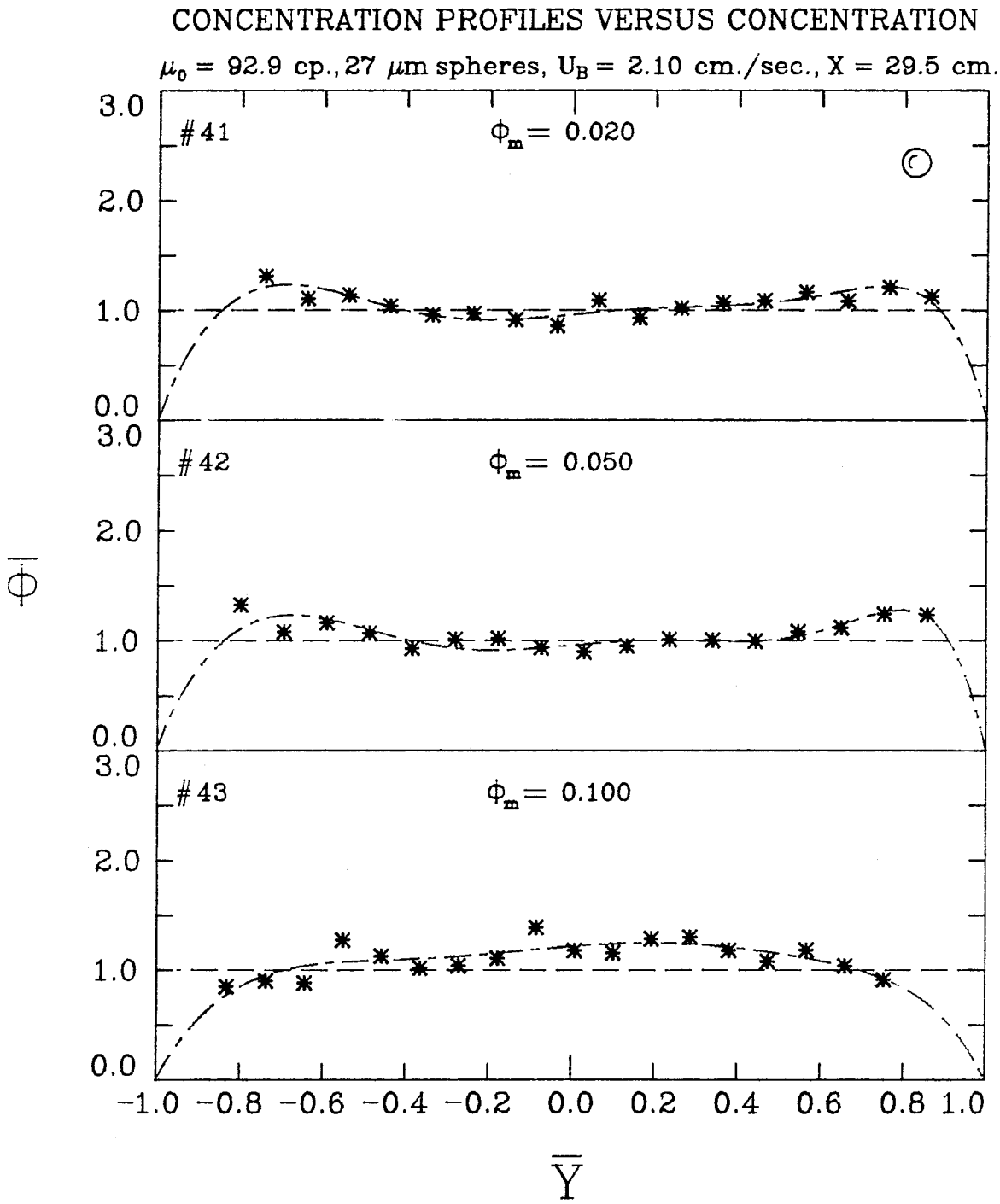
CONCENTRATION PROFILES VERSUS CONCENTRATION
μ_0 = 92.9 cp., 27 μm spheres, U_B = 2.10 cm./sec., X = 29.5 cm.
#41
Φ_m = 0.020
#42
Φ_m = 0.050
#43
Φ_m = 0.100
3.0
2.0
1.0
0.0
-1.0 -0.8 -0.6 -0.4 -0.2 0.0 0.2 0.4 0.6 0.8 1.0
$\overline{\Phi}$
$\overline{Y}$

Figure 3-19.

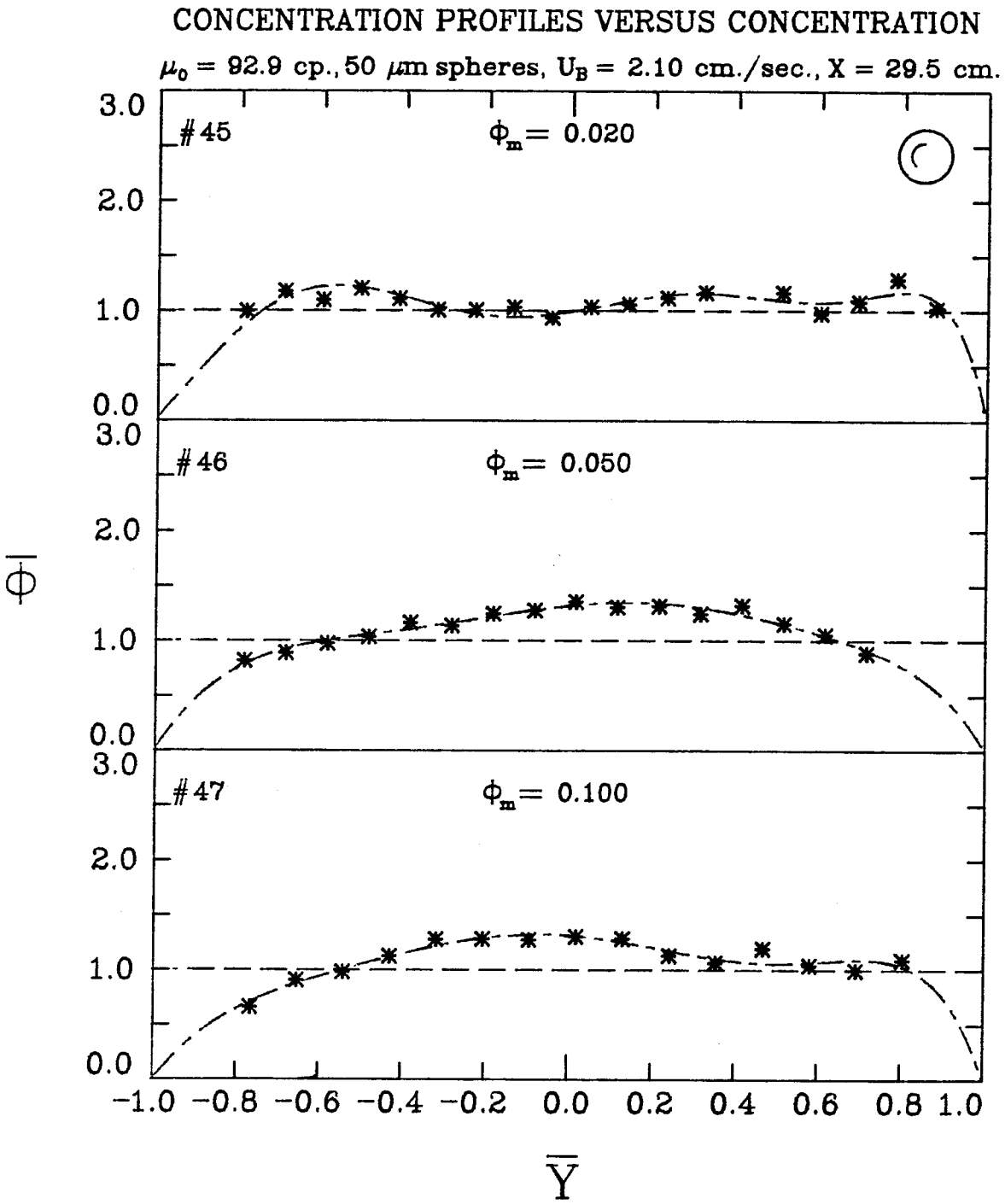
CONCENTRATION PROFILES VERSUS CONCENTRATION
μ_0 = 92.9 cp., 50 μm spheres, U_B = 2.10 cm./sec., X = 29.5 cm.
#45
Φ_m = 0.020
#46
Φ_m = 0.050
#47
Φ_m = 0.100
3.0
2.0
1.0
0.0
$\overline{\Phi}$
-1.0 -0.8 -0.6 -0.4 -0.2 0.0 0.2 0.4 0.6 0.8 1.0
$\overline{Y}$

Figure 3-20.

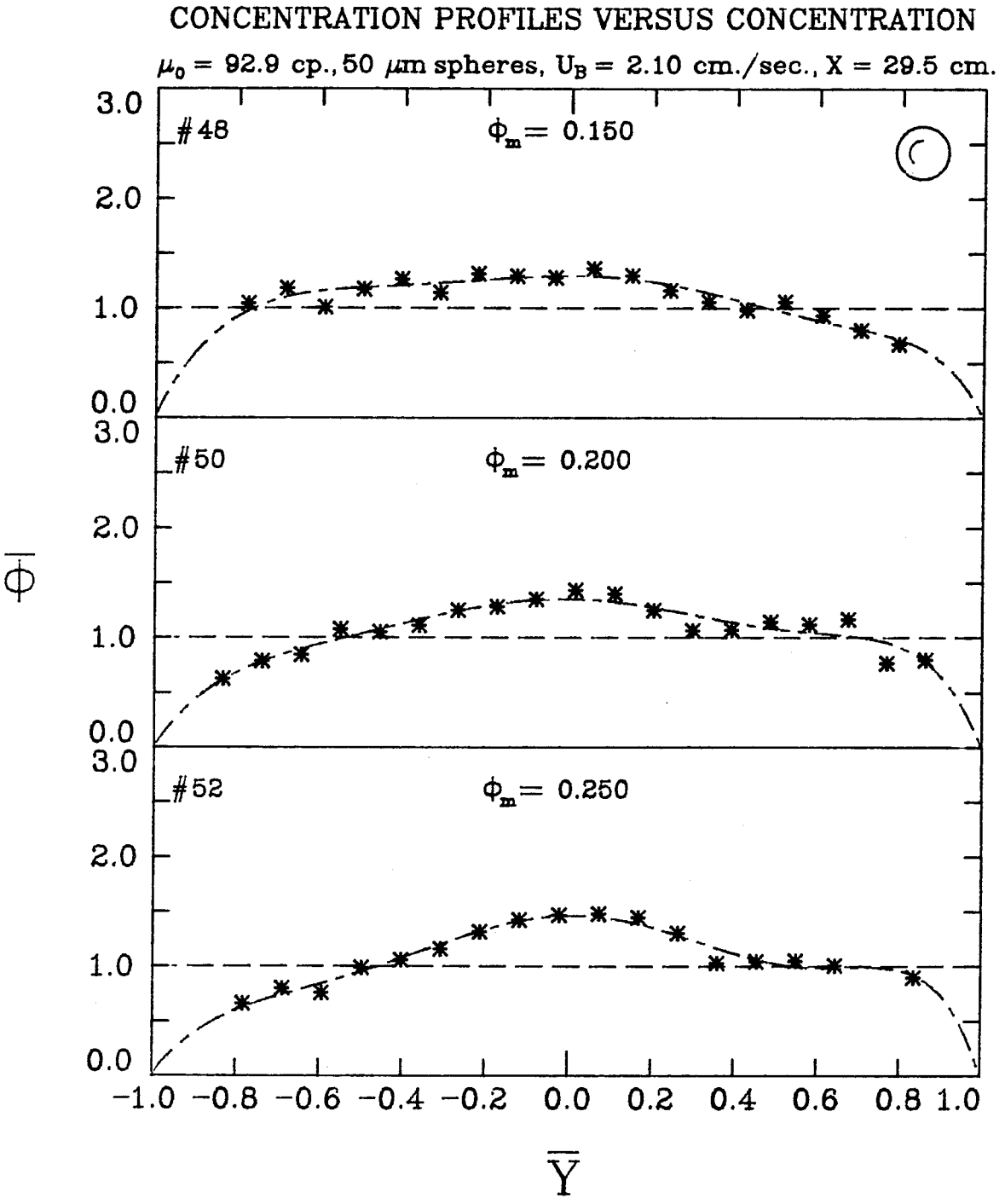
CONCENTRATION PROFILES VERSUS CONCENTRATION
μ_0 = 92.9 cp., 50 μm spheres, U_B = 2.10 cm./sec., X = 29.5 cm.
#48
Φ_m = 0.150
#50
Φ_m = 0.200
#52
Φ_m = 0.250
3.0
2.0
1.0
0.0
−1.0 −0.8 −0.6 −0.4 −0.2 0.0 0.2 0.4 0.6 0.8 1.0
$\overline{\Phi}$
$\overline{Y}$

Figure 3-21.

increased only slightly as the concentration increased beyond Φ_m=0.05, however.

Both of the velocity profiles measured for the 70 μm diameter sphere suspensions were substantially blunted. The blunting was greater than for the 50 μm sphere suspensions at identical concentrations, as expected. No comparison with the results of Karnis et al. is possible for these cases, since they did no experiments at a similar value of 2a/d.

The concentration profiles for the 70 μm sphere suspensions are summarized in Figure 3-22. Like the concentration profiles for the smaller spheres, the concentration profiles for the 70 μm sphere suspensions became increasingly peaked in the center of the channel with increasing Φ_m. Also, for a given Φ_m the central peak in the concentration profiles was somewhat higher for the 70 μm sphere suspensions than for the 50 μm sphere suspensions. Thus the height of the central peak in the concentration profiles increased with increasing sphere size, for a given Φ_m.

Some of the concentration profiles were slightly asymetric relative to the flow channel centerline. We believe that this assymmetry may have existed because the scattered light from one side of the flow channel, the left side, had a shorter distance to travel through the suspension before it reached the photodetector. This situation existed because the photodetector was to the left of the left-hand flow channel wall, as drawn in the experimental data figures. Thus signals from the left half of the flow channel would have less chance to be rescattered and hence would be more accurate than signals from the right half of the flow channel. This phenomenon would obviously become more pronounced at higher values of Φ_m. Therefore, the small humps on the right-hand sides of the concentration profiles for data sets 47, 50, and 52 are probably not a true depiction of the data.

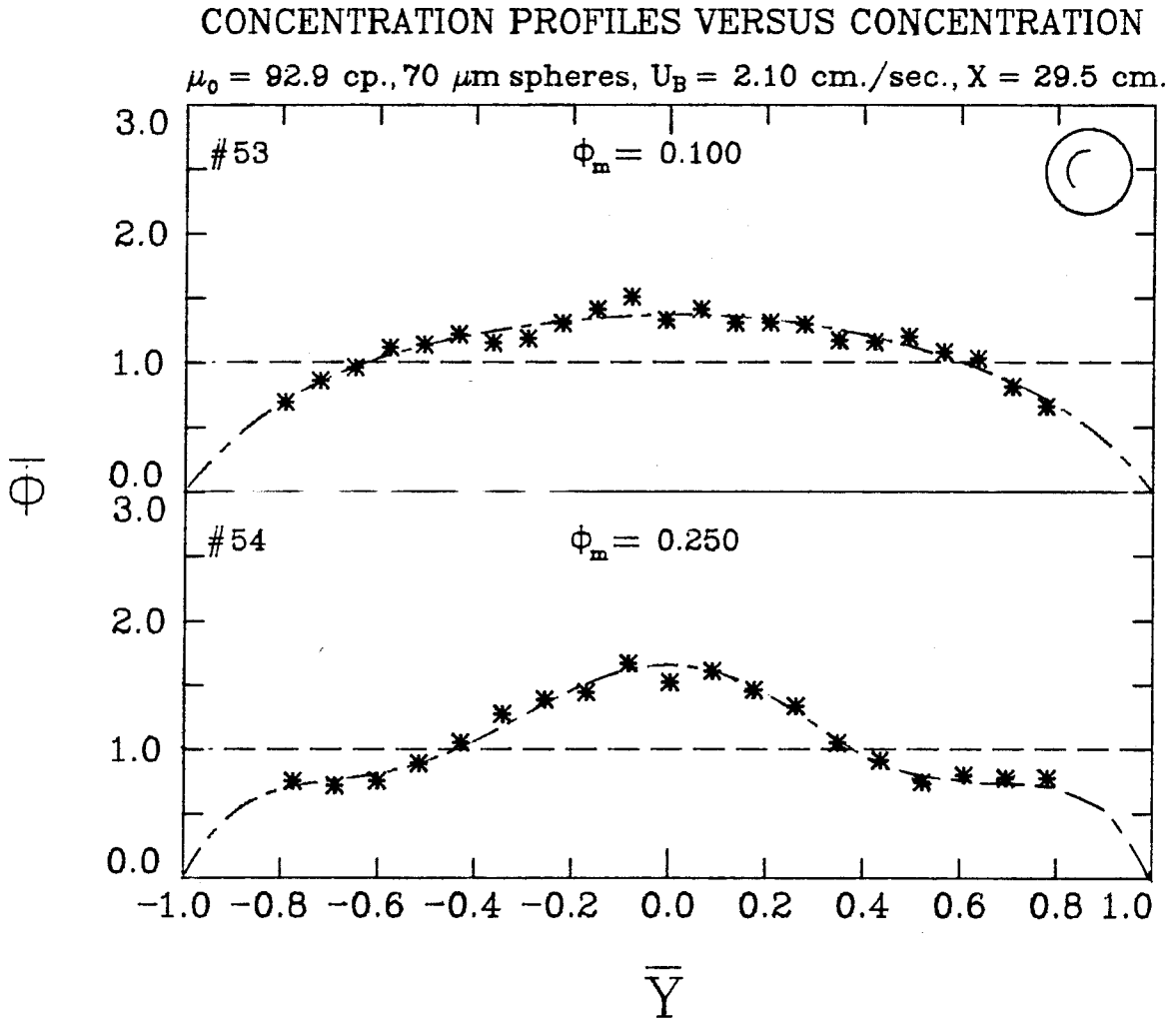
CONCENTRATION PROFILES VERSUS CONCENTRATION
μ_0 = 92.9 cp., 70 μm spheres, U_B = 2.10 cm./sec., X = 29.5 cm.
#53
Φ_m = 0.100
#54
Φ_m = 0.250
3.0
2.0
1.0
0.0
-1.0 -0.8 -0.6 -0.4 -0.2 0.0 0.2 0.4 0.6 0.8 1.0
$\overline{\Phi}$
$\overline{Y}$

Figure 3-22.

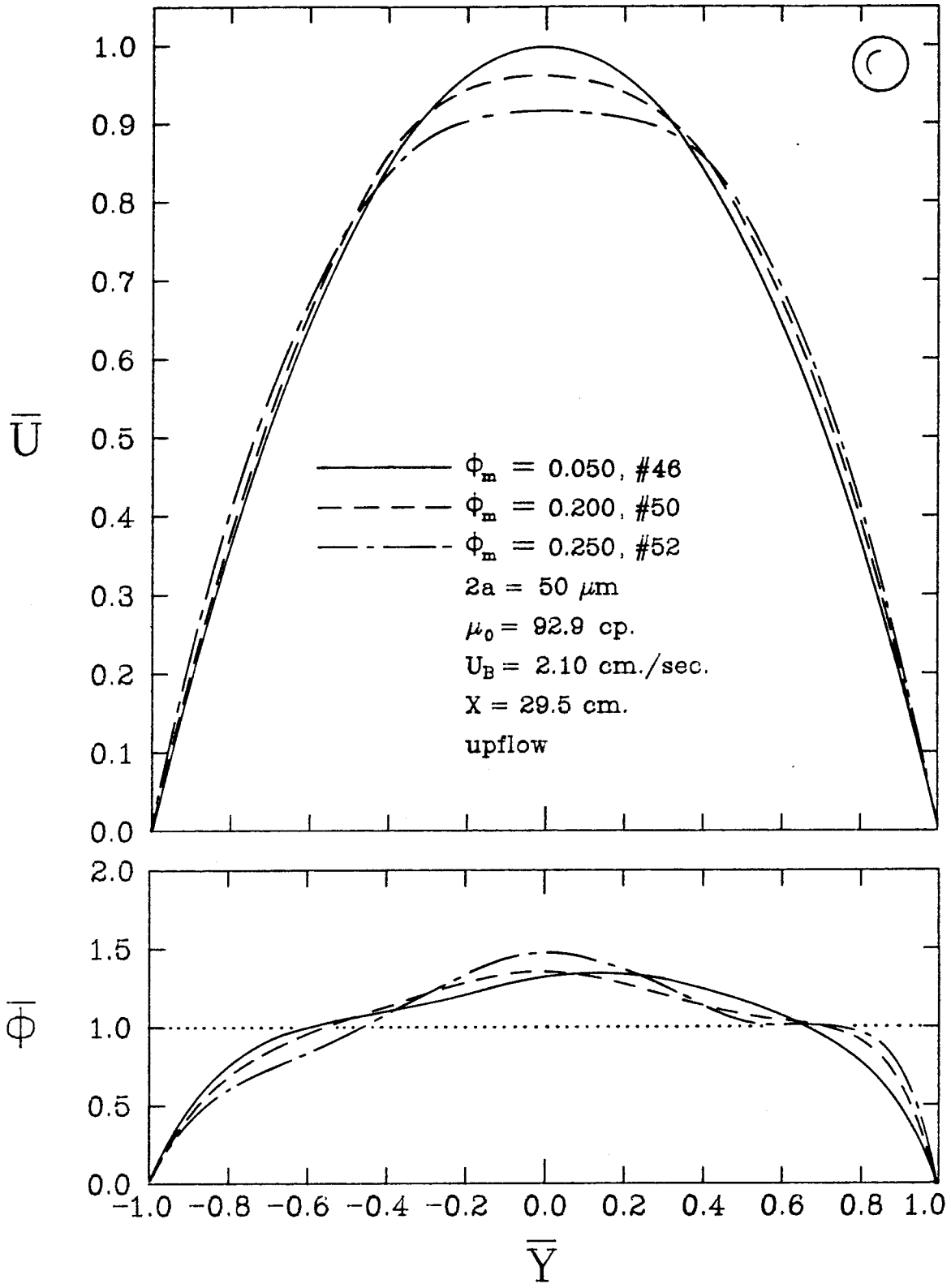

Figure 3-23. Comparison of velocity and concentration profiles for 3 different particle concentrations.

Figure 3-23 summarizes the effect of Φ_m on the velocity and concentration profiles for the 50 μm diameter sphere suspensions. As Φ_m increased, the velocity profiles became substantially blunted in the center of the channel. The concentration profiles were somewhat non-uniform, and became slightly more peaked in the center of the channel as the concentration increased.

The fact that the concentration profiles were peaked in the center of the channel when the velocity profiles were blunted suggests a possible explanation for the blunting of the velocity profiles. A higher concentration of particles in the center of the channel would lead to a higher local effective viscosity of the suspension in that region. This in turn would act to lower the velocity (and the velocity gradient) in the center of the channel relative to the region near the walls. A model used to test this hypothesis is presented in the next section.

Figures 3-24 and 3-25 show concentration profiles at two downstream positions for the 50 μm diameter sphere suspension at Φ_m=0.02 and Φ_m=0.20. For Φ_m=0.02 (Figure 3-24), the concentration profiles are similar at X=1.0 cm. and X=29.5 cm. The velocity profiles for these two cases are parabolic (see Figures 3-8 and 3-9). For Φ_m=0.20, the concentration profiles are similar, although at X=1.0 cm. the concentration profile is slightly flatter in the center of the channel, and for X=29.5 cm. the concentration increases a little more gradually from the wall to the center of the channel. Also, the corresponding velocity profiles in Figures 3-13 and 3-14 have similar shapes. The important conclusion from these results is that the concentration profiles are non-uniform near the entry, and their shape does not change much with downstream position. This indicates that the shapes of the concentration profiles are determined mostly by conditions at the flow channel entry.

In an attempt to investigate how the geometry of the flow channel entry affected the shape of the concentration profiles, an experiment was done with a

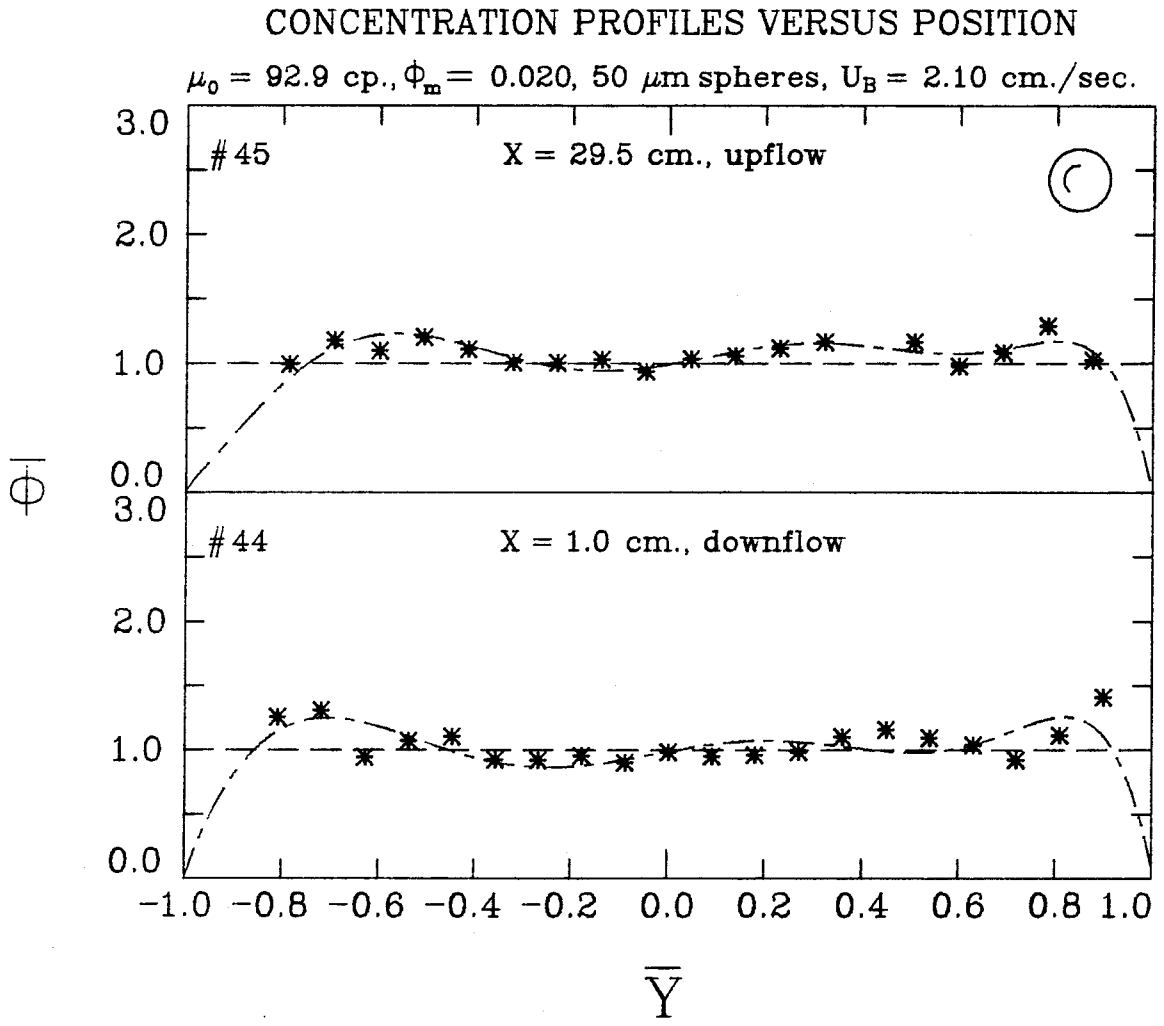
CONCENTRATION PROFILES VERSUS POSITION
μ_0 = 92.9 cp., ϕ_m = 0.020, 50 μm spheres, U_B = 2.10 cm./sec.
#45
X = 29.5 cm., upflow
#44
X = 1.0 cm., downflow
3.0
2.0
1.0
0.0
$\overline{\phi}$
-1.0 -0.8 -0.6 -0.4 -0.2 0.0 0.2 0.4 0.6 0.8 1.0
$\overline{Y}$

Figure 3-24.

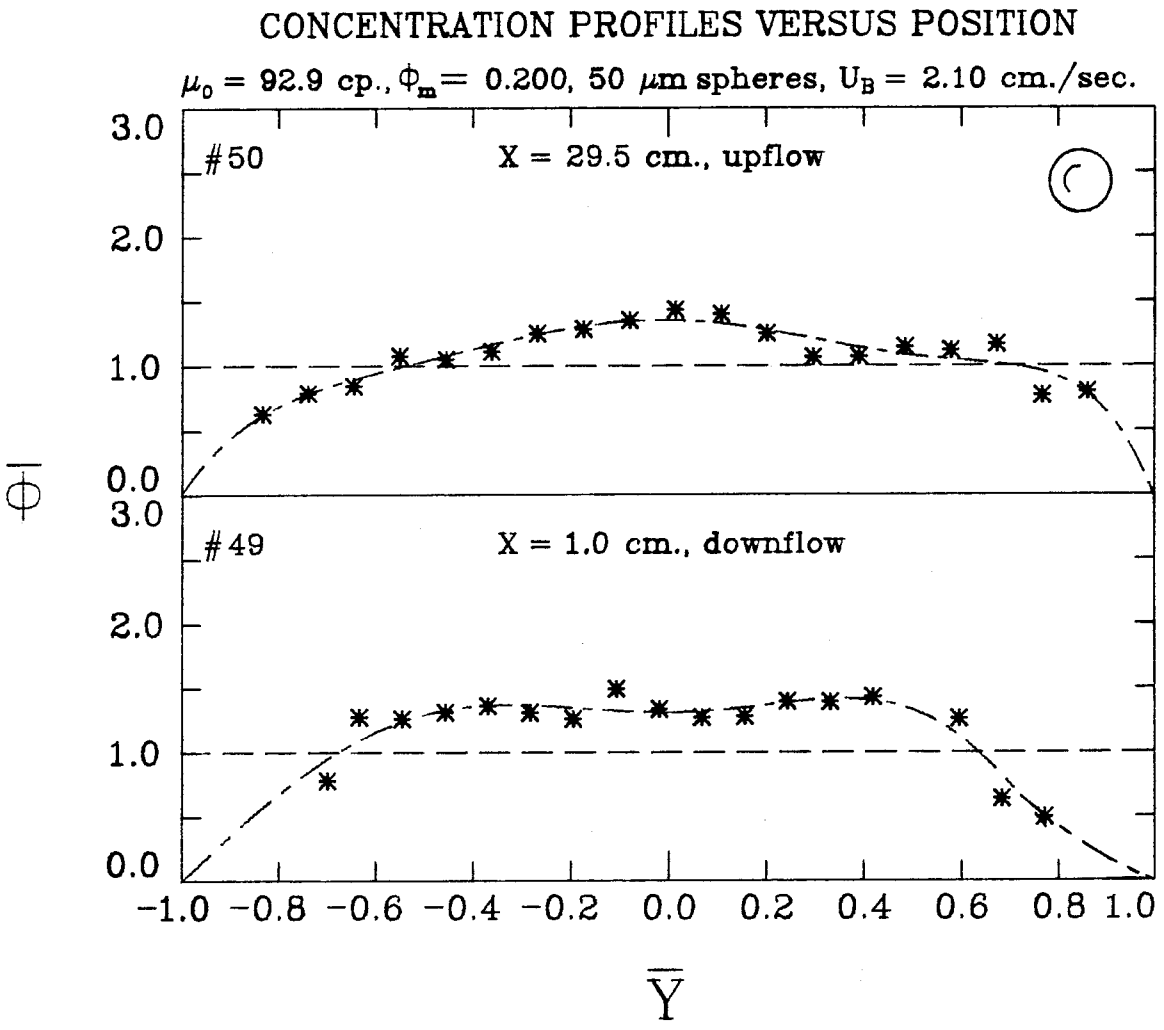
CONCENTRATION PROFILES VERSUS POSITION
μ_0 = 92.9 cp., Φ_m = 0.200, 50 μm spheres, U_B = 2.10 cm./sec.
#50
X = 29.5 cm., upflow
#49
X = 1.0 cm., downflow
3.0
2.0
1.0
0.0
-1.0 -0.8 -0.6 -0.4 -0.2 0.0 0.2 0.4 0.6 0.8 1.0
$\overline{\Phi}$
$\overline{Y}$

Figure 3-25.

modified flow channel entry (see Figure 3-3). If the initial concentration profile was produced as a result of mechanical interaction of particles near the wall with the flow channel entry, as was postulated for the dilute-suspension experiments, then changing the geometry of the entry from a nearly 90 degree angle to a 45 degree angle maybe expected to affect the resulting concentration distributions. For example, spheres which were traveling on streamlines whose minimum distance from the 90 degree corner was less than the sphere radius a (as shown in Figure 3-26) would be displaced inward upon turning the corner. A smaller number of spheres would be displaced inward for the more gradual 45 degree corner, since the streamlines are less crowded in the vicinity of the corner. When the data for the modified entry section (data set 51) is compared to the corresponding data for the original entry (data set 50), it is seen that the concentration profiles are only slightly different. The central peak is slightly higher for the modified entry, and the concentration profile is somewhat less smooth. The velocity profiles for the two cases are similar. Thus apparently for the concentrated suspensions, interaction between the particles near the wall and the flow channel entry is not a sufficient explanation for the shape of the concentration profiles.

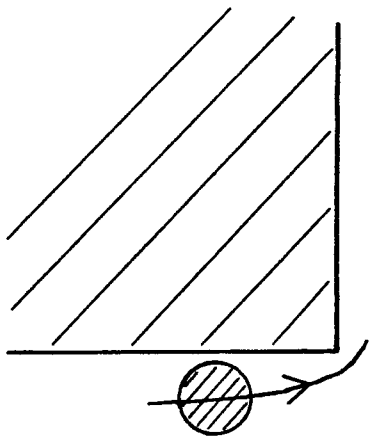

Figure 3-26. Interaction of a sphere with the flow channel entry.

The processes occurring at the entry which result in initially non-uniform concentration distributions are apparently more complicated than the above explanation would indicate. Since the concentration peaks in the center of the channel developed only at higher concentrations, it seems obvious that any mechanism describing the formation of the initial concentration profiles would need to include particle-particle interactions.

3.4. MODEL VELOCITY PROFILE CALCULATION

In order to investigate whether the non-uniform concentration distributions observed for the concentrated suspensions offered a reasonable explanation for the shape of the velocity profiles, a model velocity profile calculation was done. The method for this calculation was as follows: The viscosity at a point in the flow channel was assumed to be a function of the local concentration of spheres at that point. This assumption was questionable, since a/d was not particularly small, and thus a "point" that contained enough particles to determine the viscosity would not be small compared to d. Nevertheless, this calculation should give some indication as to whether the shape of the concentration profiles accounts for the shape of the velocity profiles. Thus an equation giving $\mu(\Phi)$ was substituted into the Navier-Stokes equations, which were solved for velocity as a function of $\bar{Y}$. The measured concentration profiles were used to give Φ as a function of $\bar{Y}$, and hence $\mu(\Phi(\bar{Y}))$. Velocity profiles were then calculated for the experiments listed in Table 3-1.

For the two-dimensional case being considered, the Navier-Stokes equations reduce to:

$$\frac{\partial \tau_{yx}}{\partial y} = \frac{\partial P}{\partial x} \qquad (3.1)$$

$$\tau_{yx} = 0 \text{ at } y=0 \quad .$$

Integrating once with respect to y and applying the boundary condition:

$$\tau_{yx} = \left[\frac{dP}{dX}\right] y \quad . \tag{3.2}$$

An equation to give viscosity as a function of Φ is now required. The equation chosen was that of Krieger and Dougherty, a commonly used equation (Jeffrey and Acrivos, 1976):

$$\mu = \mu_0(1-K\Phi)^{-B/K} \quad . \tag{3.3}$$

Here B and K are adjustable parameters determined from experimental data. These parameters were evaluated using the data of Gadala-Maria and Acrivos (1980). These data were obtained in a Couette device of an R-17 Weissenberg Rheogoniometer for neutrally-buoyant suspensions of polystyrene spheres 40-50 μm in diameter. The "asymptotic shear viscosity" at a shear rate of 24 sec^{-1} was used (for Φ_m<0.40 the viscosity was nearly independent of shear rate). The equation (3.3) was fit (by us) to the data using a least-squares computer program, giving parameter values of B=2.5092 and K=1.7032.

Using (3.3):

$$\tau_{yx} = \mu_0[1-K\Phi(y)]^{-B/K}\left[\frac{dU_x}{dy}\right] \quad . \tag{3.4}$$

Substituting (3.4) into (3.2):

$$\mu_0[1-K\Phi(y)]^{-B/K}\left[\frac{dU_x}{dy}\right] = \left[\frac{dP}{dX}\right] y \quad . \tag{3.5}$$

Rearranging:

$$dU_x = \frac{(dP/dX)}{\mu_0}\left[\frac{y}{[1-K\Phi(y)]^{-B/K}}\right] dy \quad . \tag{3.6}$$

Integrating and applying the no slip condition (U_x=0 at y=+/- (d/2)):

$$U_x = \frac{(dP/dX)}{\mu_0}\int_{d/2}^{y}\left[\frac{y'}{[1-K\Phi(y')]^{-B/K}}\right] dy' \quad . \tag{3.7}$$

Non-dimensionalizing y using:

$$\overline{Y} = \frac{y}{(d/2)} \quad , \tag{3.8}$$

gives:

$$\frac{U_x}{\left[\frac{d^2(dP/dX)}{4\mu_0}\right]} = \overline{U}_x = \int_1^{\overline{Y}} \left[\frac{\overline{Y}'}{[1-K\Phi(\overline{Y}')]^{-B/K}}\right] d\overline{Y}' \tag{3.9}$$

The integral in (3.9) was evaluated numerically using a fourth-order Runge-Kutta method. The concentration $\Phi(\overline{Y})$ was evaluated using the polynomial curve-fits to the concentration data. The results appear in Figures 3-27 to 3-37. Here the calculated velocity profiles appear as solid lines, and the curve-fits to the velocity profiles and the error bars have been omitted.

Upon observing the model velocity profiles for the 27 μm sphere suspensions, it can be seen that they are all nearly parabolic, except for data set 43 (Φ_m=0.10), which is slightly blunted. It is reasonable that there is not much blunting for these velocity profiles, since Φ_m is relatively low and the concentration profiles are relatively flat. For the 50 μm sphere suspensions, significant blunting in the model velocity profiles occurs for $\Phi_m \geq 0.10$. The model velocity profiles are also in reasonably good agreement with the measured velocity profiles.

The model velocity profile for the 70 μm sphere suspension at Φ_m=0.10 is slightly less blunted than the experimental profile, but at Φ_m=0.25 the model profile is substantially less blunted than the experimental profile. A possible explanation for this discrepancy is as follows. For these large spheres, the assumption that the viscosity at a "point" can be modeled as a function of Φ may result in a substantial error in the velocity profile calculation. This assumption will certainly become increasingly invalid as the sphere size is increased. The

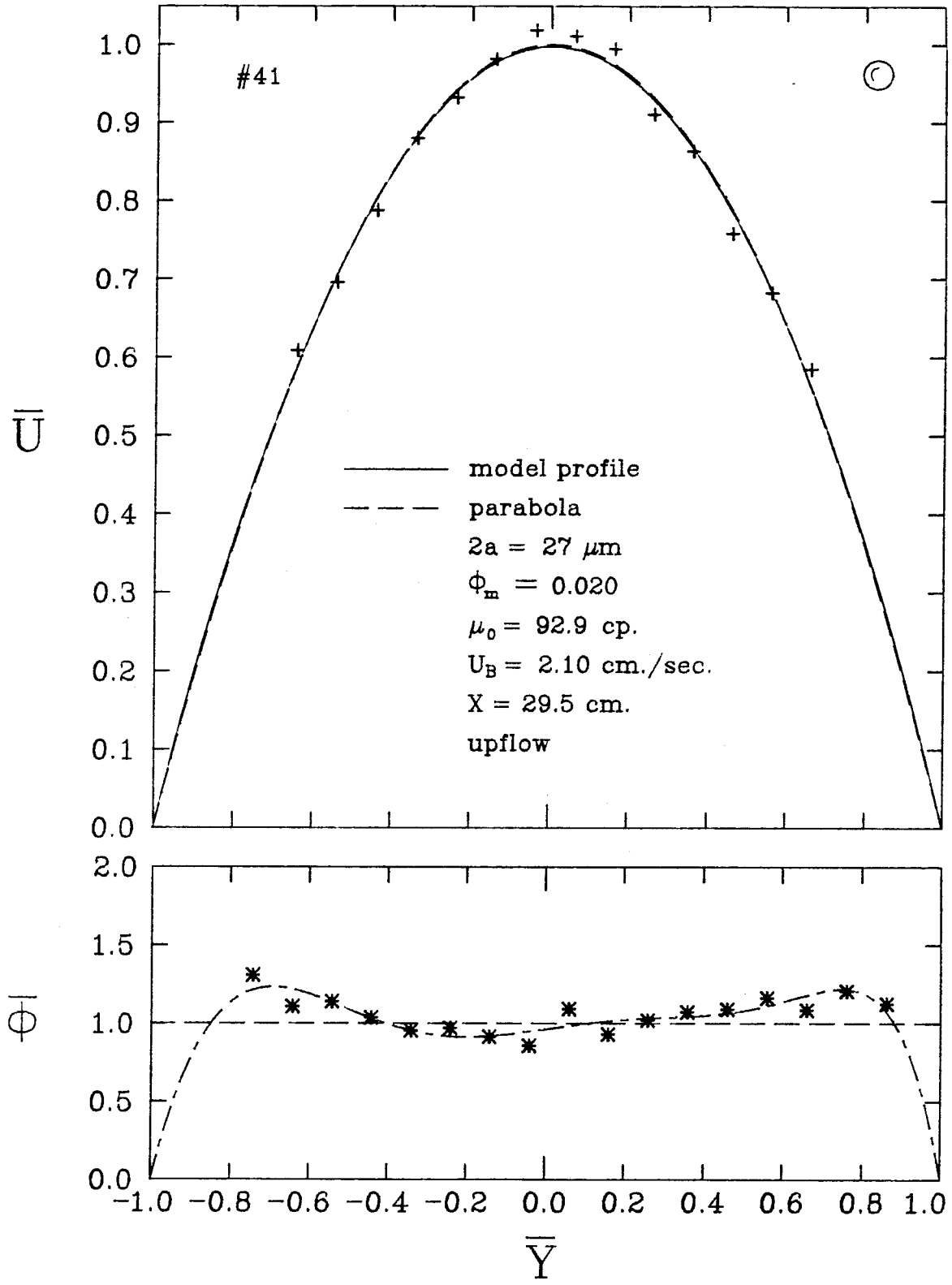

Figure 3-27. Experimental velocity and concentration profiles with model velocity profile.

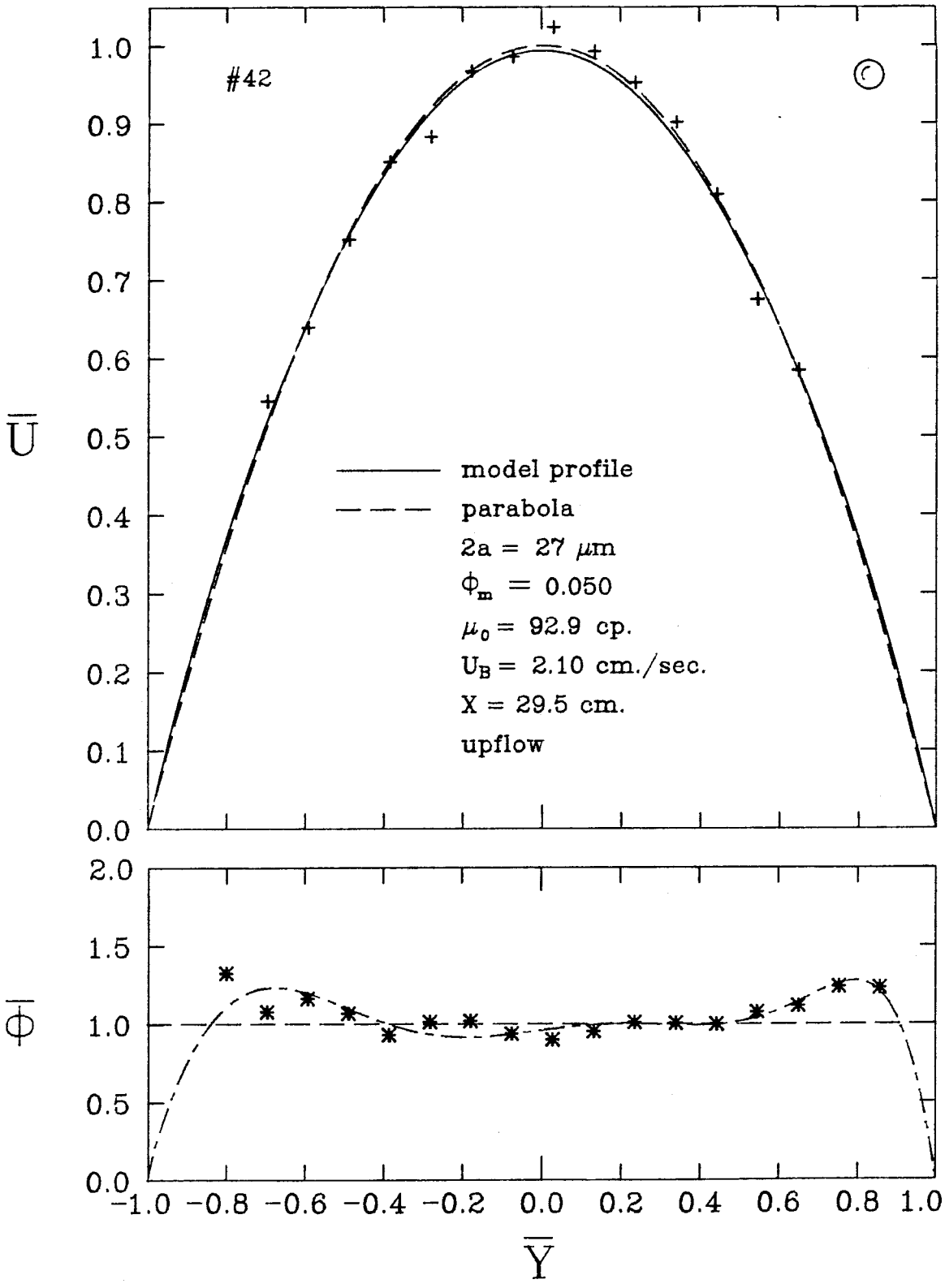

Figure 3-28. Experimental velocity and concentration profiles with model velocity profile.

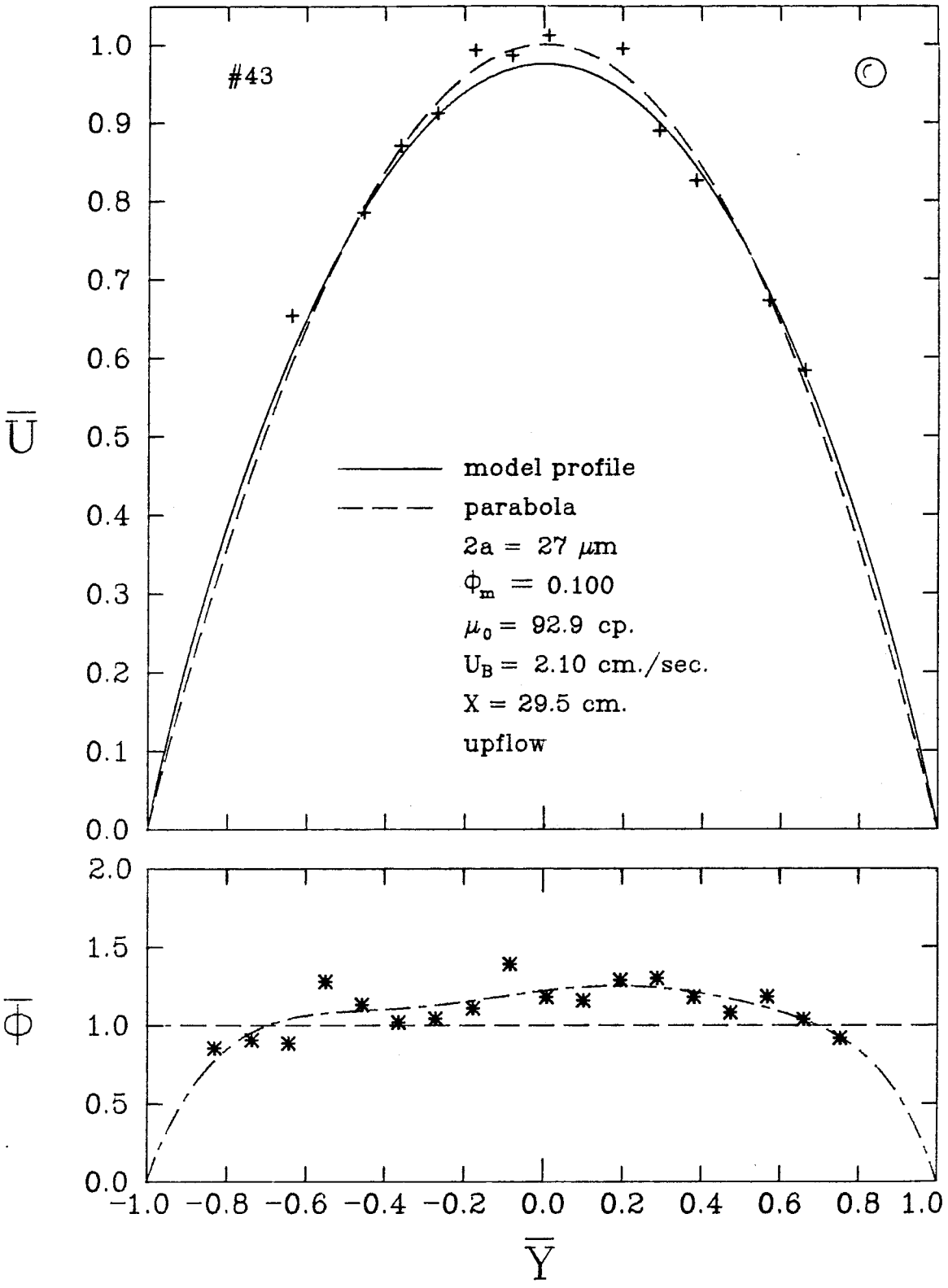

Figure 3-29. Experimental velocity and concentration profiles with model velocity profile.

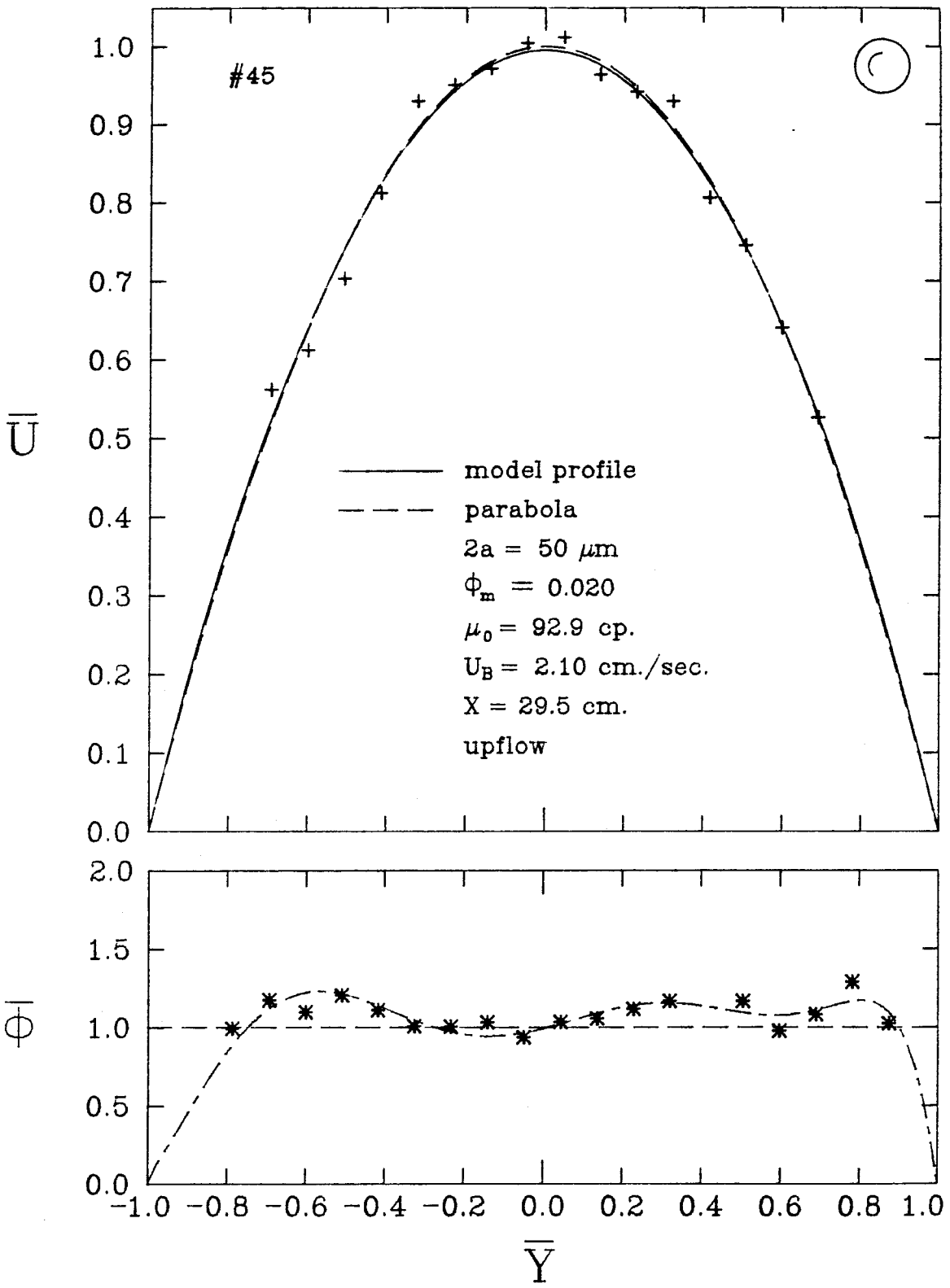

Figure 3-30. Experimental velocity and concentration profiles with model velocity profile.

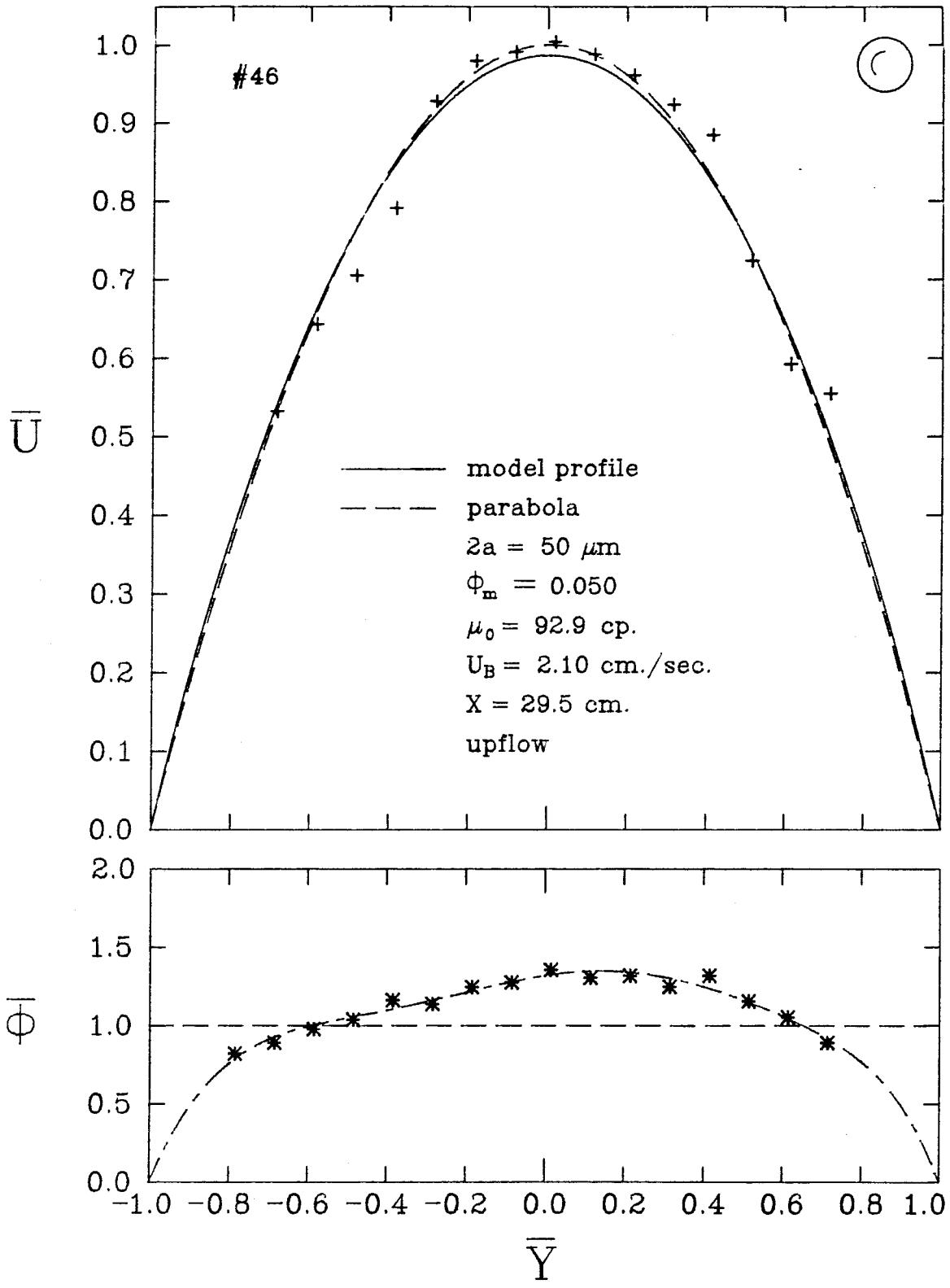

Figure 3-31. Experimental velocity and concentration profiles with model velocity profile.

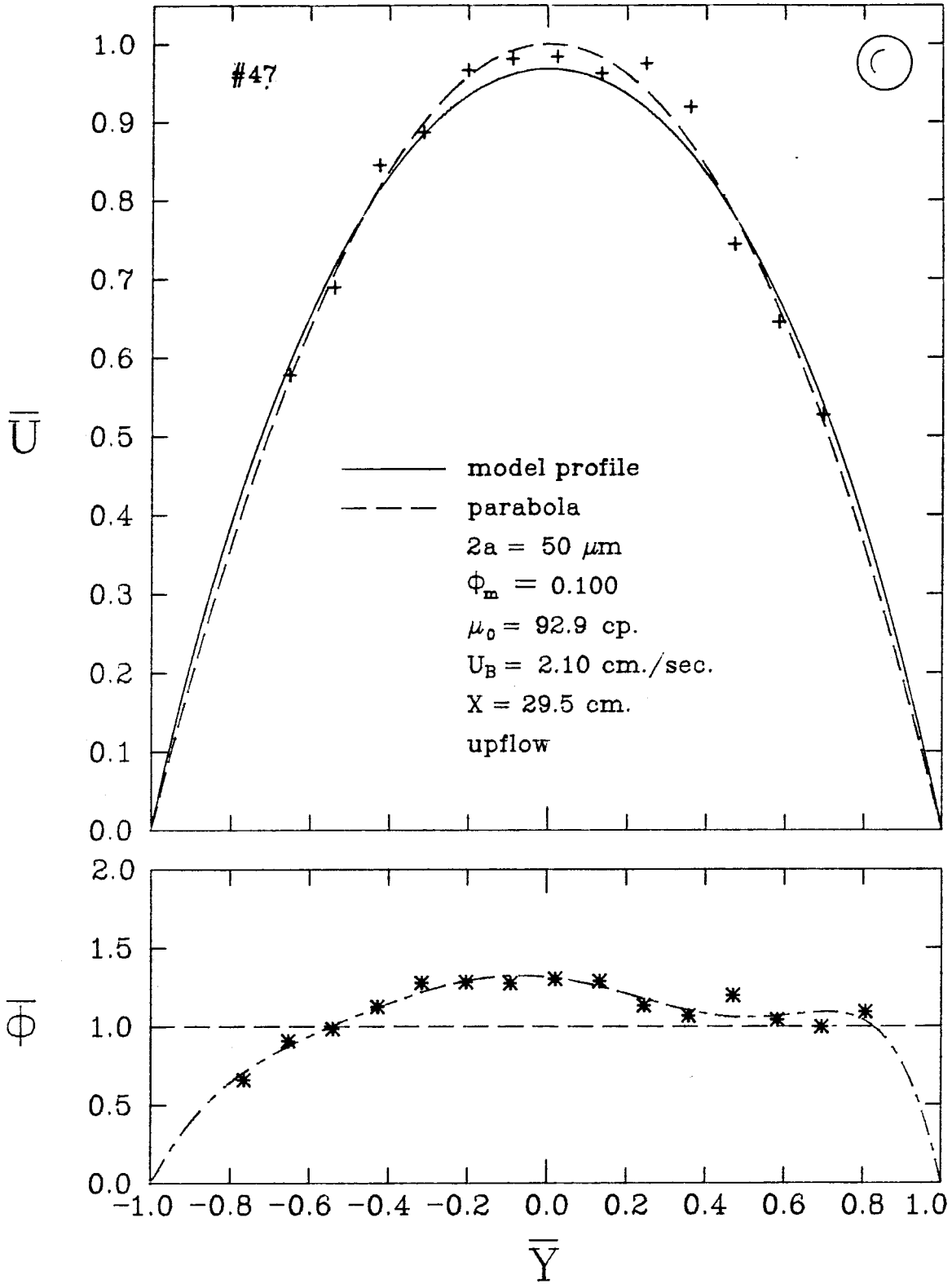

Figure 3-32. Experimental velocity and concentration profiles with model velocity profile.

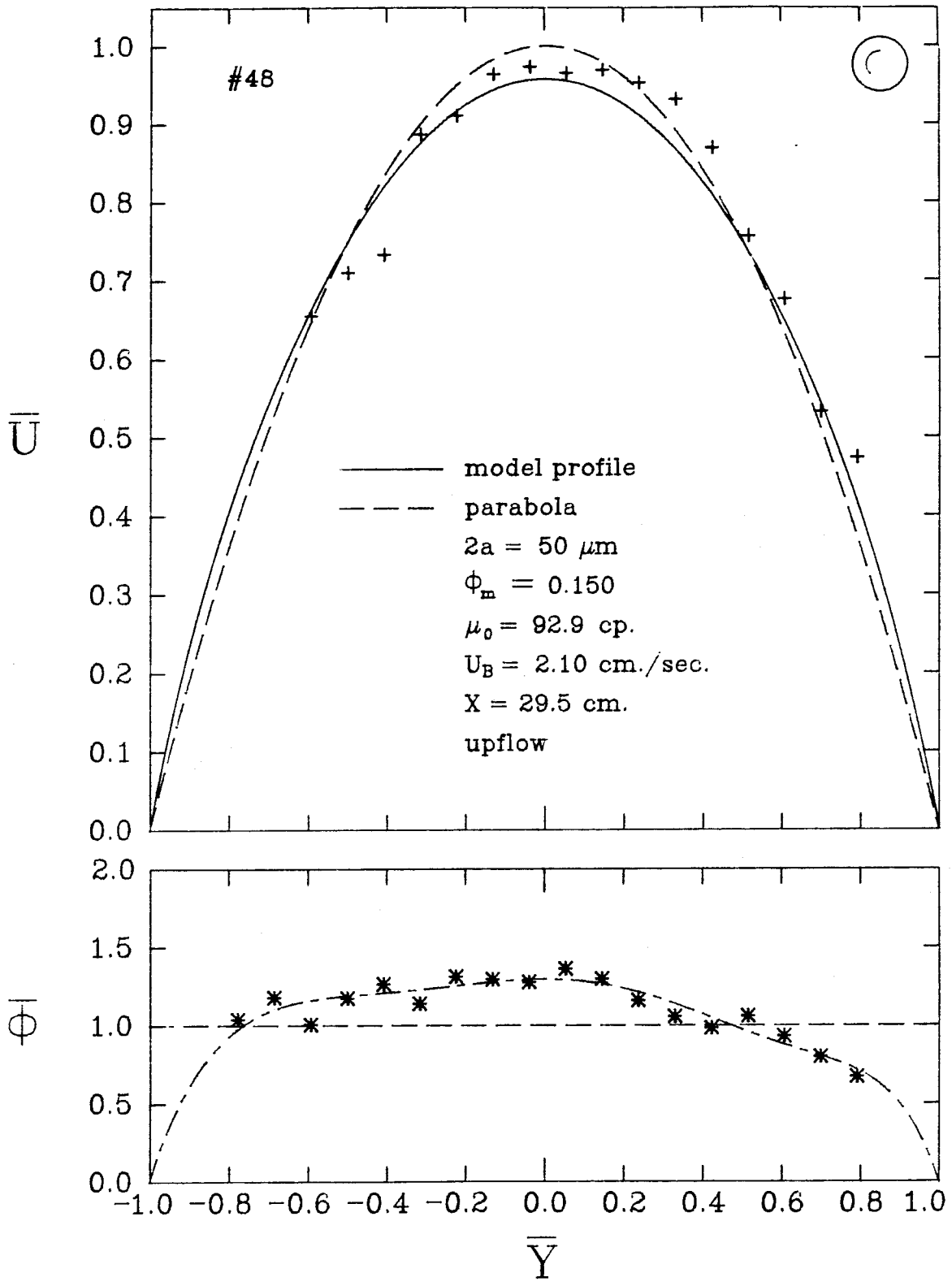

Figure 3-33. Experimental velocity and concentration profiles with model velocity profile.

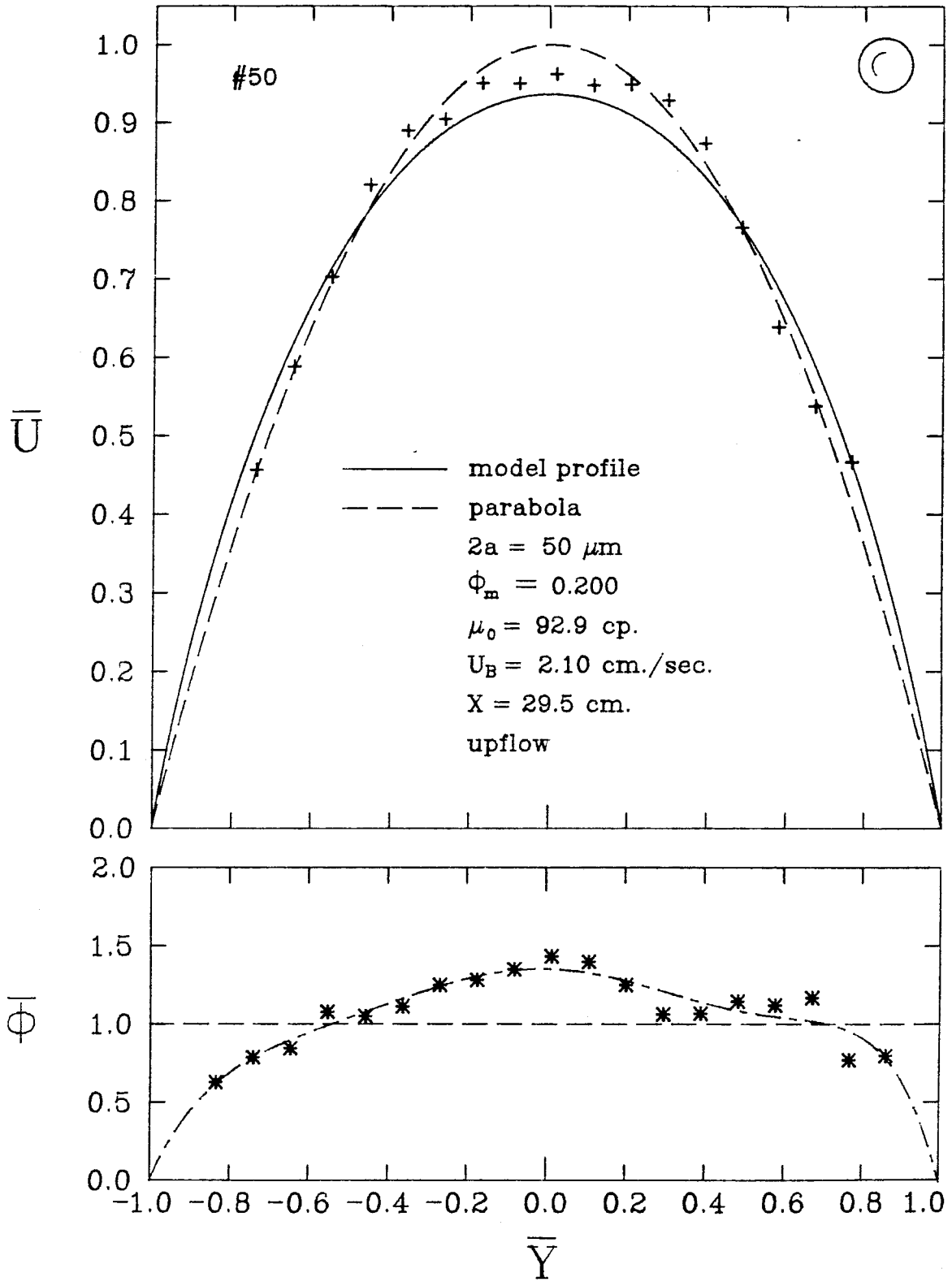

Figure 3-34. Experimental velocity and concentration profiles with model velocity profile.

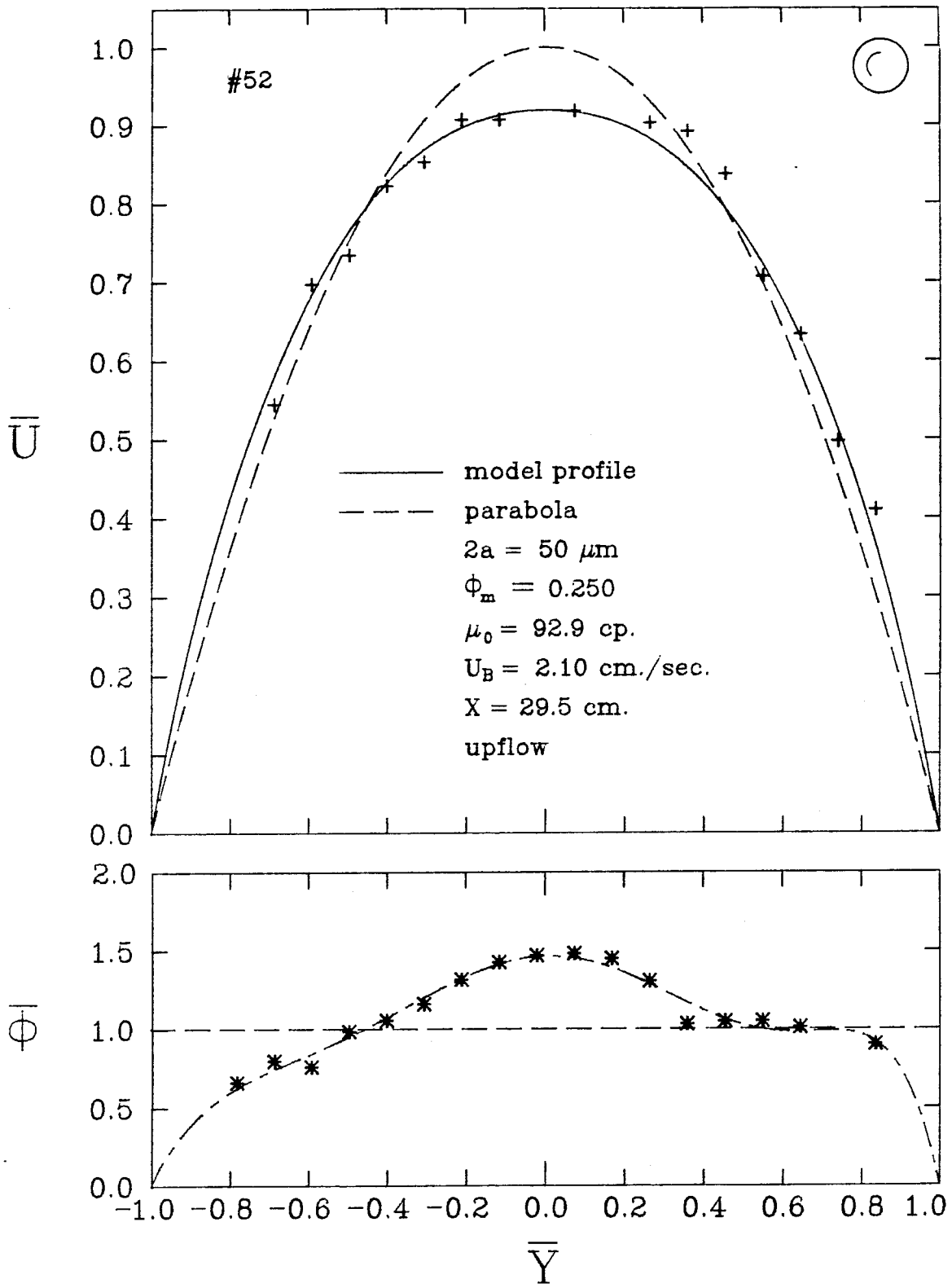

Figure 3-35. Experimental velocity and concentration profiles with model velocity profile.

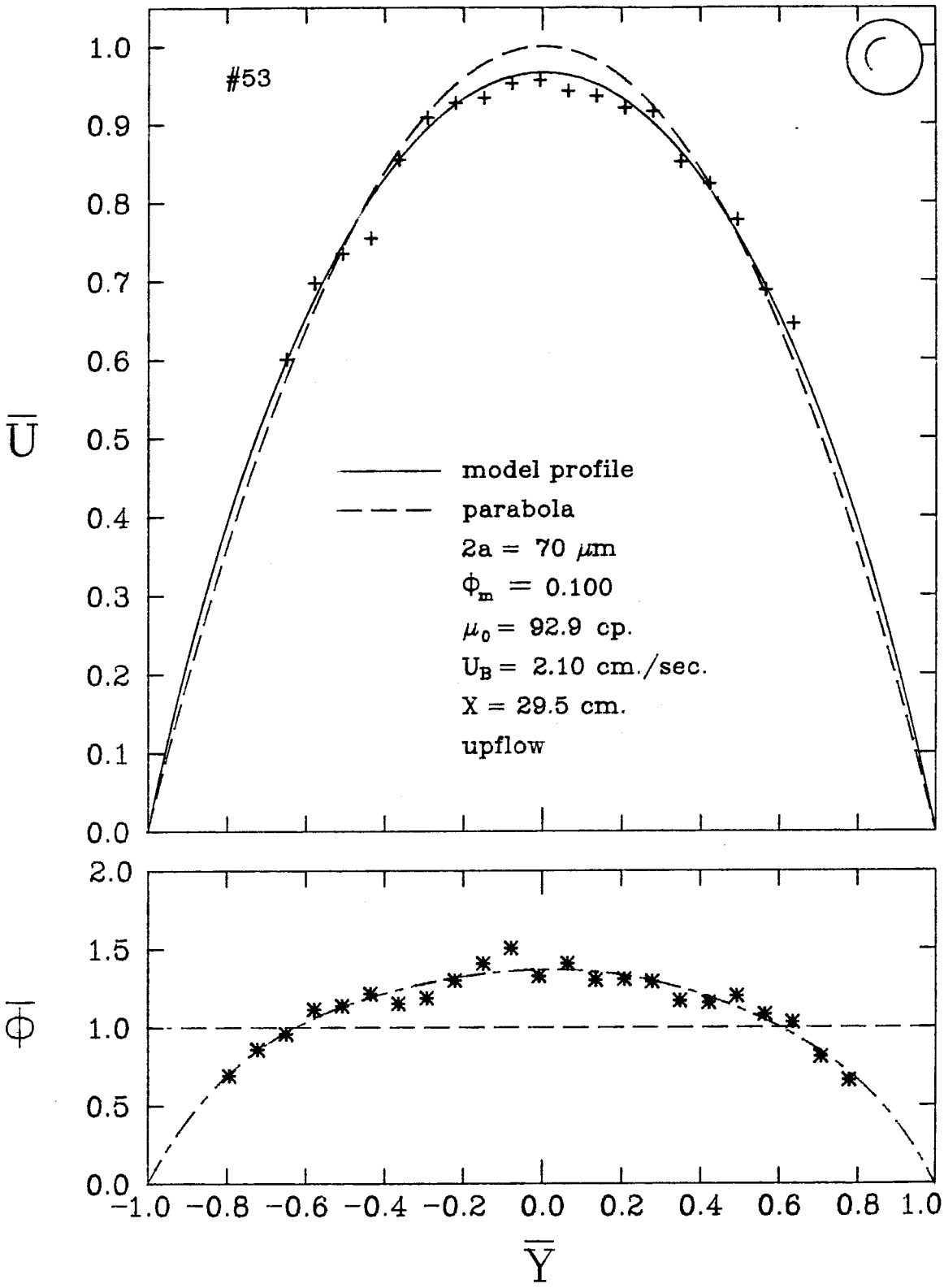

Figure 3-36. Experimental velocity and concentration profiles with model velocity profile.

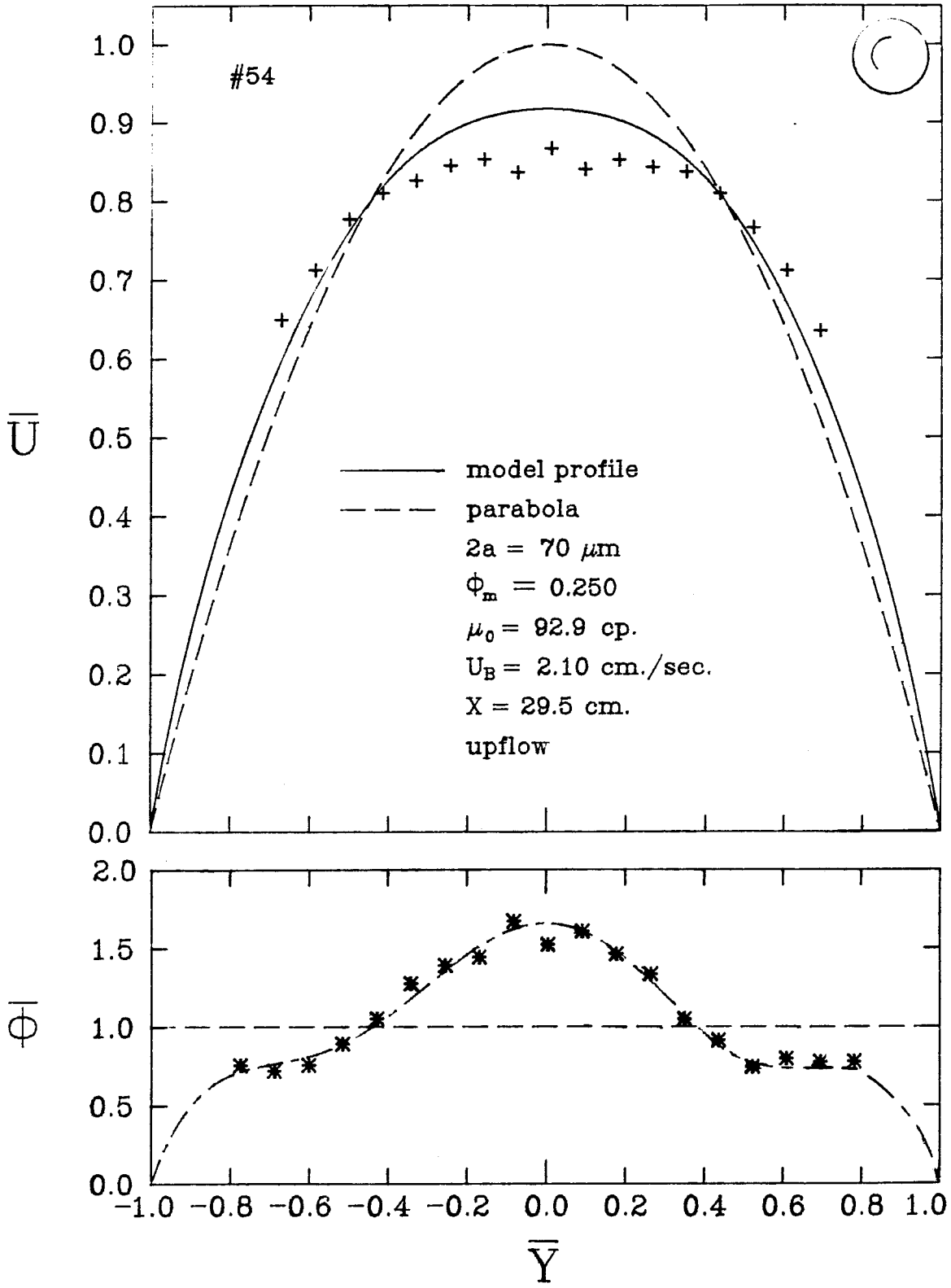

Figure 3-37. Experimental velocity and concentration profiles with model velocity profile.

fact that reasonably good agreement between model and experimental velocity profiles was obtained for the smaller spheres would seem to indicate that non-uniformity of the concentration profiles was the main factor in determining the shape of the velocity profiles, however.

3.5. CONCLUSIONS

Techniques which allowed the measurement of velocities and concentrations in moderately concentrated suspensions were demonstrated. Blunted velocity profiles were observed for 50 and 70 μm diameter sphere suspensions for $\Phi_m \geq 0.10$. This result is in agreement with a previous study by Karnis et al. Non-uniform concentration profiles were observed, which became increasingly peaked in the center of the channel as Φ_m and/or a/d increased. The concentration profiles were non-uniform near the flow channel entry, but also changed shape slightly far downstream. The model velocity profile calculation indicated that the non-uniform concentration profiles could account for the observed shape of the velocity profiles for the 27 and 50 μm sphere suspensions.

3.6. REFERENCES

Durst, F., A. Melling, and J. H. Whitelaw 1976 *Principles and Practice of Laser-Doppler Anemometry*. Academic Press.

Gadala-Maria, F. and A. Acrivos 1980 *J. Rheology* **22** , 417.

Jeffrey, D. J. and A. Acrivos 1976 *A. I. Ch. E. J.* **24** , 799.

Karnis, A., H. L. Goldsmith, and S. G. Mason 1966 J. Colloid Interface Sci. **22** , 531.

4. SUMMARY AND CONCLUSIONS

In the introduction, two major, related goals of this research were indicated. One was to discern the mechanism by which velocity profiles are blunted in suspensions of neutrally-buoyant rigid spheres in low Reynolds number tube or channel flows. The other was the development of an experimental technique capable of measuring particle concentrations in concentrated suspensions, which would help in achieving the first goal. Both of these goals were realized satisfactorily.

The concentration measurement technique was demonstrated to give reasonably rapid and accurate results for dilute and concentrated suspensions of solid particles with volume fractions as high as 0.25. To our knowledge, this is the first demonstration of a technique capable of doing so. In principle, higher concentrations could be used, if the suspensions were sufficiently transparent. Also, the technique could be applied to other flow channel geometries. Thus the technique could be applied to suspension flows other than the one studied, as long as the suspensions were transparent.

The concentration measurements provided a reasonable explanation for the blunting of velocity profiles observed for the suspension flows studied. Increases in the height of the central peak in the concentration profiles corresponded to increased blunting of the velocity profiles. This phenomenon was observed for a given sphere size as a function of sphere concentration, and for a given concentration as a function of sphere size. These results provide a reasonable explanation for the apparent puzzle which arose when the results of Karnis, Goldsmith, and Mason were published almost 20 years ago.

The main unsolved question regarding the present results is how the initially non-uniform concentration profiles were formed. Measurements in the entry region of the flow channel (even before the start of the flow channel

proper) may be useful in answering this question.